Copy 24
RM A9G13
NACA RM-A9G13
NACA RM A9G13
RESTRICTED
UNCLASSIFIED

NACA

Classification Changed to UNCLASSIFIED
By Authority of NACA Res. abstracts #46 dated 31 July 1953 (6-11-53)
Date NOV 3 1953 By J. E. Newlan

RESEARCH MEMORANDUM

TESTS OF A MODEL HORIZONTAL TAIL OF ASPECT RATIO 4.5 IN THE AMES 12-FOOT PRESSURE WIND TUNNEL.

I - QUARTER-CHORD LINE SWEPT BACK 35°

By Bruce E. Tinling and Jerald K. Dickson

Ames Aeronautical Laboratory
Moffett Field, Calif.

CASE FILE COPY
JPL LIBRARY
CALIFORNIA INSTITUTE OF TECHNOLOGY

CLASSIFIED DOCUMENT

This document contains classified information affecting the National Defense of the United States within the meaning of the Espionage Act, USC 50:31 and 32. Its transmission or the revelation of its contents in any manner to an unauthorized person is prohibited by law. Information so classified may be imparted only to persons in the military and naval services of the United States, appropriate civilian officers and employees of the Federal Government who have a legitimate interest therein, and to United States citizens of known loyalty and discretion who of necessity must be informed thereof.

NATIONAL ADVISORY COMMITTEE FOR AERONAUTICS

WASHINGTON
September 9, 1949

RESTRICTED
UNCLASSIFIED
SEP 13 1949

UNCLASSIFIED
Authority NACA Res. abstracts #46 dated 31 July 1953 - (6-11-53)
Date NOV 3 1953 By L. E. Newlan BS

UNCLASSIFIED

NATIONAL ADVISORY COMMITTEE FOR AERONAUTICS

RESEARCH MEMORANDUM

TESTS OF A MODEL HORIZONTAL TAIL OF ASPECT RATIO 4.5 IN THE AMES 12-FOOT PRESSURE WIND TUNNEL.

I - QUARTER-CHORD LINE SWEPT BACK 35°

By Bruce E. Tinling and Jerald K. Dickson

SUMMARY

Wind-tunnel tests have been conducted to evaluate the independent effects of Reynolds and Mach numbers on the aerodynamic characteristics of a horizontal tail of aspect ratio 4.5 equipped with a plain sealed elevator with a tab. The line joining the quarter-chord points of the airfoil sections was swept back 35° and the thickness distribution normal to this line was the NACA 64A010.

The Reynolds number was varied from 2,000,000 to 11,000,000 at a Mach number of 0.21, and the Mach number was varied from 0.21 to 0.94 at a Reynolds number of 2,000,000. Lift, drag, pitching moment, elevator hinge moment, tab hinge moment, streamwise distribution of static pressure at the midsemispan, and pressure difference across the elevator-nose seal were measured.

An increase of Reynolds number from 2,000,000 to 11,000,000 had little effect other than to increase the angle-of-attack range over which the variation of lift with angle of attack was linear.

Abrupt decreases in lift-curve slope occurred at a Mach number of about 0.93 and in elevator lift effectiveness at a Mach number of about 0.87. The Mach numbers at which marked changes in the elevator hinge-moment coefficients occurred were dependent upon the magnitude of angle of attack and of elevator deflection. In general, however, the changes of elevator hinge-moment coefficient were gradual as the Mach number was increased to 0.85. The tab was effective throughout the Mach number range. Calculations indicated that incorporation of sufficient sealed internal balance to reduce the variation of elevator hinge moment with elevator deflection by 50 percent at a Mach number of 0.21 would cause only a 12-percent reduction for elevator deflections greater than 4° at a Mach number of 0.93.

UNCLASSIFIED

INTRODUCTION

A systematic investigation of control-surface characteristics has been undertaken at the Ames Aeronautical Laboratory to determine experimentally the control-effectiveness and hinge-moment parameters for comparison with those predicted by lifting-surface theory. References 1 through 4 present results of low-speed wind-tunnel tests of both swept and unswept horizontal tails of several aspect ratios, all having the same taper ratio and airfoil section.

The tests reported herein were conducted to evaluate the effects of compressibility and dynamic scale on the control-surface characteristics of a horizontal tail with 35° of sweepback. The low-speed aerodynamic characteristics of a geometrically similar horizontal tail have been reported in reference 2. Since this model also represents a wing with a full-span flap or elevon, drag and pitching-moment data are included in addition to lift and hinge-moment data.

NOTATION

C_D drag coefficient $\left(\frac{\text{drag}}{qS}\right)$

C_{h_e} elevator hinge-moment coefficient $\left(\frac{\text{elevator hinge moment}}{2q\ M_{A_e}}\right)$

C_{h_t} tab hinge-moment coefficient $\left(\frac{\text{tab hinge moment}}{2q\ M_{A_t}}\right)$

C_L lift coefficient $\left(\frac{\text{lift}}{qS}\right)$

C_m pitching-moment coefficient about the quarter point of the mean aerodynamic chord $\left(\frac{\text{pitching moment}}{qS\bar{c}}\right)$

M Mach number $\left(\frac{V}{a}\right)$

P pressure coefficient $\left(\frac{p_l-p}{q}\right)$

$P_{Cr_{\Lambda=35^\circ}}$ critical pressure coefficient, corresponding to a Mach number of 1.0 in a direction perpendicular to the quarter-chord line of the airfoil section

$\frac{\Delta p}{q}$ pressure coefficient across the elevator-nose seal (pressure below the seal minus pressure above the seal divided by the free-stream dynamic pressure)

R	Reynolds number $\left(\frac{\rho V \bar{c}}{\mu}\right)$
M_{A_e}	first moment of the elevator area behind the hinge line about the hinge line, feet cubed
M_{A_t}	first moment of the tab area behind the tab hinge line about the tab hinge line, feet cubed
S	horizontal-tail area, square feet
V	airspeed, feet per second
a	speed of sound, feet per second
$b/2$	semispan, measured perpendicular to the plane of symmetry, feet
c	chord, measured parallel to the plane of symmetry, feet
$\bar{c}$	mean aerodynamic chord $\left(\frac{\int_0^{b/2} c^2\, dy}{\int_0^{b/2} c\, dy}\right)$, feet
c_e'	chord of the elevator behind the hinge line measured perpendicular to the hinge line, feet
p_l	local static pressure, pounds per square foot
p	free-stream static pressure, pounds per square foot
q	free-stream dynamic pressure, pounds per square foot
y	lateral distance normal to plane of symmetry, feet
α	corrected angle of attack, degrees
α_u	angle of attack, uncorrected for tunnel-wall interference and angle-of-attack counter correction, degrees
δ_e	elevator deflection (positive to increase lift) measured in a plane normal to the elevator hinge line, degrees
δ_t	tab deflection (positive to increase lift) measured in a plane normal to the tab hinge line, degrees
ρ	density of air, slugs per cubic foot
μ	absolute viscosity, slugs per foot second

$C_{L_\alpha} = \left(\frac{\partial C_L}{\partial \alpha}\right)_{\delta_e=\delta_t=0}$ (measured through α=0), per degree

$C_{L_{\delta_e}} = \left(\frac{\partial C_L}{\partial \delta_e}\right)_{\alpha=\delta_t=0}$ (measured through δ_e=0), per degree

$\alpha_{\delta_e} = -\left(\frac{C_{L_{\delta_e}}}{C_{L_\alpha}}\right)_{C_L=0}$

$C_{m_{\delta_e}} = \left(\frac{\partial C_m}{\partial \delta_e}\right)_{\alpha=\delta_t=0}$ (measured through δ_e=0), per degree

$C_{h_{e_\alpha}} = \left(\frac{\partial C_{h_e}}{\partial \alpha}\right)_{\delta_e=\delta_t=0}$ (measured through α=0), per degree

$C_{h_{e_{\delta_e}}} = \left(\frac{\partial C_{h_e}}{\partial \delta_e}\right)_{\alpha=\delta_t=0}$ (measured through δ_e=0), per degree

$C_{h_{e_{\delta_t}}} = \left(\frac{\partial C_{h_e}}{\partial \delta_t}\right)_{\alpha=\delta_e=0}$ (measured through δ_t=0), per degree

The subscripts outside the parentheses represent the factors held constant during the measurement of the parameters.

MODEL

The semispan model tested in this investigation represented a horizontal tail of aspect ratio 4.5 and taper ratio 0.5. The airfoil section was the NACA 64A010 (table I) in planes inclined 35° to the plane of symmetry (fig. 1). The quarter-chord line of the airfoil sections was swept back 35°. This line was at 27.8 percent of the chord measured parallel to the plane of symmetry. The tip shape was formed by rotating the section parallel to the undisturbed stream about a line inboard of the tip a distance equal to the maximum tip ordinate.

The model was equipped with a full-span, radius-nose, sealed elevator, the chord of which was 30 percent of the chord of the airfoil sections. The ratio of elevator area behind the hinge line to the total model area was 0.271. The elevator was attached to the stabilizer by hinges at 34, 80, and 96 percent of the semispan. These hinges and a close-fitting block at the plane of symmetry divided the sealed balance chamber into

three separate sections. The seals were fitted closely to the ends of each section to reduce leakage to a minimum. The elevator was equipped with an unsealed tab, the area of which was 6.5 percent of the elevator area and which extended from 23.7 to 44.8 percent of the semispan. The elevator and the tab gaps are shown in figure 1.

The stabilizer was constructed of solid steel and the elevator of aluminum alloy. The model was mounted vertically with the wind-tunnel floor serving as a reflection plane as shown in figure 2. The rotating turntable upon which the model was mounted is directly connected to the force-measuring apparatus. The elevator and tab hinge moments were measured with resistance-type electric strain gages. The elevator gage was beneath the turntable cover plates, and the tab gage was contained within the elevator. The elevator deflection was remotely controlled and the tab deflection was set by means of an indexing system built into the tab and elevator. The gap between the elevator and the reflection plane was approximately 0.02 inch when the elevator was undeflected.

A streamwise row of orifices was provided at 50 percent of the semispan to measure the chordwise distribution of static pressure. Six orifices were located in the balance chamber, one on either side of the seal at 16, 48, and 90 percent of the semispan, to measure the pressure differences across the elevator-nose seal.

CORRECTIONS TO DATA

The data have been corrected for the effects of tunnel-wall interference, for constriction due to the presence of the tunnel walls, and for model-support tare forces.

Tunnel-Wall Interference

Corrections to the data for the effects of tunnel-wall interference have been evaluated by the methods of reference 5, using the theoretical span loading calculated by the methods of reference 6. The corrections added to the drag and to the angle of attack were:

$$\Delta\alpha = 0.329\ C_L, \text{ degrees}$$

$$\Delta C_D = 0.00502\ C_L^2$$

No attempt was made to separate the tunnel-wall interference effects resulting from lift due to elevator deflection and lift due to angle of attack. No corrections were applied to the pitching-moment or hinge-moment data.

Constriction Effects

The data have been corrected for the constriction effects due to the presence of the tunnel walls. The corrections have not been modified to allow for the effect of sweep. The following table shows the magnitude of the corrections to Mach number and to dynamic pressure:

Corrected Mach number	Uncorrected Mach number	$\frac{q \text{ uncorrected}}{q \text{ corrected}}$
0.210	0.210	1.001
.600	.600	1.001
.800	.798	1.002
.850	.848	1.003
.900	.896	1.005
.930	.923	1.008
.940	.932	1.009

Tares

A correction to the drag data was necessary to allow for forces on the exposed surface of the turntable. This correction was determined from tests with the model removed from the turntable. The correction was found to vary with Reynolds number only and is presented in the following table:

$R \times 10^{-6}$	C_D tare
1.00	0.0071
2.00	.0063
3.00	.0060
7.00	.0058
11.00	.0056

No attempt was made to evaluate tares due to possible interference effects between the model and the turntable.

TESTS

Reynolds Number Effects

To determine the effects of Reynolds number on the aerodynamic characteristics of the horizontal tail, lift, drag, pitching moment, and elevator hinge moment were measured for a Mach number of 0.21 at Reynolds numbers of 2,000,000, 3,000,000, 7,000,000, and 11,000,000. For these tests, the angle-of-attack range was from -10° to 24°, the elevator deflections were 0°, -10°, and -20°, and the tab was undeflected. For Mach numbers of 0.60, 0.80, and 0.90, similar data were obtained at Reynolds numbers of 1,000,000 and 2,000,000 with the elevator and the tab undeflected.

Mach Number Effects

To determine the effects of compressibility on the aerodynamic characteristics of the horizontal tail, lift, drag, pitching moment, elevator hinge moment, tab hinge moment, pressure difference across the elevator-nose seal, and streamwise distribution of static pressure were measured at a Reynolds number of 2,000,000 at Mach numbers of 0.21, 0.60, 0.80, 0.85, 0.90, 0.93, and 0.94. At Mach numbers less than 0.80, the angle-of-attack range was from -10° to 24°, and the elevator-deflection range was from -25° to 6°. At Mach numbers above 0.80, the angular ranges were limited by wind-tunnel power. Lift and hinge-moment measurements were made with tab deflections of 0°, 5°, 10°, and 15° throughout the complete range of Mach numbers and elevator deflections at uncorrected angles of attack of 0°, 4°, and 8°.

Effects of Standard Roughness and of Removal of the Elevator-Nose Seal

Tests were also made to evaluate the separate effects of standard leading-edge roughness (reference 7), and of removing the elevator-nose seal on the lift, drag, pitching-moment, and elevator hinge-moment characteristics. Data were obtained at a Reynolds number of 2,000,000 over the angle-of-attack range for elevator deflections of 4°, 0°, and -15° with the tab undeflected at all test Mach numbers up to 0.93.

RESULTS AND DISCUSSION

The results of tests conducted to evaluate the effects of Reynolds number on the aerodynamic characteristics of the horizontal tail are presented in figures 3 and 4, and results of tests conducted to evaluate the effects of Mach number are presented in figures 5 through 12. The data from tests conducted to evaluate the separate effects of leading-edge roughness and of removal of the elevator-nose seal are compared with those obtained with the model in the normal condition in figures 13 through 16. An index of the figures presenting the results is given in the appendix.

Certain data are presented for values of uncorrected angle of attack α_u where:

$$\alpha = 0.99\ \alpha_u + \Delta\alpha$$

The constant 0.99 is the ratio between the geometric angle of attack and the uncorrected angle of attack indicated by the angle-of-attack counter. The uncorrected angle of attack does not differ from the corrected value by more than 0.26° for any of the test points presented.

Effect of Reynolds Number

Low speed.- The effects of increasing the Reynolds number from 2,000,000 to 11,000,000 at a Mach number of 0.21 on the lift, drag, pitching-moment, and elevator hinge-moment characteristics are presented in figure 3. The angle of attack at which the lift curves became nonlinear was increased by approximately 3° when the Reynolds number was increased from 2,000,000 to 11,000,000. This effect may be correlated with that shown in the pitching-moment data of figure 3(c) where the abrupt forward movement of the aerodynamic center, which is associated with a loss of lift over the outer sections of a swept-back lifting surface (reference 8), occurred at higher lift coefficients as the Reynolds number was increased. This delay in the loss of lift over the outer section was accompanied by more positive elevator hinge moments (fig. 3(b)), and by reductions in the drag (fig. 3(d)) at the higher Reynolds numbers.

Increasing the Reynolds number caused very little change in the location of the aerodynamic center (at $C_L=0$) for elevator deflections of 0° and -10°. However, a forward movement of the aerodynamic center of 7 percent of the mean aerodynamic chord accompanied an increase in Reynolds number from 2,000,000 to 7,000,000 with the elevator deflected -20°.

The close agreement of the lift and elevator hinge-moment coefficients obtained at the various Reynolds numbers over the linear range of the data of figures 3(a) and 3(b) indicates that C_{L_α}, $C_{L_{\delta_e}}$, $C_{h_{e_\alpha}}$, and $C_{h_{e_{\delta_e}}}$ were not sensitive to changes in Reynolds numbers between 2,000,000 and 11,000,000.

The slope parameters measured from the results of tests of a geometrically similar model conducted in the Ames 7- by 10-foot wind tunnel (reference 2) are presented for comparison with those evaluated from results of the present tests in the following table:

Slope parameter	Ames 7- by 10-foot wind tunnel (reference 2)	Ames 12-foot pressure wind tunnel
C_{L_α}	0.061	0.059
$C_{L_{\delta_e}}$	.032	.032
$C_{h_{e_\alpha}}$	-.0024	-.0025
$C_{h_{e_{\delta_e}}}$	-.0078	-.0080
Aerodynamic center, percent $\bar{c}$ ($C_L=0$, $\delta_e=0$)	25.0	27.6

All measurements of slope parameters were made from data obtained at a Reynolds number of 3,000,000 with the exception of the values of

$C_{L_{\delta_e}}$ and $C_{h_{e_{\delta_e}}}$ from the Ames 12-foot pressure wind tunnel. These values were measured from data obtained at a Reynolds number of 2,000,000.

The agreement between the lift and hinge-moment parameters from the two investigations can be considered excellent. The reason for the difference of 2.6 percent of the mean aerodynamic chord in the location of the aerodynamic center is not known.

High subsonic speeds.- Figure 4 presents data obtained at Reynolds numbers of 2,000,000 and 1,000,000 at Mach numbers of 0.60, 0.80, and 0.90. These data show that the reduction of Reynolds number resulted in a reduction of lift-curve slope and a forward movement of the aerodynamic center. The greatest effect occurred at a Mach number of 0.90 where the lift-curve slope was reduced by 0.003 per degree and the aerodynamic center at zero lift was moved forward 2 percent of the mean aerodynamic chord. The change in Reynolds number from 2,000,000 to 1,000,000 resulted in no important change in the drag for lift coefficients less than 0.4 or in the elevator hinge moment.

Effect of Mach Number

The aerodynamic characteristics of the horizontal tail at a Reynolds number of 2,000,000 for a range of Mach numbers from 0.21 to 0.94 are presented in figures 5 through 12.

Lift.- The variation of lift coefficient with angle of attack is presented in figure 5. At a Mach number of 0.21, the elevator was effective in producing changes in lift throughout the elevator-deflection and angle-of-attack range. As the Mach number was increased, the range of elevator deflections for which the elevator was effective at angles of attack greater than 12° was progressively reduced. It is not known if this effect exists at Mach numbers greater than 0.85, as insufficient wind-tunnel power was available to test at angles of attack greater than 12° at these speeds. The variation of lift coefficient with elevator deflection at an angle of attack of 0° is presented in figure 17. These data show that the elevator effectiveness was approximately constant over a range of elevator deflections between $\pm 6^{\circ}$ at all Mach numbers.

The effects of Mach number on the values of $C_{L_{\delta_e}}$, $C_{L_{\alpha}}$, and α_{δ_e} are shown in figure 18. The elevator-effectiveness parameter $C_{L_{\delta_e}}$ increased gradually from 0.032 at a Mach number of 0.21 to 0.038 at a Mach number of 0.87, and decreased abruptly with further increase in Mach number. The stabilizer effectiveness parameter $C_{L_{\alpha}}$ increased from 0.059 per degree at a Mach number of 0.21 to 0.082 per degree at a Mach number of 0.93 in close agreement with the variation predicted from reference 6. Increasing the Mach number from 0.93 to 0.94 resulted in an abrupt decrease of $C_{L_{\alpha}}$. At low speeds, the value of α_{δ_e} was -0.54

and was little affected by compressibility at Mach numbers up to 0.70. At higher Mach numbers, the absolute value of α_{δ_e} decreased, the decrease becoming very rapid at Mach numbers above 0.85. At a Mach number of 0.94, the magnitude of α_{δ_e} had decreased to 65 percent of its low-speed value.

Hinge moment.- The elevator hinge-moment coefficients for various Mach numbers up to 0.94 are presented in figure 6 as a function of angle of attack and in figure 7 as a function of elevator deflection. At the higher Mach numbers the slopes of the curves vary considerably with angle of attack and with elevator deflection; therefore, the hinge-moment parameters $C_{h_{e_{\delta_e}}}$ and $C_{h_{e_\alpha}}$ are not indicative of the hinge-moment characteristics of the horizontal tail and any discussion in terms of these parameters would be misleading. At Mach numbers less than about 0.85, increasing the Mach number caused gradual changes in the elevator hinge-moment coefficients for elevator deflections and angles of attack between $\pm 6^\circ$. The Mach numbers at which rapid changes in the elevator hinge-moment coefficients occurred were dependent upon the elevator deflection and the angle of attack. This is illustrated in figure 19(a) which presents the variation of elevator hinge-moment coefficient with Mach number for several angles of attack at 0° elevator deflection and in figure 19(b) which presents the variation of elevator hinge-moment coefficient with Mach number for several elevator deflections at an uncorrected angle of attack of 0°.

Tab effectiveness.- The variation of elevator hinge-moment coefficient with elevator deflection for several tab deflections is presented in figure 7. The tab-effectiveness parameter $C_{h_{e_{\delta_t}}}$, measured at 0° elevator deflection, had a value of -0.0035 and was little affected by compressibility. This is evident from the data of figure 20 which presents the elevator hinge-moment coefficient produced by tab deflection ΔC_{h_e} as a function of Mach number. For negative elevator deflections the tab effectiveness decreased with increasing Mach number, especially at the larger tab deflections. With an elevator deflection of -10° the tab was ineffective when deflected more than 10° at Mach numbers above 0.90. The change in lift coefficient due to deflection of the tab is shown in figure 17.

The tab hinge-moment coefficients are presented in figure 8 to permit application of the tab-effectiveness data to the design of a simple or spring-tab installation.

Pressure difference across the elevator-nose seal.- The variation with elevator deflection of the pressure coefficient across the elevator-nose seal is presented in figure 9. The low-speed data are not in close accord with those of reference 2. The comparatively greater spanwise variation of pressure coefficient across the elevator-nose seal than is shown in reference 2 may be attributed to the division of the balance chamber into three sections between which air could not flow. The hinge

line of the model tested in this investigation was slightly offset, which required a distortion of the curtains to prevent a discontinuity at the hinge line. Evidence of this offset of the elevator hinge line is given by the pressure-distribution data shown in figure 12. Leakage around the ends of the seal in each section of the balance chamber may have had an effect on the balancing pressures, particularly in the tip section of the balance chamber where the ratio of leakage area to vent area between the curtains and the elevator was the greatest.

Inspection of the data presented in figure 9 reveals that, in general, the rate of change of the pressure coefficient across the elevator-nose seal with elevator deflection, measured at 0° elevator deflection, became more positive as the Mach number was increased to 0.93. At a Mach number of 0.21, the rate of rise of balancing pressure with elevator deflection decreased abruptly at large negative elevator deflections. At 0° angle of attack, for example, the balancing pressure in the middle section of the chamber did not increase when the elevator was deflected more than -20°. As the Mach number was increased, a decrease of balancing effectiveness occurred at progressively smaller elevator deflections. At a Mach number of 0.93 and at an angle of attack of 0°, the balancing pressure in the middle chamber increased little as the elevator was deflected beyond -4°.

In order to evaluate the reduction of elevator hinge moment obtainable through the use of a sealed internal aerodynamic balance, the hinge-moment coefficients for an elevator with a balance plate extending from 0 to 96 percent of the span with a chord of $0.35c_e'$ have been computed. The total elevator-deflection range would be limited to approximately 36° if this amount of balance were employed. In computing the hinge-moment characteristics of the balanced elevator, it was assumed that the pressure difference indicated by each pair of orifices existed uniformly over the balance plate between the center lines of the hinges which limited that section of the balance chamber wherein the orifices were located. The computed hinge moments of the balanced elevator are compared with the measured hinge moments of the radius-nose sealed elevator in figure 21. These computations show that, at a Mach number of 0.21, use of the sealed internal balance would result in a 50-percent reduction in $\frac{\partial C_{h_e}}{\partial \delta_e}$ for elevator deflections less than -14°. As the Mach number was increased, the range of elevator deflection for which $\frac{\partial C_{h_e}}{\partial \delta_e}$ was substantially reduced by the internal balance was progressively decreased. At a Mach number of 0.93, for example, the value of $\frac{\partial C_{h_e}}{\partial \delta_e}$ was reduced by only about 12 percent at elevator deflections greater than 4°. At this Mach number the value of $\frac{\partial C_{h_e}}{\partial \delta_e}$ was approximately zero for elevator deflections between $\pm 1^{\circ}$. Any greater

amount of internal balance would result in overbalance for small elevator deflections. The range of angle of attack for which $\frac{\partial C_{h_e}}{\partial \alpha}$ was reduced by the incorporation of the internal balance became progressively smaller as the Mach number was increased.

Pitching moment.- The pitching-moment coefficients about the quarter point of the mean aerodynamic chord are presented as a function of lift coefficient in figure 10. At low speed, loss of lift over the outer sections, which caused static longitudinal instability as indicated by the break in the pitching-moment curves, occurred at a lift coefficient of about 0.6 with the elevator undeflected and at lower lift coefficients as the elevator was deflected negatively. An increase in Mach number to 0.90 caused little change in the lift coefficient at which static longitudinal instability occurred. This instability did not occur at Mach numbers of 0.93 and 0.94 within the angle-of-attack range for which data were obtained.

The rate of change of pitching-moment coefficient with lift coefficient shows that the static longitudinal stability of the horizontal tail increased as the Mach number was increased. This effect is summarized in figure 22 where the location of the aerodynamic center (for $\delta_e=0^\circ$ at $C_L=0$) is presented as a function of Mach number. At low speeds, the aerodynamic center was at 27.6 percent of the mean aerodynamic chord and its location varied only slightly with Mach number up to 0.85. A rapid rearward movement of the aerodynamic center occurred as the Mach number was increased from 0.85 to 0.94.

The pitching moment due to deflection of the elevator increased with Mach number as illustrated in figure 22, where the negative value of the parameter $C_{m_{\delta_e}}$ is shown to increase from -0.0098 per degree at a Mach number of 0.21 to -0.0165 at a Mach number of 0.94.

Drag.- The drag data of figure 11 are summarized in figure 23 where the minimum drag coefficient, maximum lift-drag ratio, and the lift coefficient at which the maximum lift-drag ratio occurred are presented as a function of Mach number. The Mach number for drag divergence, defined as the Mach number at which $\frac{\partial C_D}{\partial M} = 0.10$, was approximately 0.91 when the elevator was undeflected. The maximum lift-drag ratio was 20.5 at a Mach number of 0.21. The effects of compressibility on the maximum lift-drag ratio were small up to a Mach number of about 0.80, but marked decreases occurred with further increases in Mach number. At a Mach number of 0.94 the maximum lift-drag ratio was about one-third of that at low speed. The lift coefficient for maximum lift-drag ratio increased with Mach number at Mach numbers greater than about 0.60.

Pressure distribution.– The streamwise distribution of static pressure at the midsemispan was measured to correlate the effects of Mach number, as evaluated from force measurements, with changes in the surface pressures and to provide data for structural design. These pressure-distribution data are presented in figure 12 for various elevator deflections and angles of attack for the same Mach numbers for which force data are presented.

The magnitude of the pressure coefficient which corresponds to sonic velocity normal to the quarter-chord line was calculated from the following equation based on simple sweep theory:

$$P_{Cr_{\Lambda=35^\circ}} = \frac{2}{\gamma M^2}\left[\left(\frac{2}{\gamma+1} + \frac{\gamma-1}{\gamma+1} M^2 \cos^2 35^\circ\right)^{\frac{\gamma}{\gamma-1}} - 1\right] \qquad (1)$$

where γ is the ratio of specific heats and is equal to 1.4. The values of $P_{Cr_{\Lambda=35^\circ}}$ calculated from the above equation are shown in figure 12 in order to indicate the conditions for which there was supersonic flow in a direction normal to the quarter-chord line at the midsemispan.

The reason for the reduction of elevator effectiveness at the higher Mach numbers is evident from the data of figure 12. At low speeds, the decrement in lift due to negative elevator deflection was distributed over the airfoil chord. However, at the higher Mach numbers, deflection of the elevator produced very little change in the surface pressures forward of points on the stabilizer where the flow was indicated to be supersonic normal to the quarter-chord line. At small elevator deflections, increasing the Mach number beyond 0.90 caused supersonic flow over the elevator. The resultant change in the load distribution over the elevator can be correlated with the large increase in elevator hinge-moment coefficient shown in figure 19(b) for an elevator deflection of -4° between the Mach numbers of 0.90 and 0.94.

Effects of Leading-Edge Roughness

Results of tests conducted with standard roughness, applied to the leading edge as described in reference 7, are presented in figures 13 through 16. Results of tests without leading-edge roughness are also presented in these figures for purposes of comparison.

Loss of lift over the outer sections of the tail occurred at slightly lower angles of attack at Mach numbers greater than 0.60 when leading-edge roughness was applied. (See figs. 13 and 15.) The stabilizer effectiveness and elevator effectiveness were reduced when

roughness was applied to the leading edge. These effects are summarized in figure 24 where the values of C_{L_α} and $C_{L_{\delta_e}}$, which were measured from the data of figure 13, are presented as a function of Mach number. It was assumed in measuring $C_{L_{\delta_e}}$ that the elevator effectiveness was constant between deflections of 0° and 4°. The greatest reduction in effectiveness occurred at a Mach number of 0.93 where C_{L_α} and $C_{L_{\delta_e}}$ were each reduced by 0.012 per degree.

Inspection of the data of figure 14 shows that leading-edge roughness caused sizable reductions in elevator hinge moments when the elevator was deflected.

Leading-edge roughness caused a large forward shift of the aerodynamic center at Mach numbers greater than 0.70. Figure 25 shows this effect to be greatest at a Mach number of 0.93 where the aerodynamic center (measured for $\delta_e=0$ at $C_L=0$) was shifted from 36.7 to 28.8 percent of the mean aerodynamic chord.

As would be expected, application of leading-edge roughness resulted in increased drag. (See fig. 16.) Figure 25 shows that the increment of minimum drag coefficient due to leading-edge roughness was about 0.0060 at low speed and about 0.0040 at a Mach number of 0.93.

Effect of Removal of Elevator-Nose Seal

The effect of removal of the elevator-nose seal is shown in figures 13 through 15 where comparison is made between data obtained with the elevator nose sealed and with the elevator nose unsealed.

The data of figure 13 show that unsealing the elevator nose had no important effect on the variation of lift with angle of attack. The elevator effectiveness, however, was reduced. This effect is summarized in figure 24 where $C_{L_{\delta_e}}$ is presented as a function of Mach number. The maximum reduction in $C_{L_{\delta_e}}$ was 0.004 per degree, which occurred at a Mach number of 0.60.

In general, unsealing the elevator-nose gap caused slight increases in the elevator hinge moment when the elevator was deflected.

CONCLUDING REMARKS

The results of wind-tunnel tests conducted to evaluate the independent effects of Reynolds number and of Mach number on the aerodynamic characteristics of a horizontal tail of aspect ratio 4.5 with the quarter-chord line swept back 35° have been presented.

Results of tests at a Mach number of 0.21 over a range of Reynolds numbers from 2,000,000 to 11,000,000 indicated that:

1. An increase of Reynolds number increased the angle-of-attack range over which the variation of lift with angle of attack was linear.

2. The aerodynamic characteristics of the horizontal tail were not sensitive to scale between Reynolds numbers of 2,000,000 and 11,000,000 within the angle-of-attack range for which the variation of lift with angle of attack was linear.

Results of tests at a Reynolds number of 2,000,000 over a range of Mach numbers from 0.21 to 0.94 indicated that:

1. An increase in Mach number from 0.21 to 0.93 resulted in an increase in lift-curve slope from 0.059 to 0.082 per degree; further increase in Mach number to 0.94 caused an abrupt decrease in lift-curve slope.

2. The elevator-effectiveness parameter $C_{L_{\delta_e}}$ increased from 0.032 to 0.038 per degree between Mach numbers of 0.21 and 0.87, and decreased rapidly as the Mach number was increased to 0.94.

3. The Mach number at which marked changes in the elevator hinge-moment coefficients occurred was dependent upon the angle of attack and elevator deflection; however, the changes in the elevator hinge-moment coefficients at angles of attack and elevator deflections between $\pm 6^{\circ}$ were gradual as the Mach number was increased to 0.85.

4. The tab was effective in producing a balancing increment in elevator hinge moment throughout the Mach number range.

5. Incorporation of sealed internal balance sufficient to cause a 50-percent reduction in the variation of elevator hinge moment with elevator deflection at a Mach number of 0.21 caused only a 12-percent reduction at a Mach number of 0.93 for elevator deflections greater than 4°.

Results of tests made to evaluate the effect of leading-edge roughness indicated that:

1. Leading-edge roughness caused reductions in the lift-curve slope and in the elevator effectiveness.

2. Leading-edge roughness caused a sizable reduction in the elevator hinge moment when the elevator was deflected.

Results of tests made to evaluate the effect of unsealing the elevator-nose gap indicated that:

1. Unsealing the elevator-nose gap had no important effect on the lift-curve slope, but reduced the elevator effectiveness.

2. In general, unsealing the elevator-nose gap caused slight increases in the elevator hinge moment when the elevator was deflected.

Ames Aeronautical Laboratory,
National Advisory Committee for Aeronautics,
Moffett Field, Calif.

APPENDIX

The following tables have been included to provide a convenient index to the data of this report:

FORCE AND MOMENT CHARACTERISTICS

Reynolds Number Variable

Results presented	R	M	α, deg	δ_e, deg	δ_t, deg	Figure number
C_L vs α	2,000,000 to 11,000,000	0.21	-10 to 24	0,-10,-20	0	3(a)
C_{h_e} vs α	↓	↓	↓	↓	↓	3(b)
C_L vs C_m	↓	↓	↓	↓	↓	3(c)
C_L vs C_D	↓	↓	↓	↓	↓	3(d)
C_L vs α	1,000,000 and 2,000,000	0.60,0.80, 0.90	↓	0	↓	4(a)
C_{h_e} vs α	↓	↓	↓	↓	↓	4(b)
C_L vs C_m	↓	↓	↓	↓	↓	4(c)
C_L vs C_D	↓	↓	↓	↓	↓	4(d)

Mach Number Variable
[R=2,000,000]

Results presented	M	α, deg	δ_e, deg	δ_t, deg	Figure number
C_L vs α	0.21	−10 to 24	6 to −25	0	5(a)
	.60				5(b)
	.80				5(c)
	.85	−10 to 20			5(d)
	.90	−10 to 12	6 to −20		5(e)
	.93	−10 to 10	6 to −20		5(f)
	.94	−8 to 8	4 to −10		5(g)
C_{h_e} vs α	.21	−10 to 24	6 to −25		6(a)
	.60				6(b)
	.80				6(c)
	.85	−10 to 20			6(d)
	.90	−10 to 12	6 to −20		6(e)
	.93	−10 to 10	6 to −20		6(f)
	.94	−8 to 8	4 to −10		6(g)
C_{h_e} vs δ_e	.21	0,4,8	6 to −25	0 to 15	7(a)
	.60				7(b)
	.80				7(c)
	.85				7(d)
	.90		6 to −20		7(e)
	.93		6 to −20		7(f)
	.94	0,4	4 to −10		7(g)
C_{h_t} vs δ_e	.21	0,4,8	6 to −25		8(a)
	.60				8(a)
	.80				8(a)
	.85	0,4,8	6 to −25		8(b)
	.90				8(b)
	.93				8(b)
	.94				8(b)
$\Delta p/q$ vs δ_e	.21	−8 to 24	6 to −25	0	9(a)
	.60				9(b)
	.80				9(c)
	.85	−8 to 20			9(d)
	.90	−8 to 8	6 to −20		9(e)
	.93	−8 to 8	6 to −20		9(f)
	.94	−4 to 8	4 to −10		9(g)
C_L vs C_m	.21	−10 to 24	6 to −25		10(a)
	.60				10(b)
	.80				10(c)
	.85	−10 to 20			10(d)
	.90	−10 to 12	6 to −20		10(e)
	.93	−10 to 10	6 to −20		10(f)
	.94	−8 to 8	4 to −10		10(g)
C_L vs C_D	.21	−10 to 24	6 to −25		11(a)
	.60				11(b)
	.80				11(c)
	.85	−10 to 20			11(d)
	.90	−10 to 12	6 to −20		11(e)
	.93	−10 to 10	6 to −20		11(f)
	.94	−8 to 8	4 to −10		11(g)

STREAMWISE DISTRIBUTION OF STATIC PRESSURE AT THE MIDSEMISPAN

[R=2,000,000; $\delta_t=0^\circ$]

Results presented	M	α, deg	δ_e, deg	Figure number
P vs percent chord	0.21	0,4,8	0,-4,-10 -15,-20	12(a)
↓	.21	12,16,20	↓	12(b)
	.60	0,4,8		12(c)
	.60	12,16,20		12(d)
	.80	0,4,8		12(e)
	.80	12,16,20		12(f)
	.85	0,4,8		12(g)
	.85	12,16,20		12(h)
	.90	0,4,8		12(i)
	.93	↓	↓	12(j)
	.94		0,-4,-10	12(k)

SEPARATE EFFECTS OF LEADING-EDGE ROUGHNESS
AND REMOVAL OF ELEVATOR-NOSE SEAL

[R=2,000,000; $\delta_e=4^\circ$, 0°, -15°; $\delta_t=0^\circ$]

Results presented	M	α, deg	Figure number
C_L vs α	0.21	−10 to 24	13(a)
	.60		13(b)
	.80		13(c)
	.85	−10 to 20	13(d)
	.90	−10 to 12	13(e)
	.93	−10 to 10	13(f)
C_{h_e} vs α	.21	−10 to 24	14(a)
	.60		14(b)
	.80		14(c)
	.85	−10 to 20	14(d)
	.90	−10 to 12	14(e)
	.93	−10 to 10	14(f)
C_L vs C_m	.21	−10 to 24	15(a)
	.60		15(b)
	.80		15(c)
	.85	−10 to 20	15(d)
	.90	−10 to 12	15(e)
	.93	−10 to 10	15(f)
C_L vs C_D	.21	−10 to 24	16(a)
	.60		16(b)
	.80		16(c)
	.85	−10 to 20	16(d)
	.90	−10 to 12	16(e)
	.93	−10 to 10	16(f)

SUMMARY FIGURES

[R=2,000,000; M=0.21 to 0.94]

Results presented	α, deg	δ_e, deg	δ_t, deg	Figure number
C_L vs δ_e	0	6 to −25	0 to 15	17
C_{L_α}, $C_{L_{\delta_e}}$ and α_{δ_e} vs M	- - - - -	- - - -	- - - -	18
C_{h_e} vs M	−8 to 24	0	0	19(a)
C_{h_e} vs M	0	6 to −25	0	19(b)
ΔC_{h_e} vs M	0	0,−6,−10	5,10,15	20
[1]C_{h_e} vs δ_e and C_{h_e} vs α	−10 to 24	6 to −25	0	21
Aerodynamic-center location (for C_L=0 at δ_e=0) and $C_{m_{\delta_e}}$ vs M	- - - - -	- - - -	- - - -	22
Maximum L/D, C_L for maximum L/D and minimum C_D vs M	- - - - -	0 to −15	0	23
[2]C_{L_α}, $C_{L_{\delta_e}}$, and α_{δ_e} vs M	- - - - -	- - - -	- - - -	24
[2]Aerodynamic-center location (for C_L=0 at δ_e=0) and minimum C_D vs M	- - - - -	- - - -	- - - -	25

[1]Shows the computed effect of a sealed internal aerodynamic balance on the elevator hinge-moment coefficients.

[2]Shows separate effects of leading-edge roughness and removal of elevator-nose seal.

REFERENCES

1. Dods, Jules B., Jr.: Wind-Tunnel Investigation of Horizontal Tails. I - Unswept and 35° Swept-Back Plan Forms of Aspect Ratio 3. NACA RM A7K24, 1948.

2. Dods, Jules B., Jr.: Wind-Tunnel Investigation of Horizontal Tails. II - Unswept and 35° Swept-Back Plan Forms of Aspect Ratio 4.5. NACA RM A8B11, 1948.

3. Dods, Jules B., Jr.: Wind-Tunnel Investigation of Horizontal Tails. III - Unswept and 35° Swept-Back Plan Forms of Aspect Ratio 6. NACA RM A8H30, 1948.

4. Dods, Jules B., Jr.: Wind-Tunnel Investigation of Horizontal Tails. IV - Unswept Plan Form of Aspect Ratio 2 and a Two-Dimensional Model. NACA RM A8J21, 1948.

5. Sivells, James C., and Deters, Owen J.: Jet-Boundary and Plan-Form Corrections for Partial-Span Models With Reflection Plane, End Plate, or No End Plate in a Closed Circular Wind Tunnel. NACA Rep. 843, 1946.

6. DeYoung, John: Theoretical Additional Span Loading Characteristics of Wings With Arbitrary Sweep, Aspect Ratio, and Taper Ratio. NACA TN 1491, 1947.

7. Abbott, Ira H., von Doenhoff, Albert E., and Stivers, Louis S., Jr.: Summary of Airfoil Data. NACA Rep. 824, 1945.

8. Shortal, Joseph A., and Maggin, Bernard: Effect of Sweepback and Aspect Ratio on Longitudinal Stability Characteristics of Wings at Low Speeds. NACA TN 1093, 1946.

TABLE I.– COORDINATES FOR THE NACA 64A010 AIRFOIL SECTION

[All dimensions in percent of chord]

Upper and Lower Surfaces

Station	Ordinate
0	0
.50	.804
.75	.969
1.25	1.225
2.50	1.688
5.00	2.327
7.50	2.805
10.00	3.199
15.00	3.813
20.00	4.272
25.00	4.606
30.00	4.837
35.00	4.968
40.00	4.995
45.00	4.894
50.00	4.684
55.00	4.388
60.00	4.021
65.00	3.597
70.00	3.127
75.00	2.623
80.00	2.103
85.00	1.582
90.00	1.062
95.00	.541
100.00	.021
L.E. radius, 0.687; T.E. radius, 0.023	

Dimensions shown in inches unless otherwise noted.

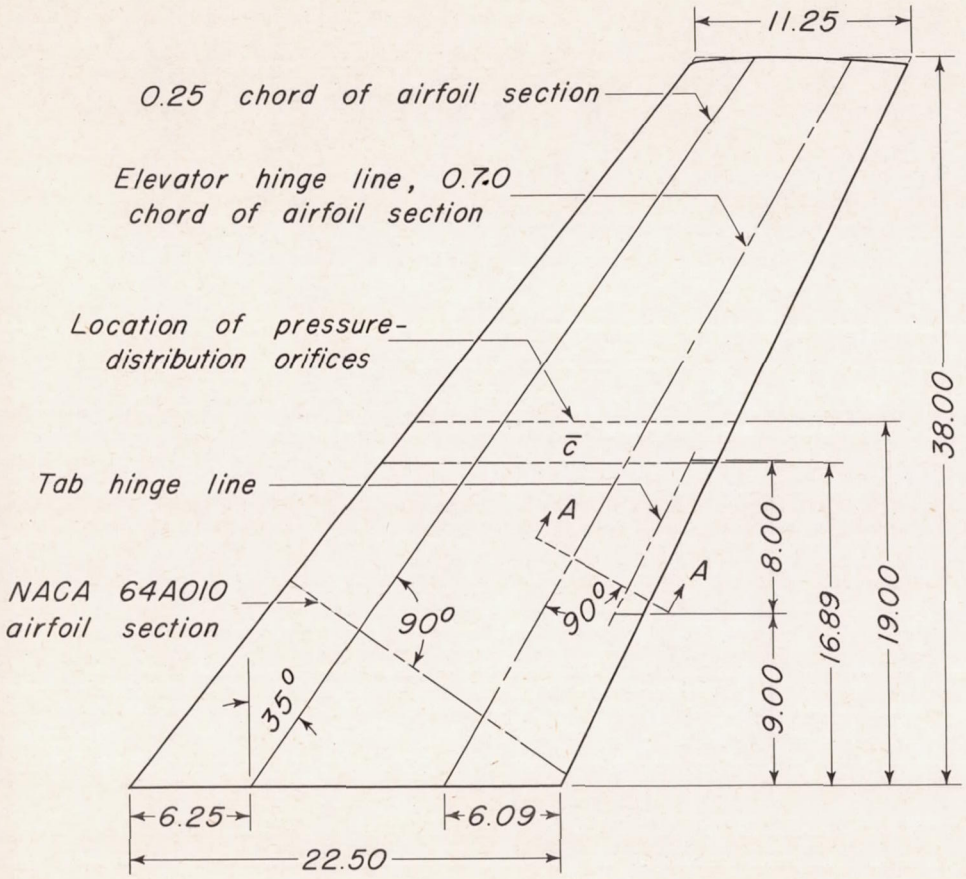

Aspect ratio	4.5
Taper ratio	0.5
Area semispan	4.443 ft²
Elevator area	1.204 ft²
Tab area	0.0777 ft²
$\bar{c}$	1.458 ft

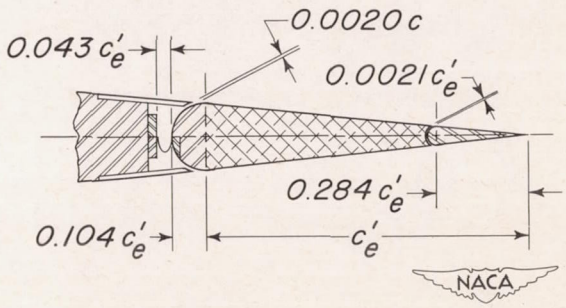

Section A-A

Figure 1.– The horizontal tail model with 35° of sweepback.

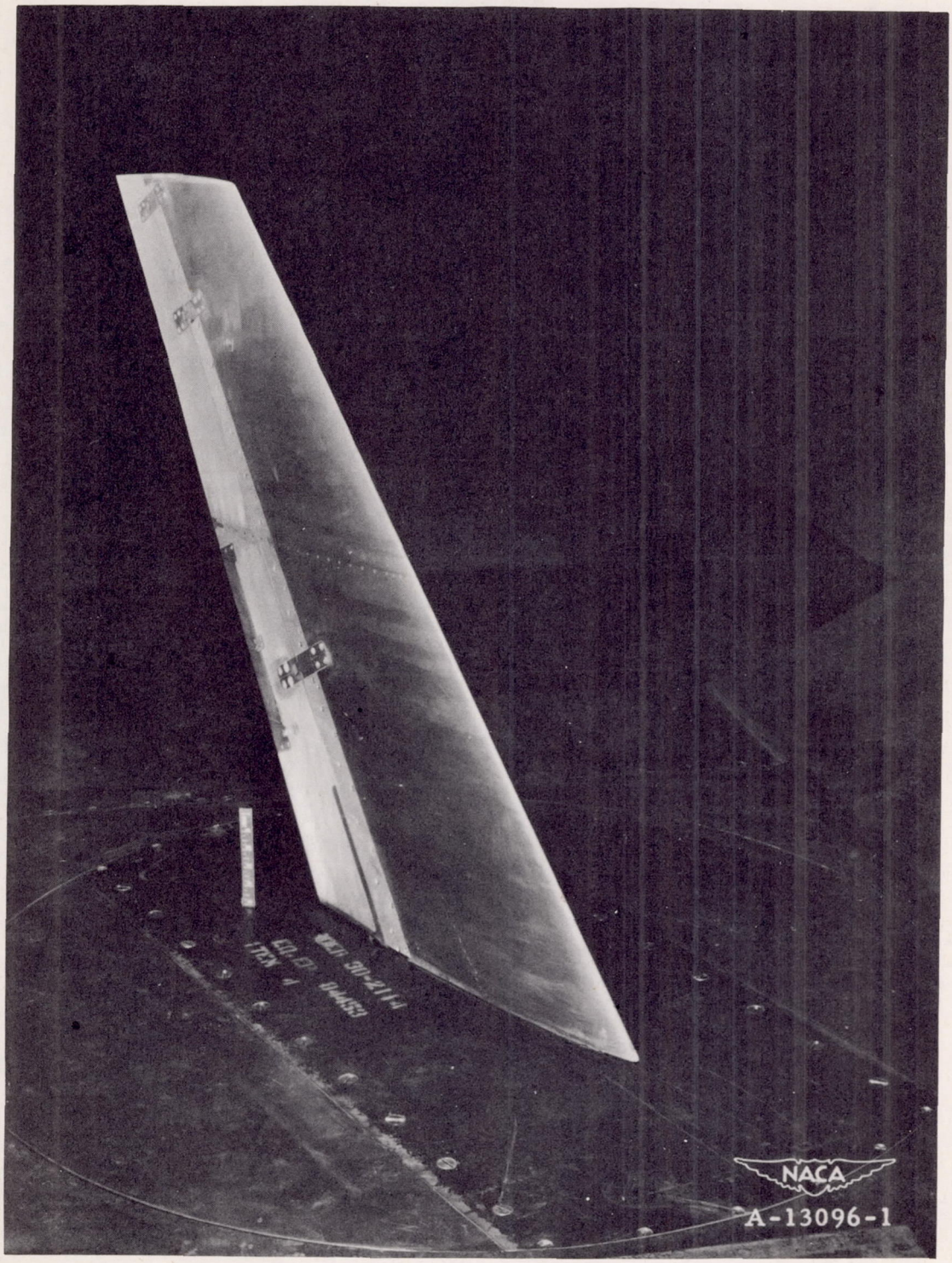

Figure 2.- Semispan horizontal tail model mounted in the 12-foot pressure wind tunnel.

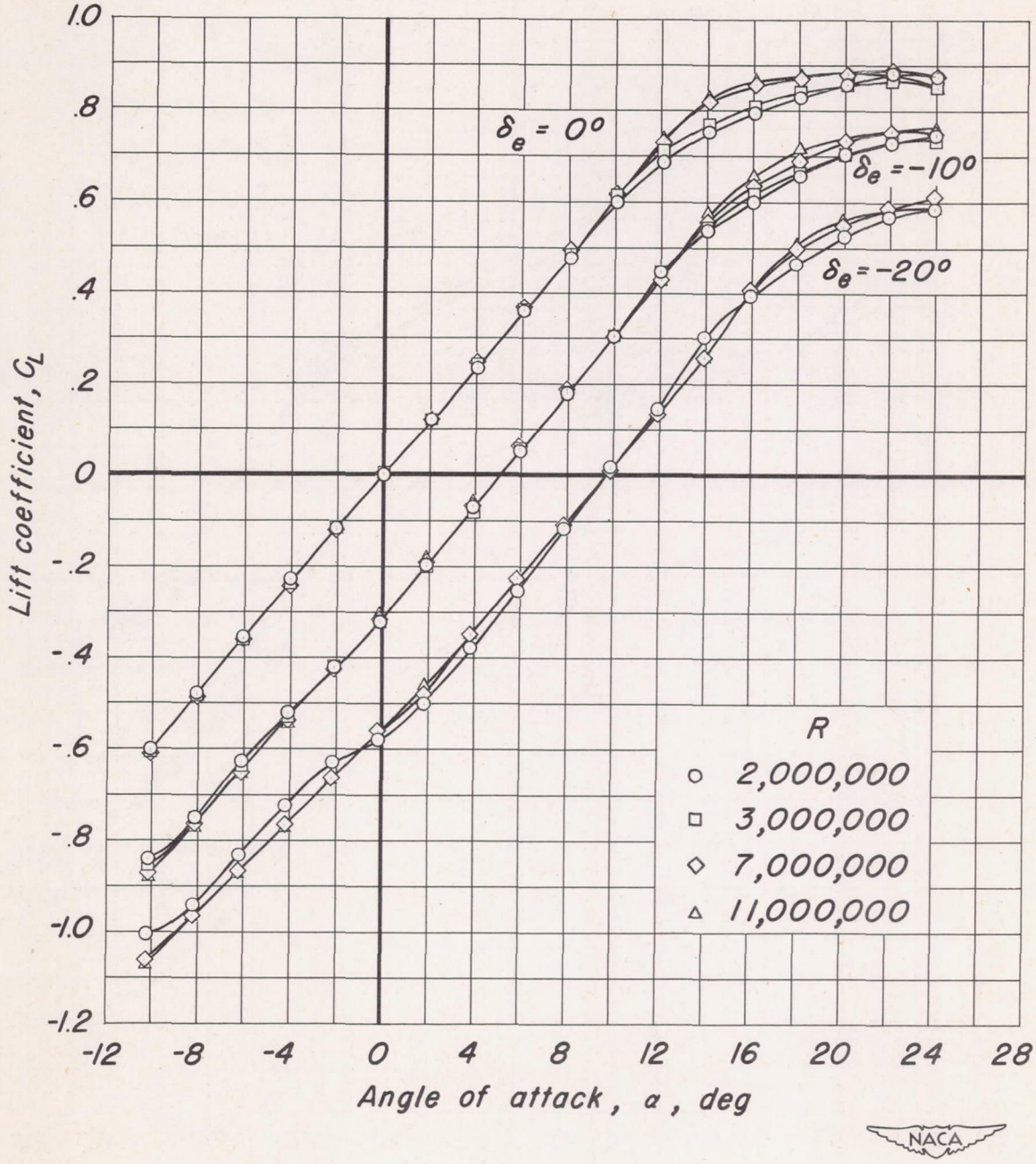

(a) C_L vs α.

Figure 3.– The effect of Reynolds number on the low-speed aerodynamic characteristics. M, 0.21; δ_t, 0°.

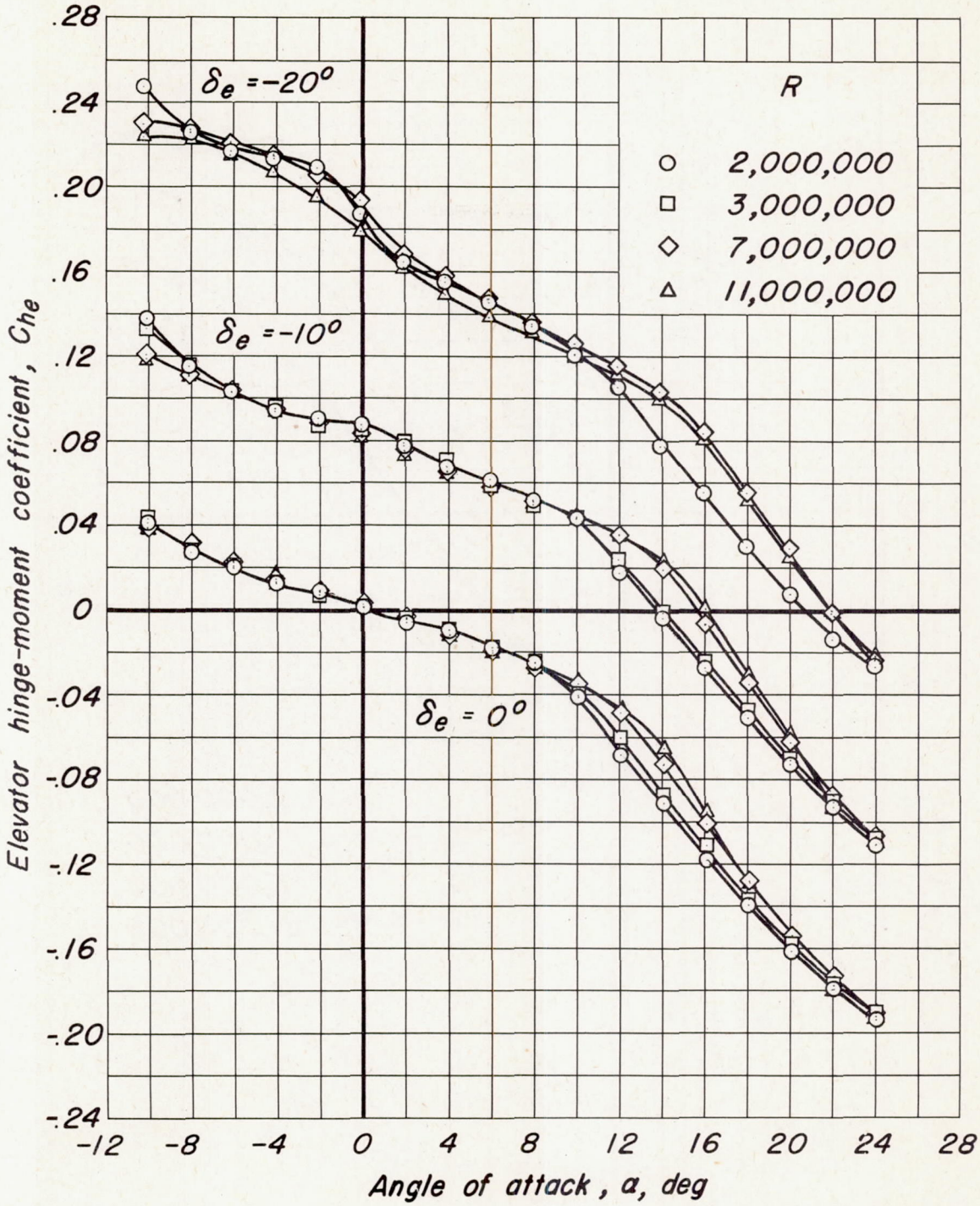

(b) C_{h_e} vs α.

Figure 3.– Continued.

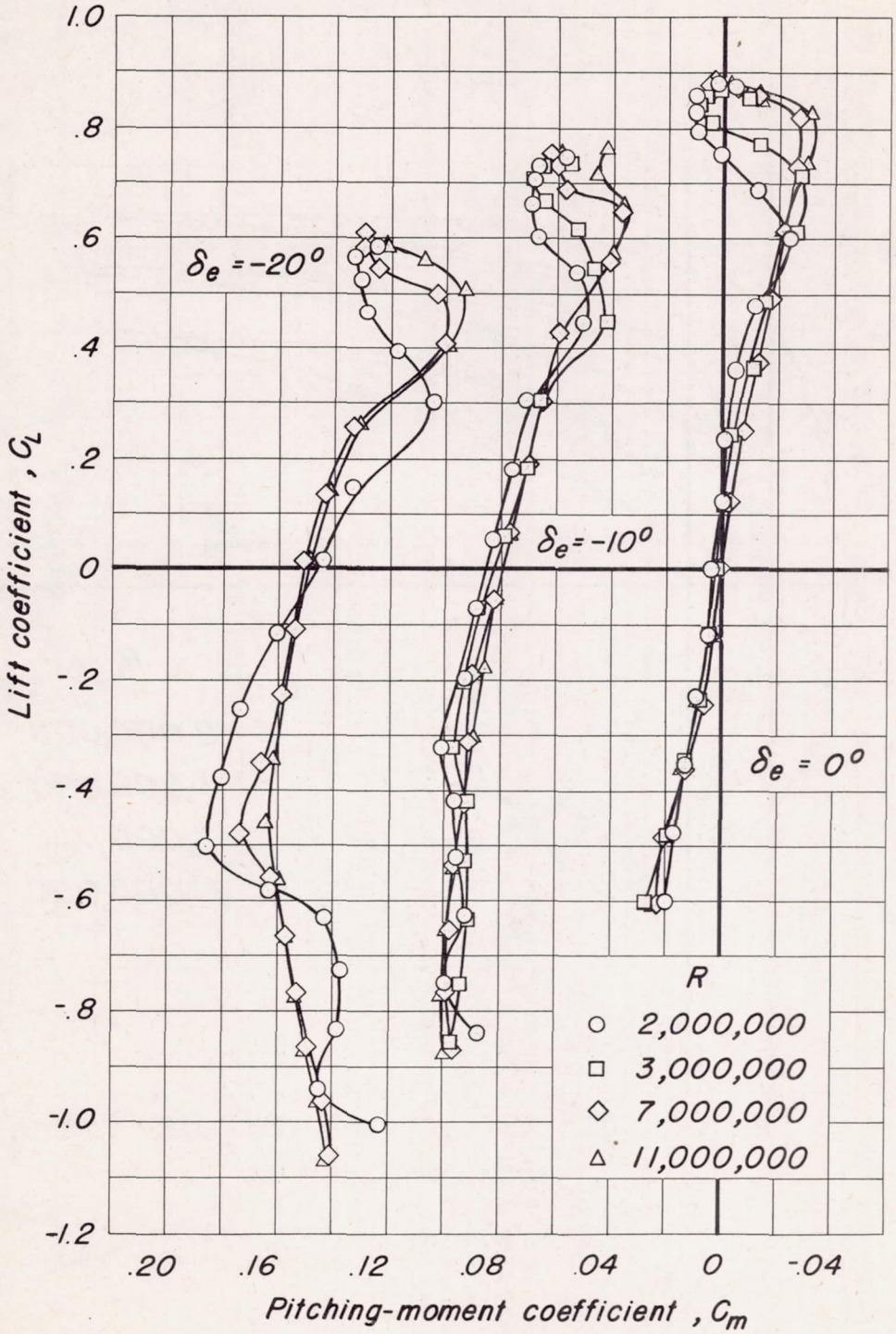

(c) C_L vs C_m.

Figure 3.– Continued.

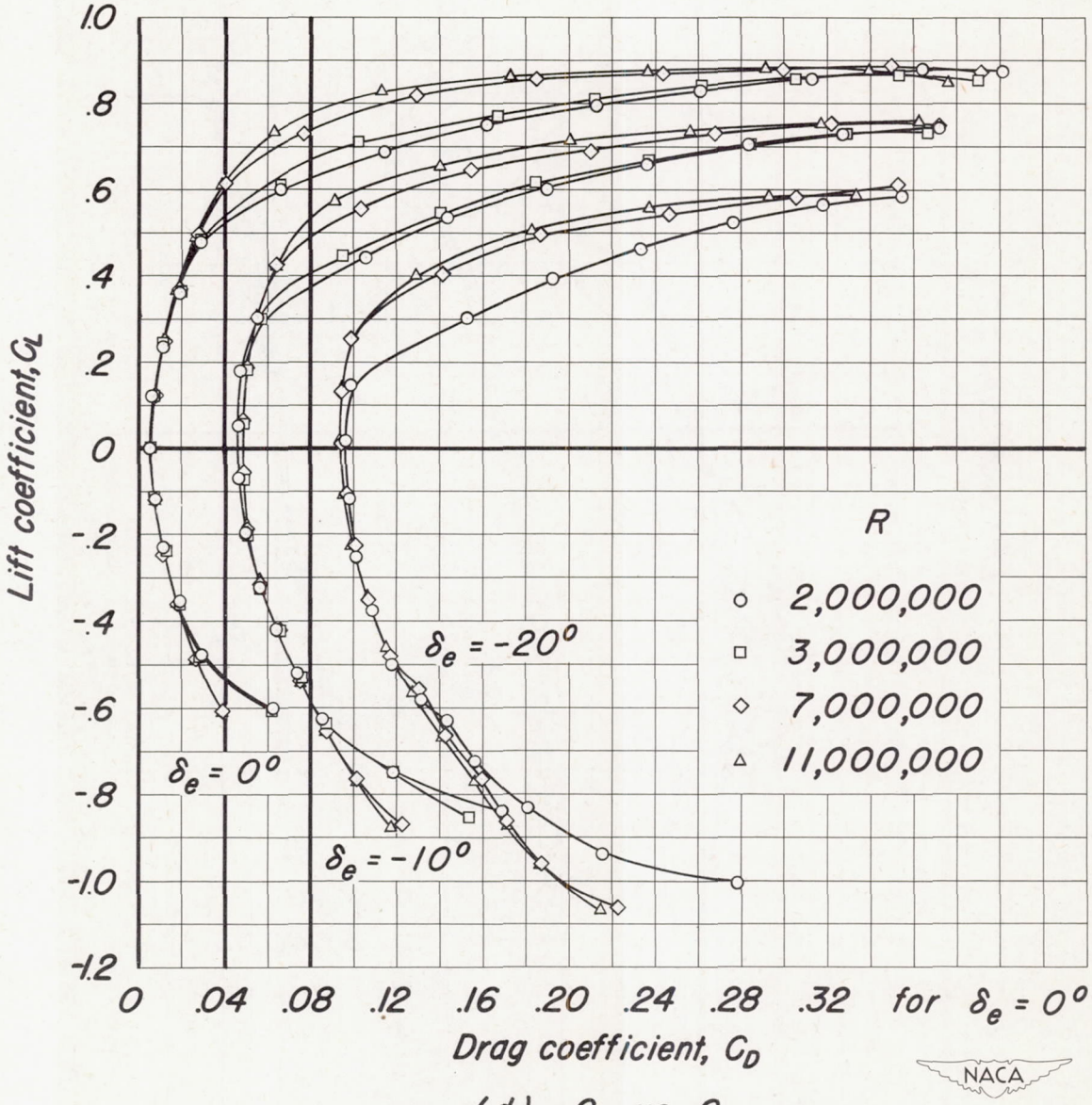

(d) C_L vs C_D.

Figure 3.– Concluded.

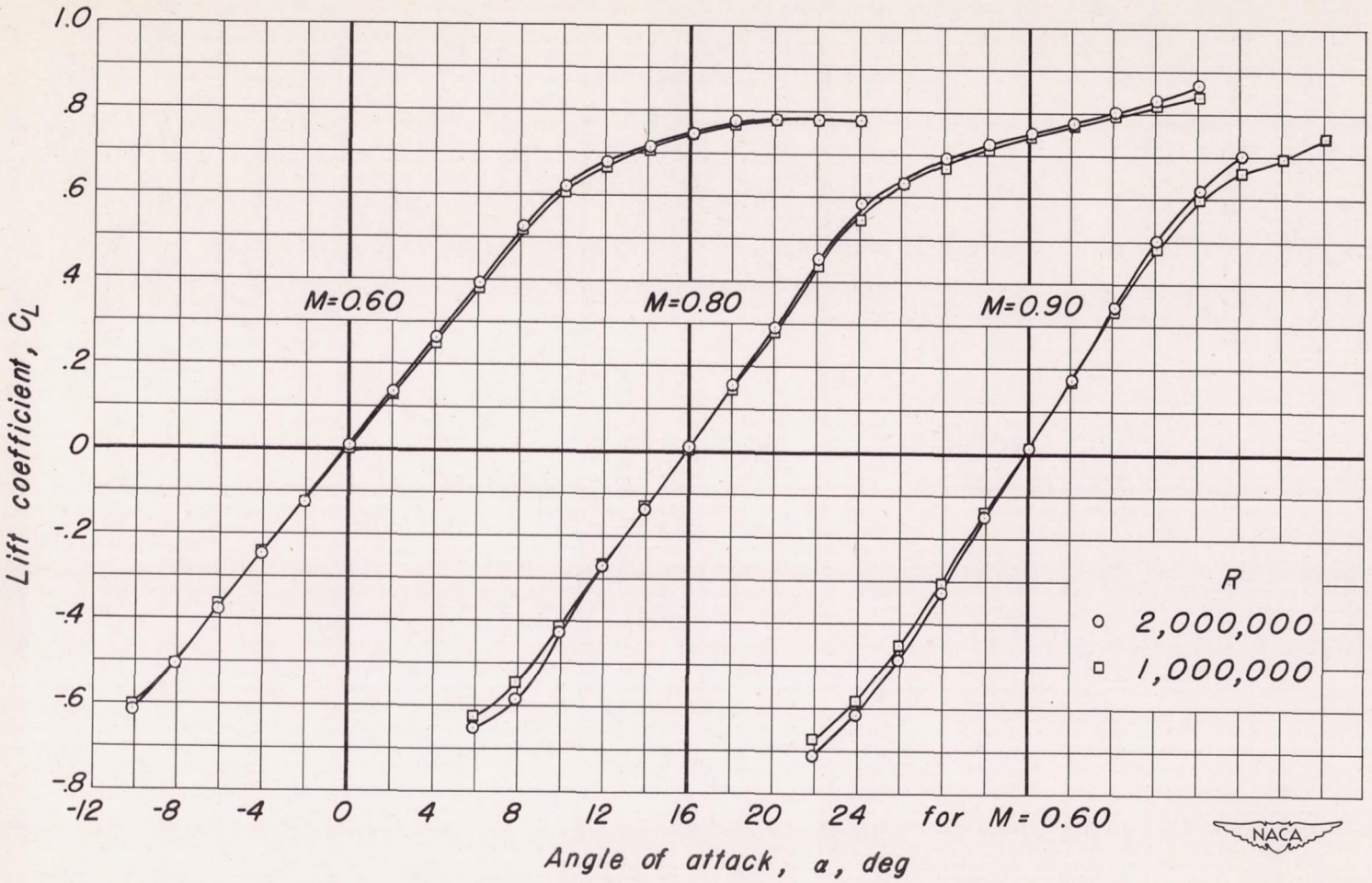

(a) C_L vs α.

Figure 4.– The effect of Reynolds number on the high-speed aerodynamic characteristics. δ_e, 0°; δ_t, 0°.

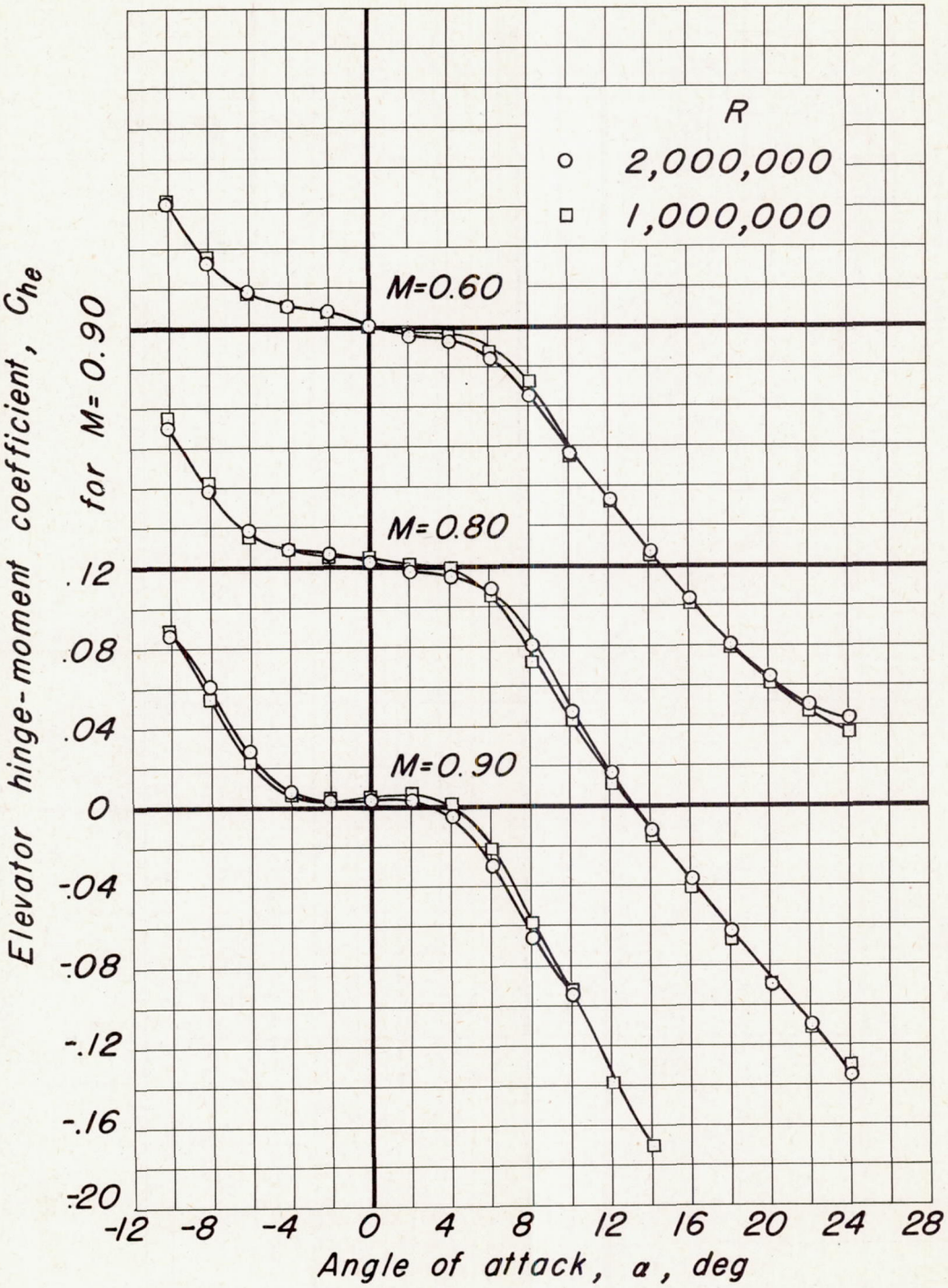

(b) C_{h_e} vs α.

Figure 4.—Continued.

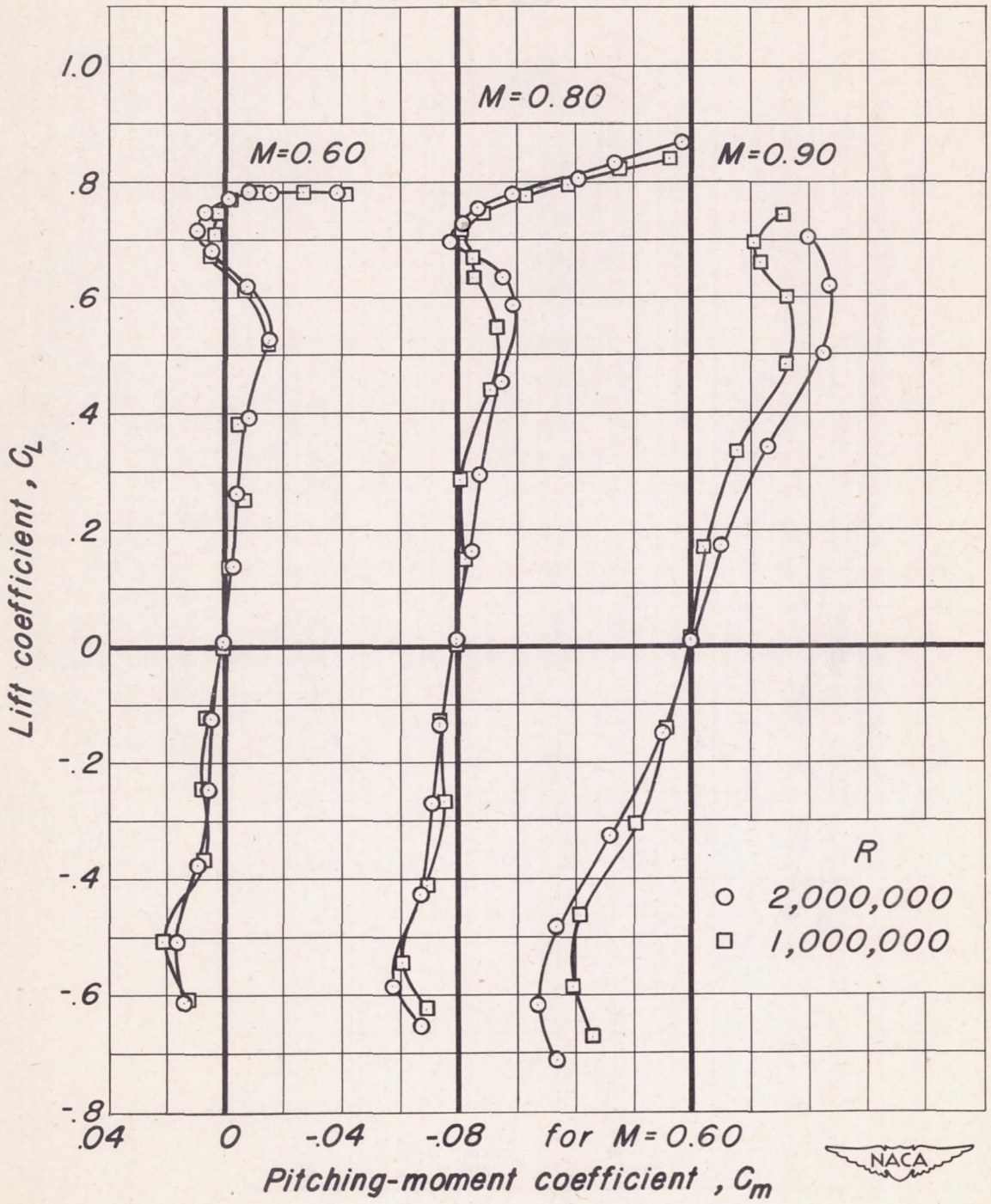

(c) C_L vs C_m.

Figure 4.– Continued.

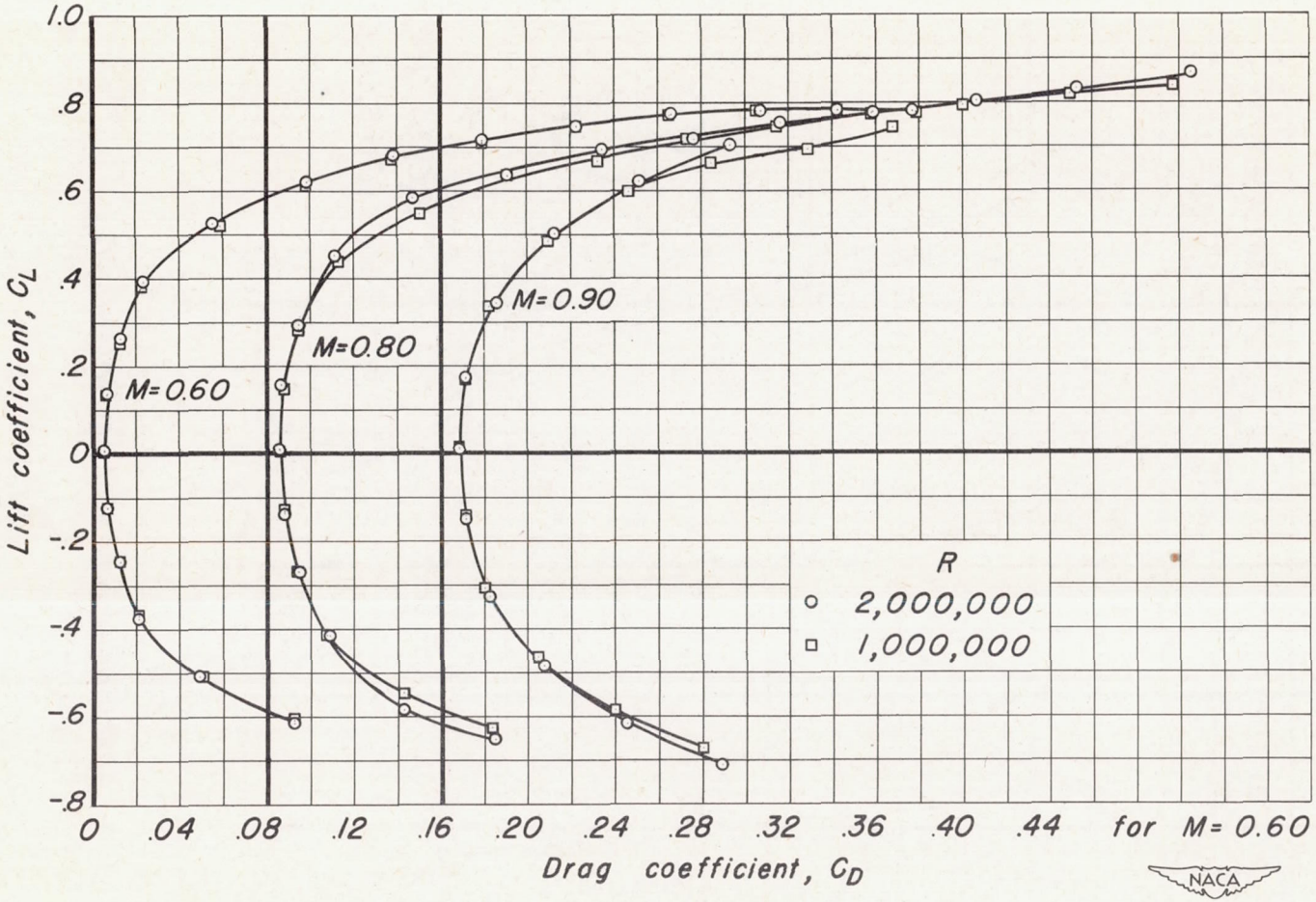

(d) C_L vs C_D.

Figure 4.– Concluded.

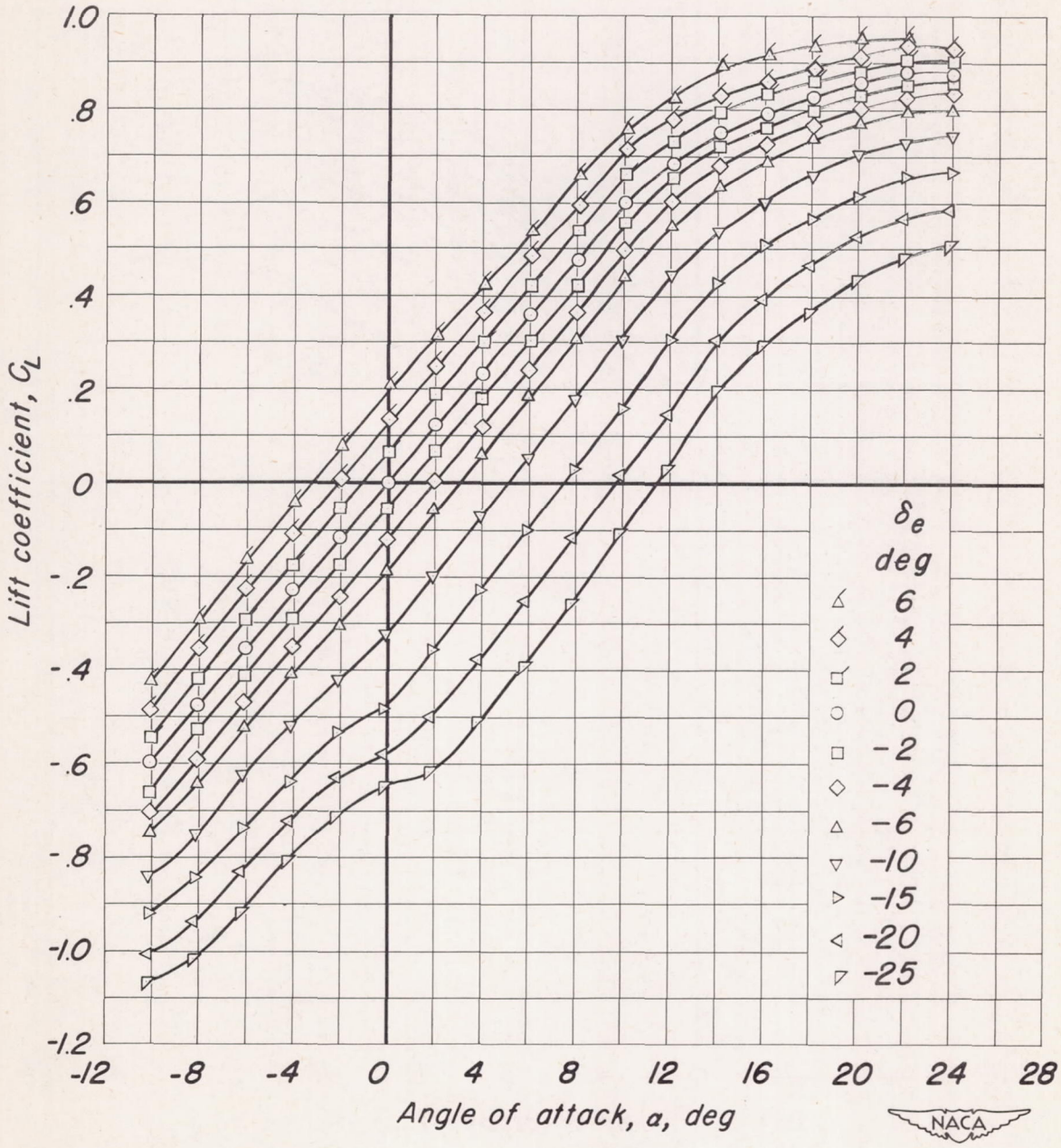

(a) M, 0.21.

Figure 5.– The variation of lift coefficient with angle of attack. δ_t, 0°; R, 2,000,000.

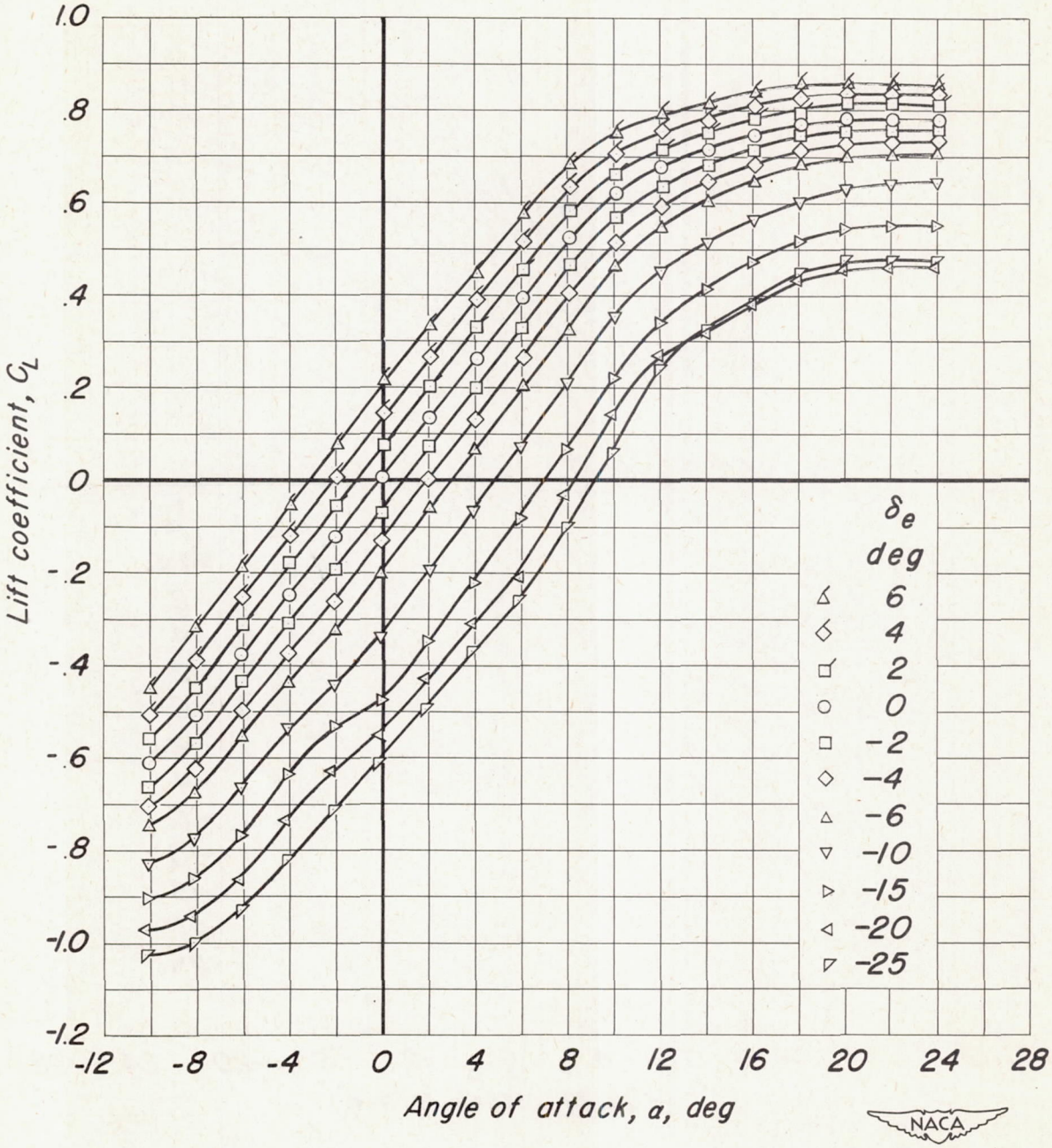

(b) M, 0.60.

Figure 5.— Continued.

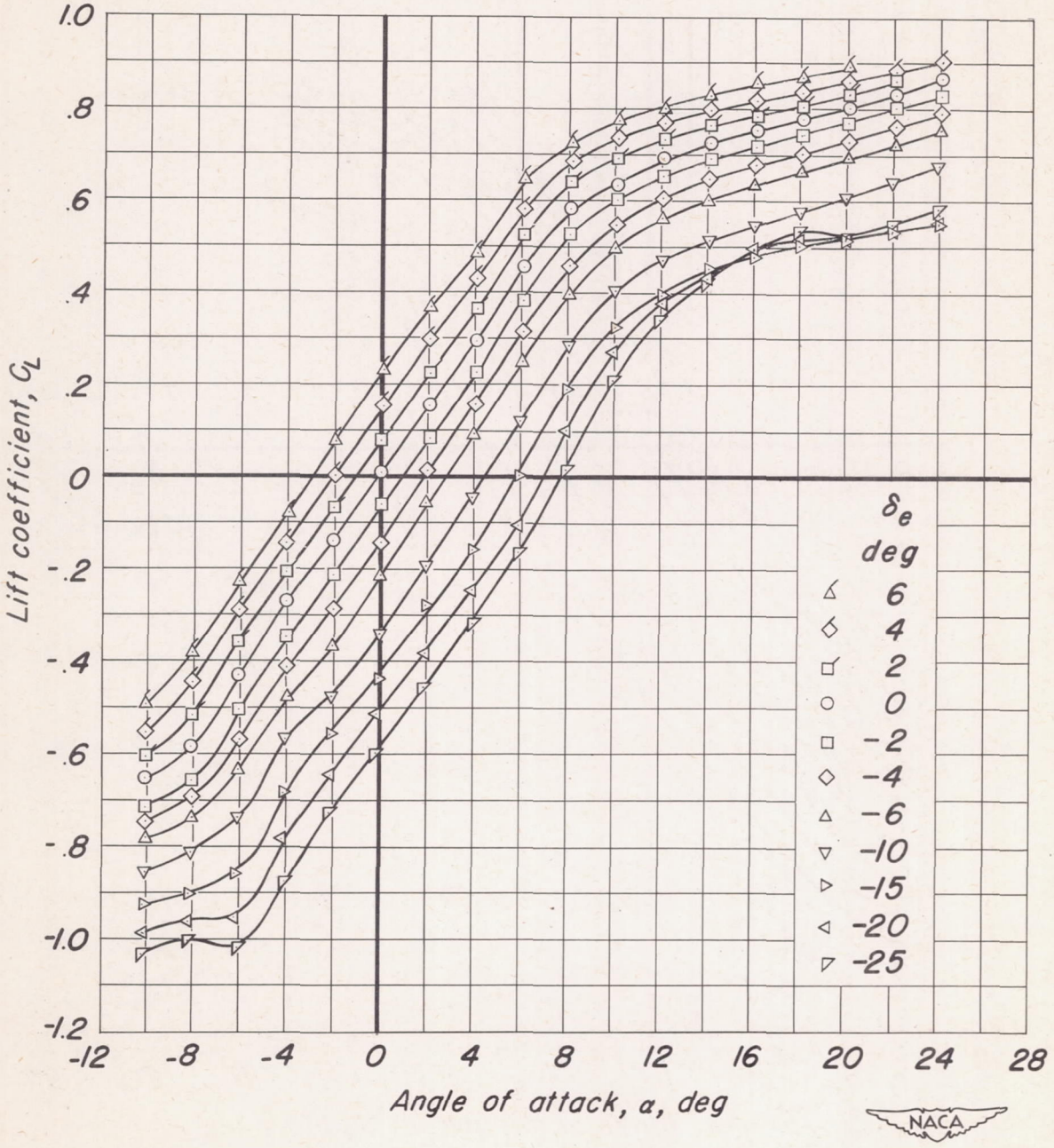

(c) M, 0.80.

Figure 5.– Continued.

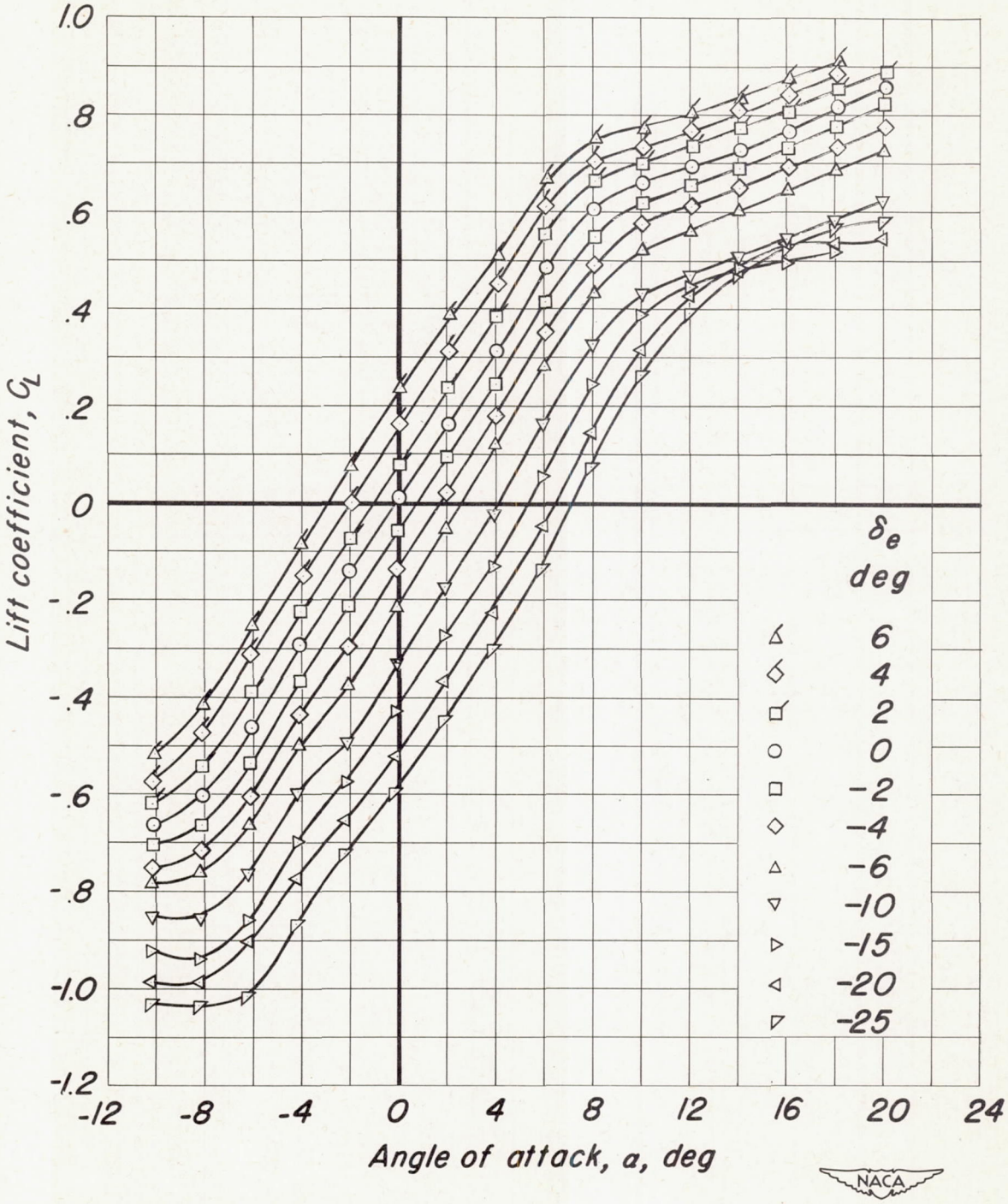

(d) M, 0.85.

Figure 5.—Continued.

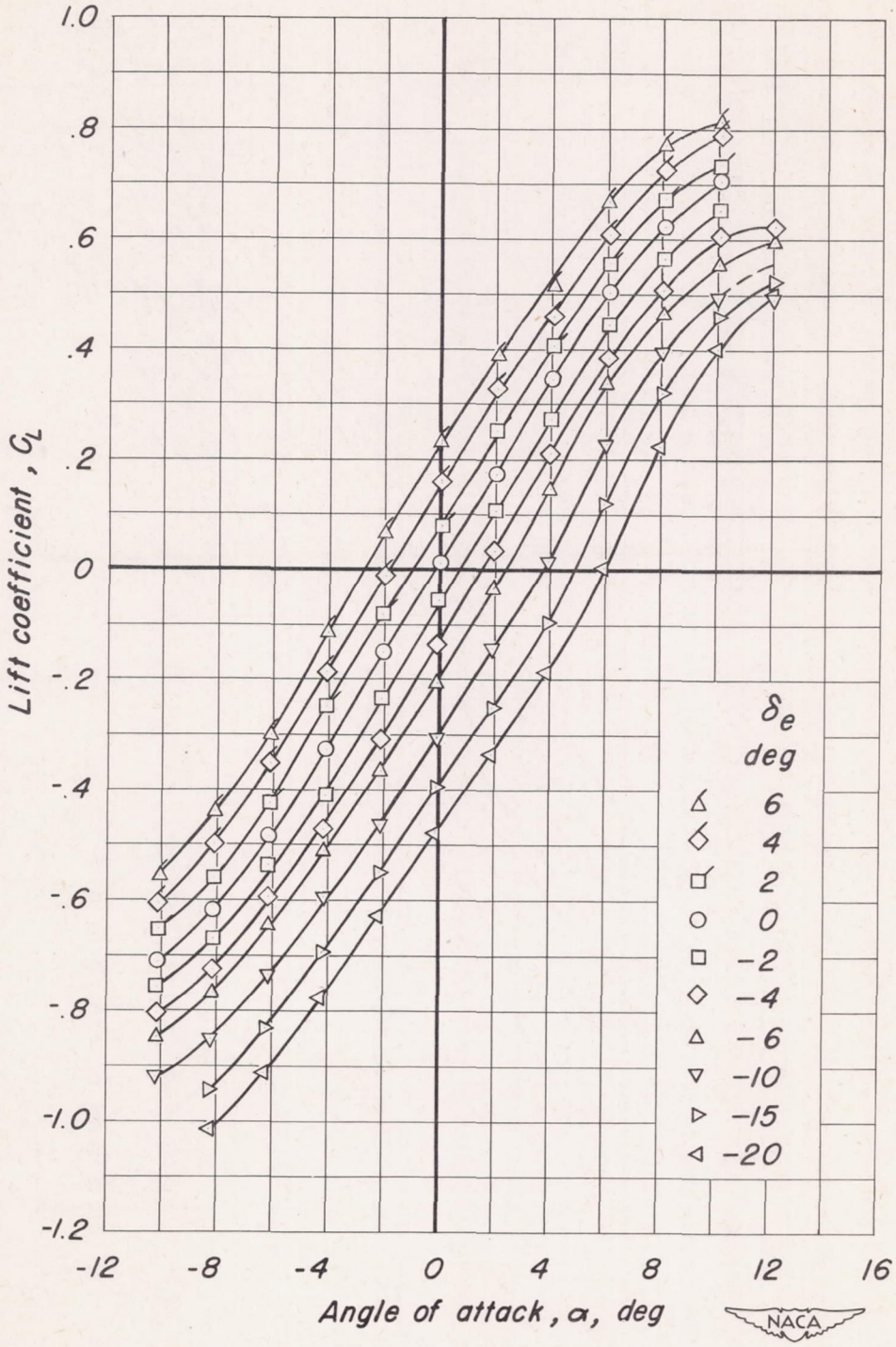

(e) M, 0.90.

Figure 5.– Continued.

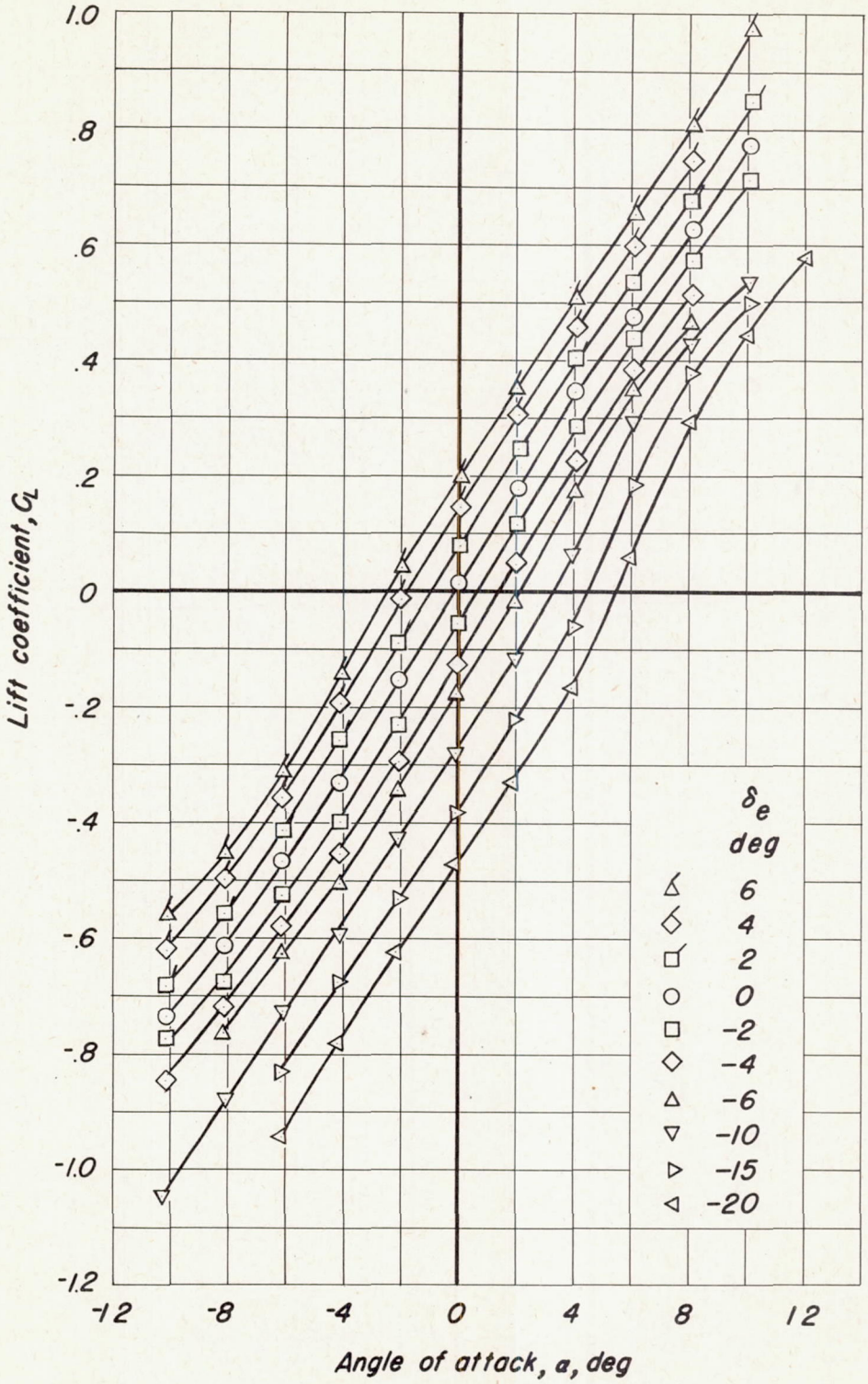

(f) M, 0.93.

Figure 5.— Continued.

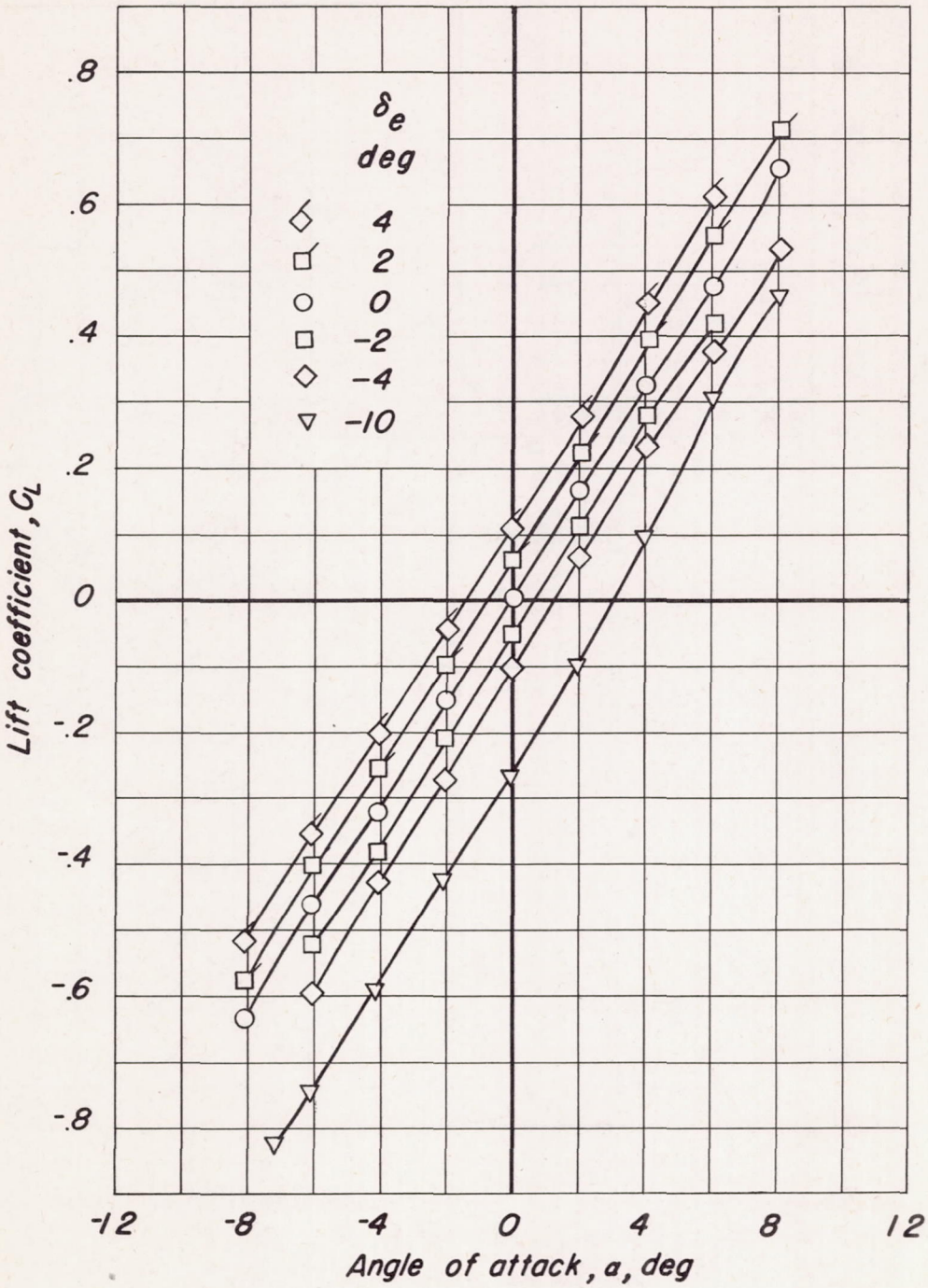

(g) M, 0.94.

Figure 5.— Concluded.

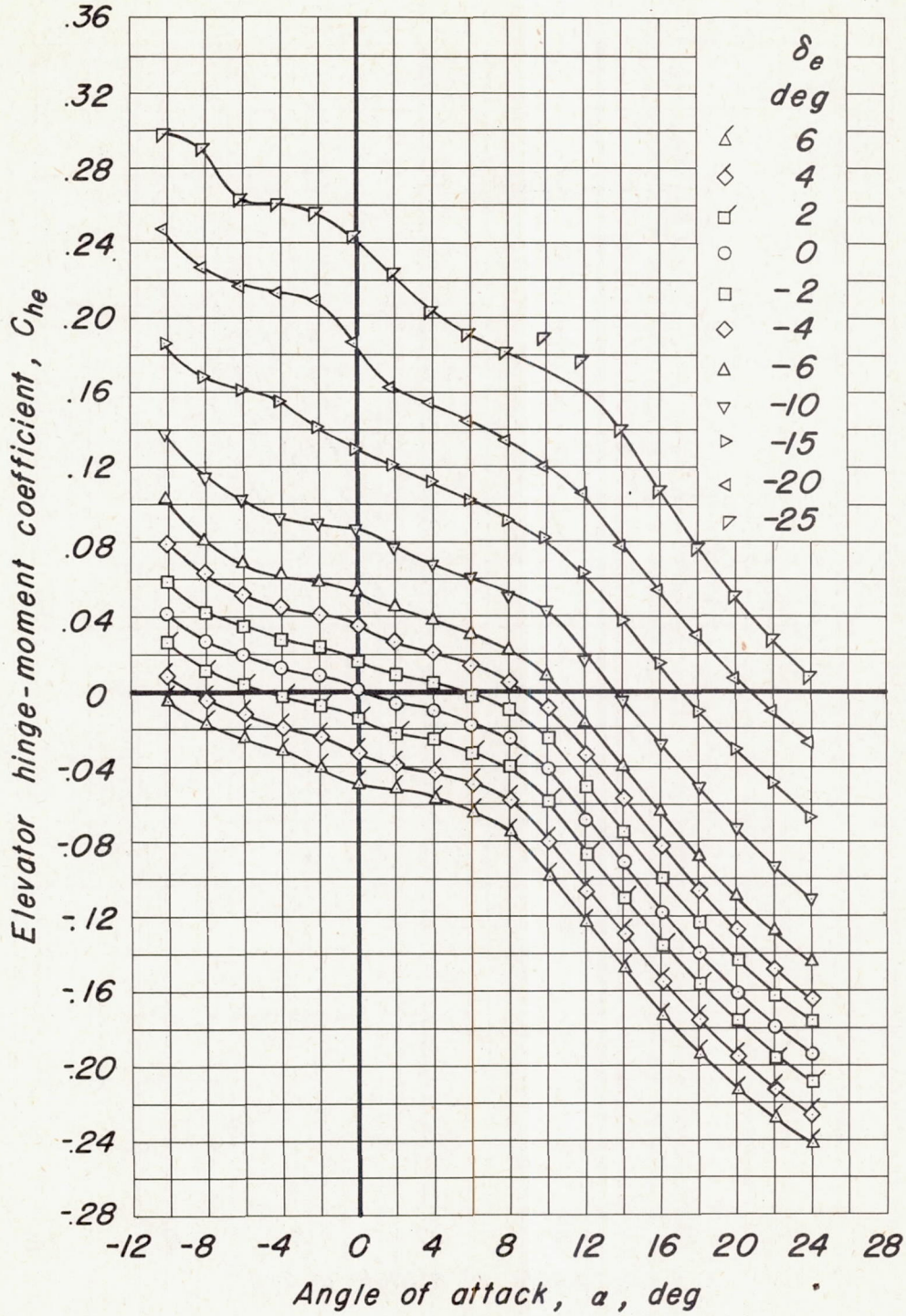

(a) M, 0.21.

NACA

Figure 6.– The variation of elevator hinge-moment coefficient with angle of attack. δ_t, 0°; R, 2,000,000.

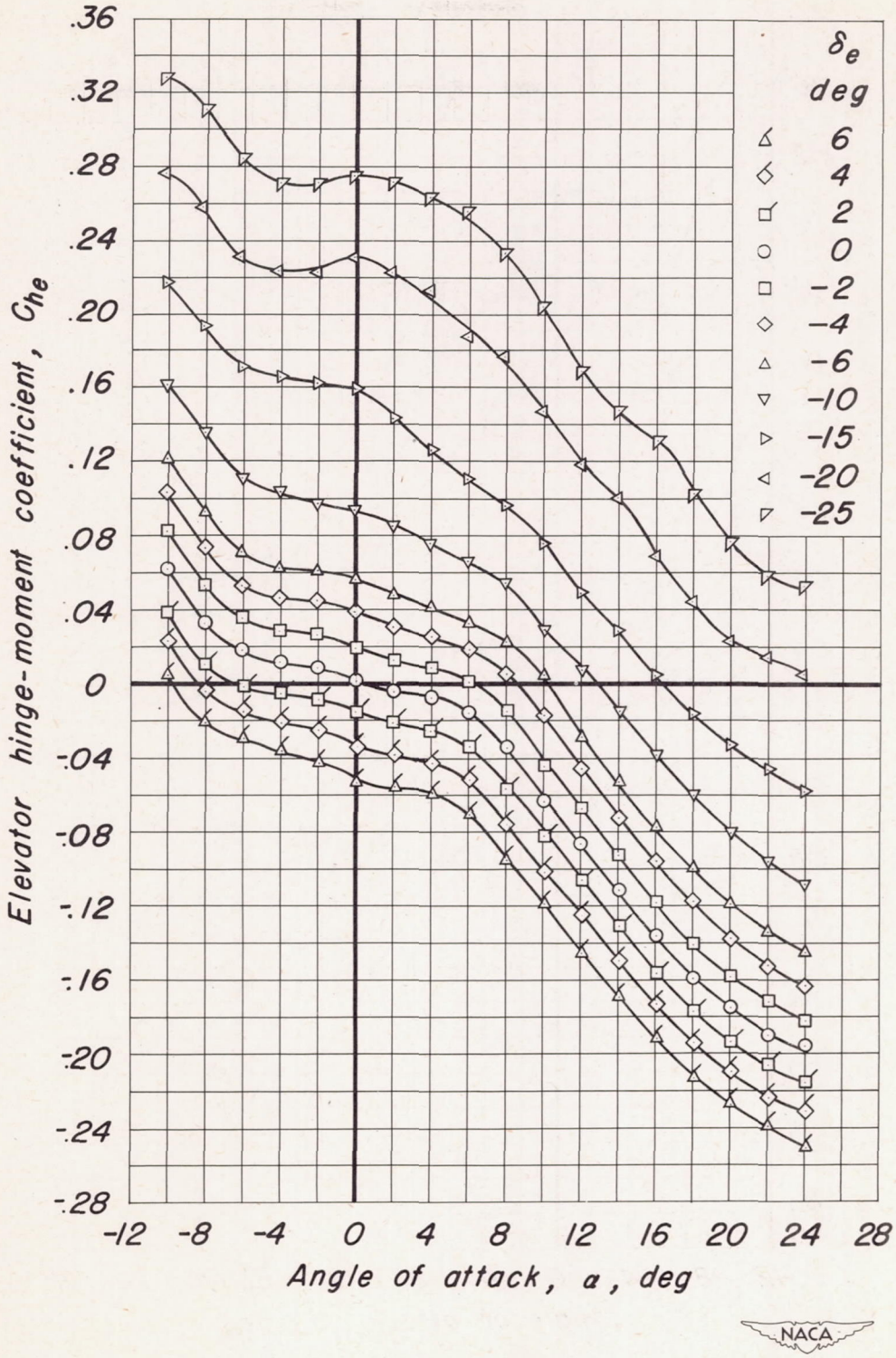

(b) M, 0.60.

Figure 6.— Continued.

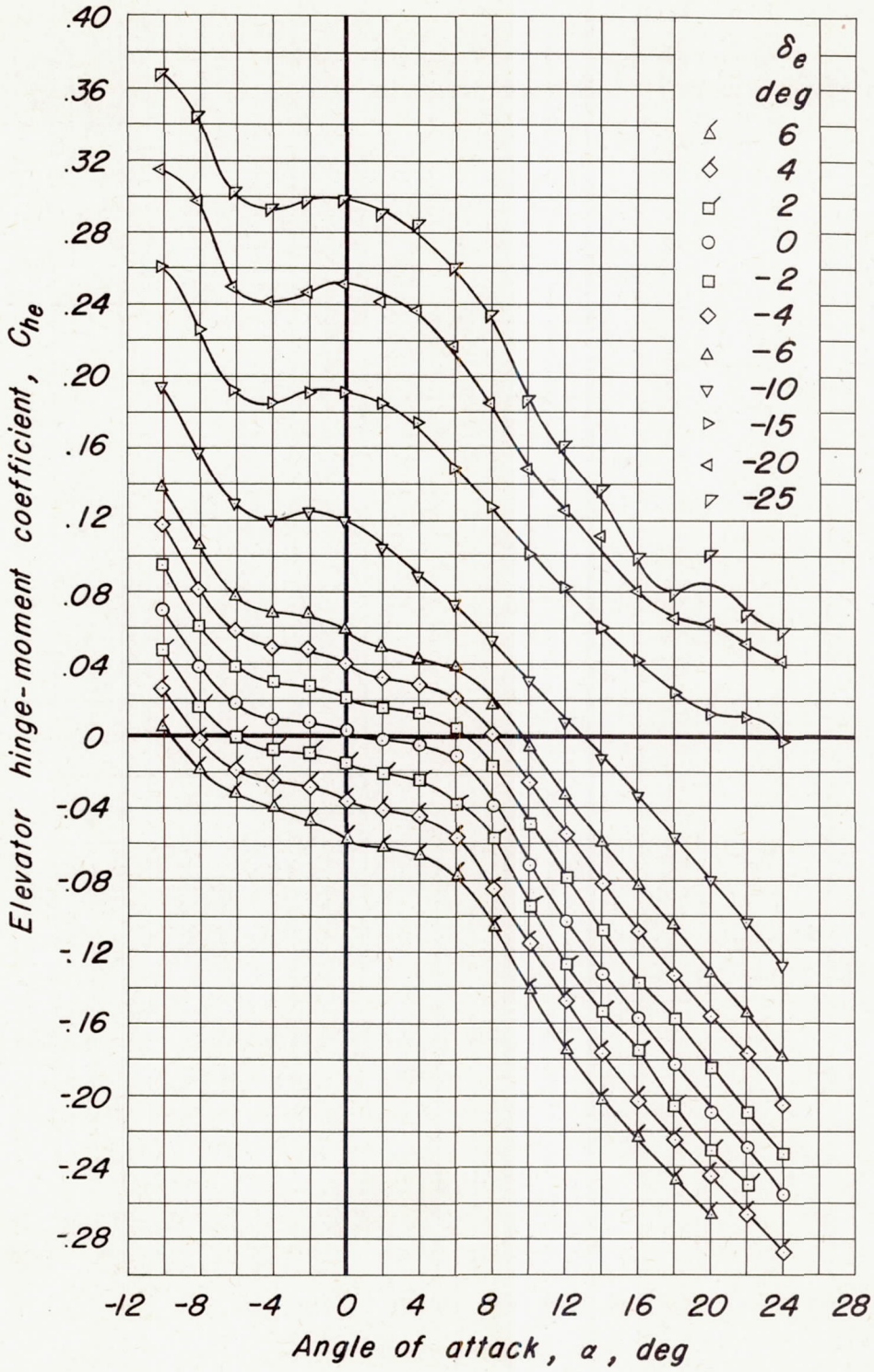

(c) M, 0.80.

Figure 6.— Continued.

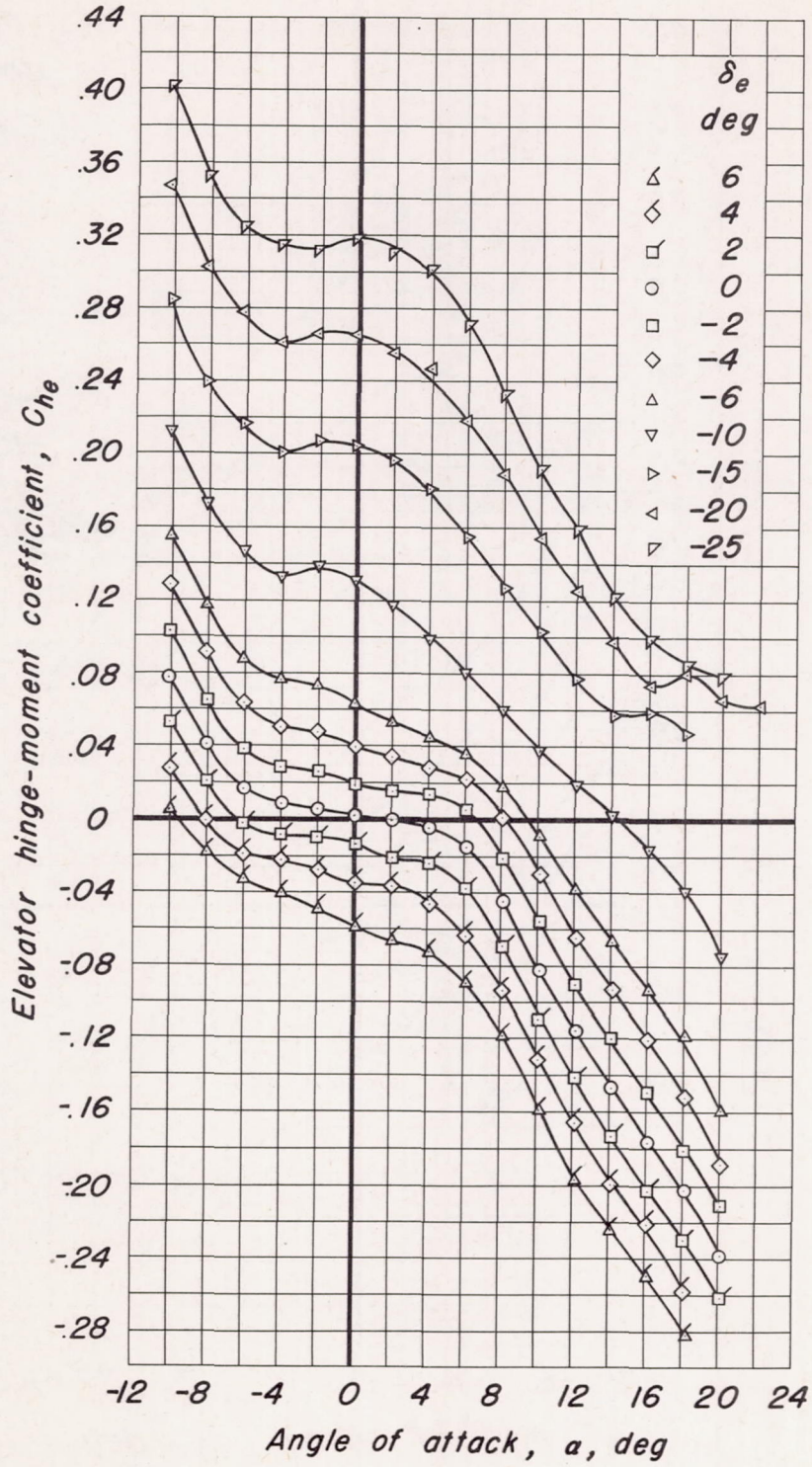

(d) M, 0.85.

Figure 6.— Continued.

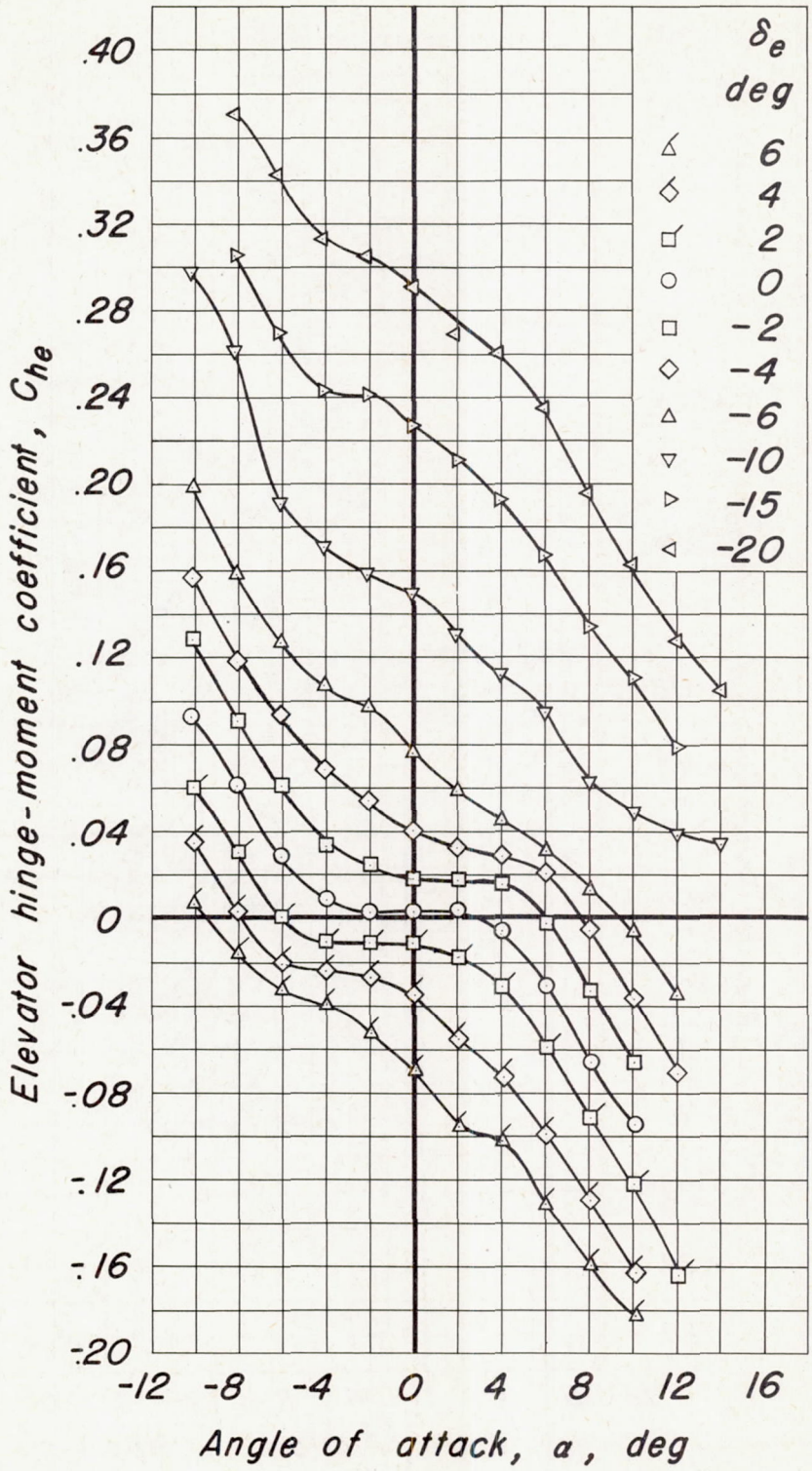

(e) M, 0.90.

Figure 6.— Continued.

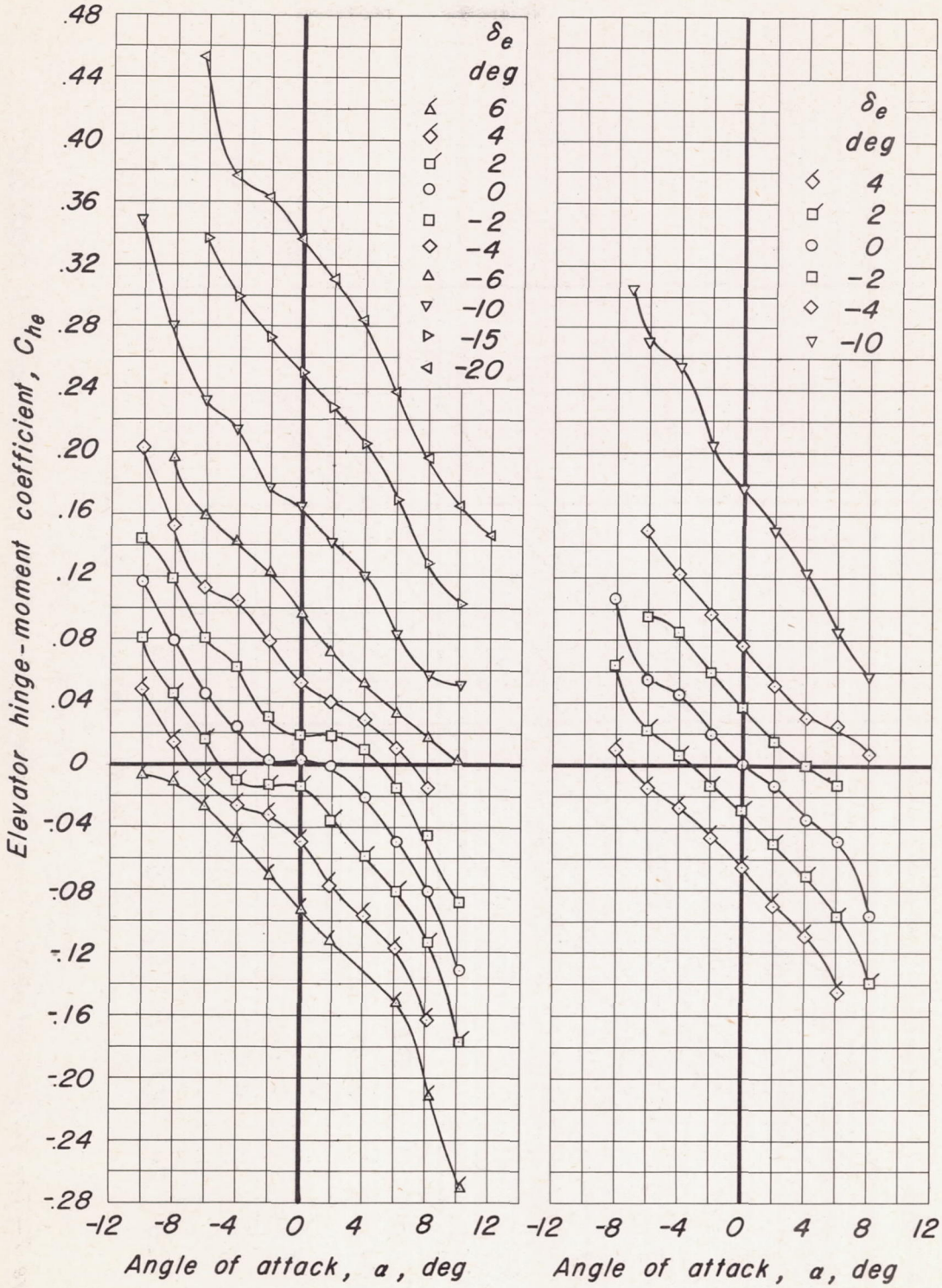

(f) M, 0.93. (g) M, 0.94.

Figure 6.—Concluded.

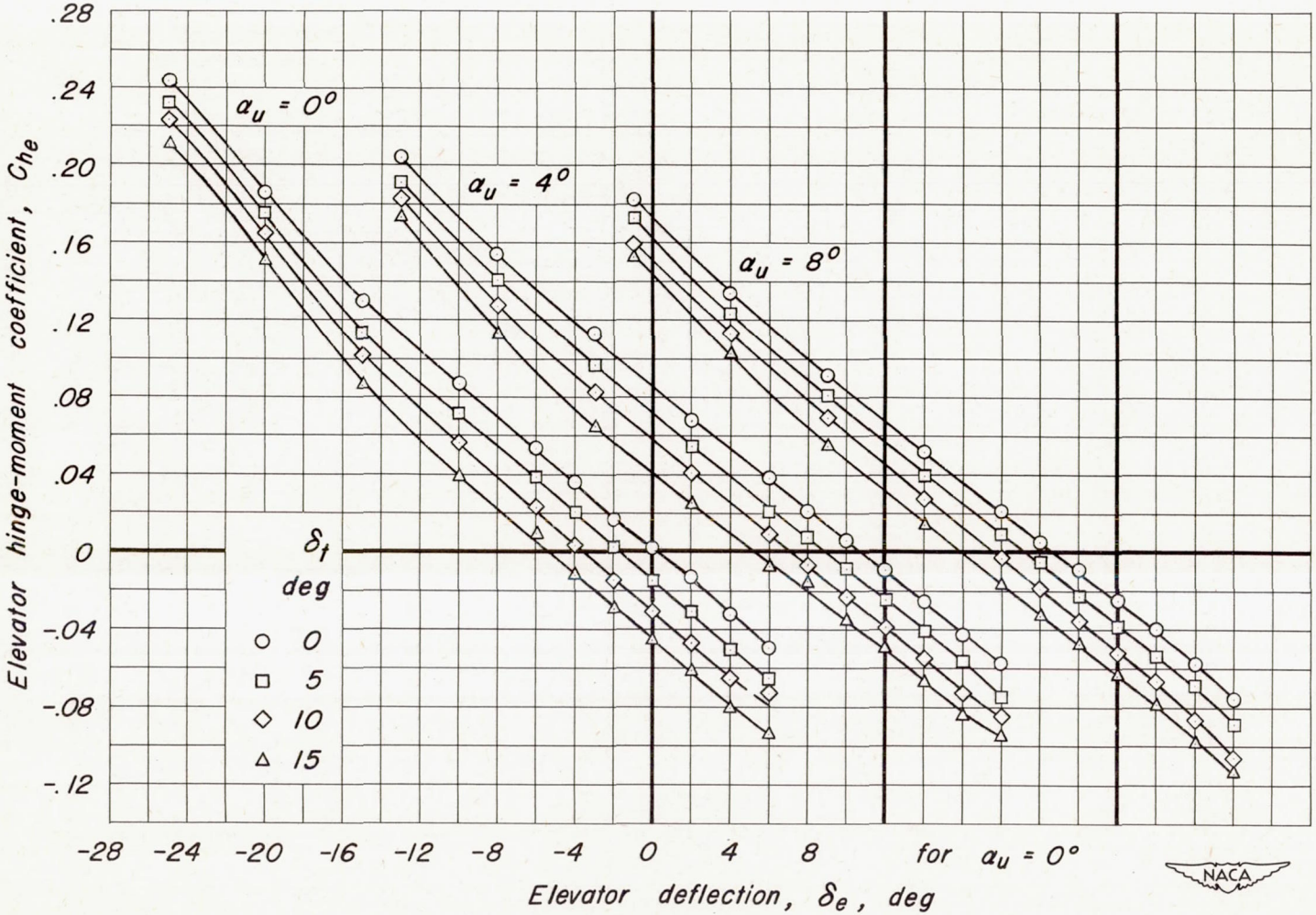

(a) M, 0.21.

Figure 7.– The variation of elevator hinge-moment coefficient with elevator deflection. R, 2,000,000.

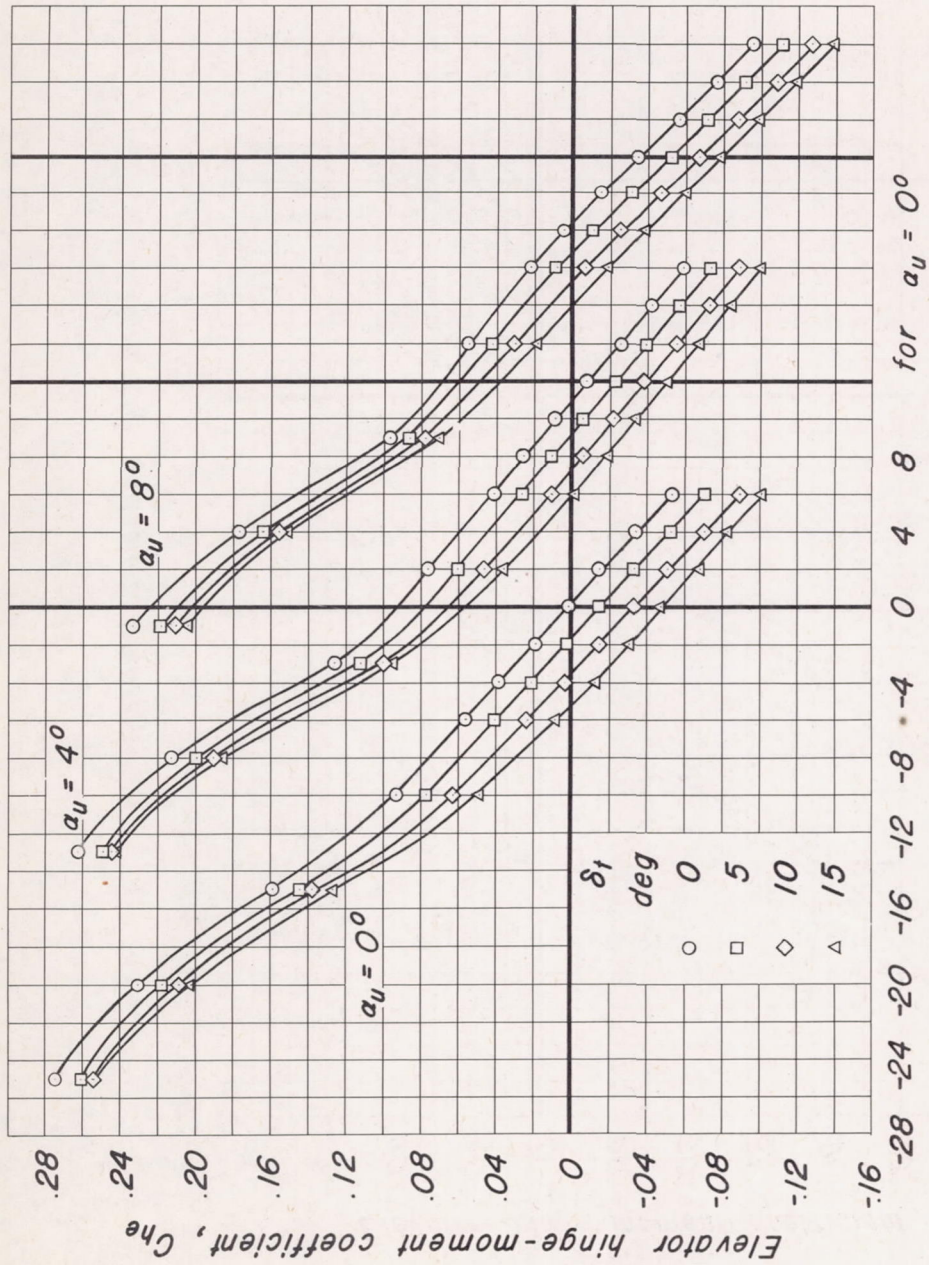

(b) M, 0.60.

Figure 7.– Continued.

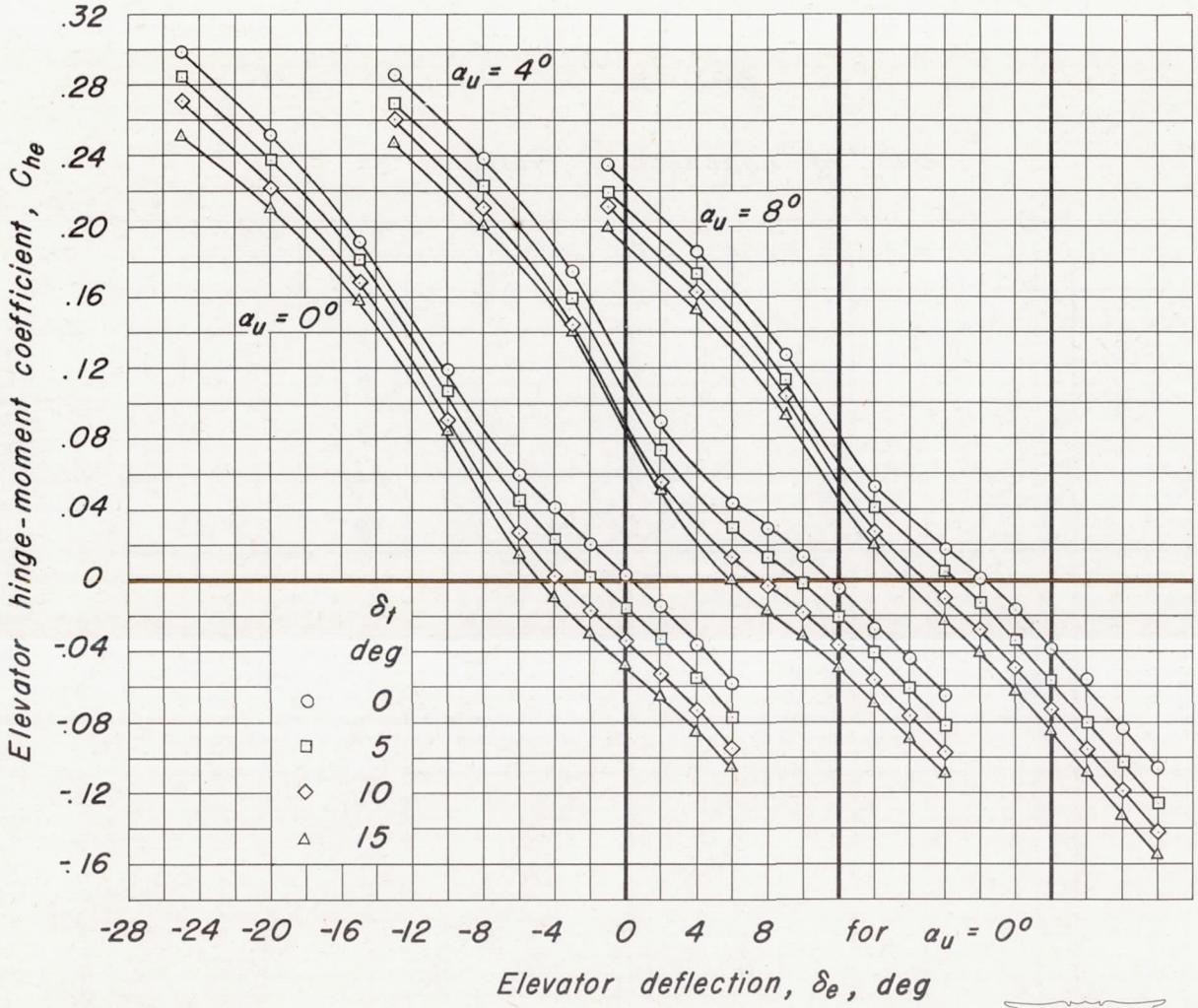

(c) M, 0.80.

Figure 7.– Continued.

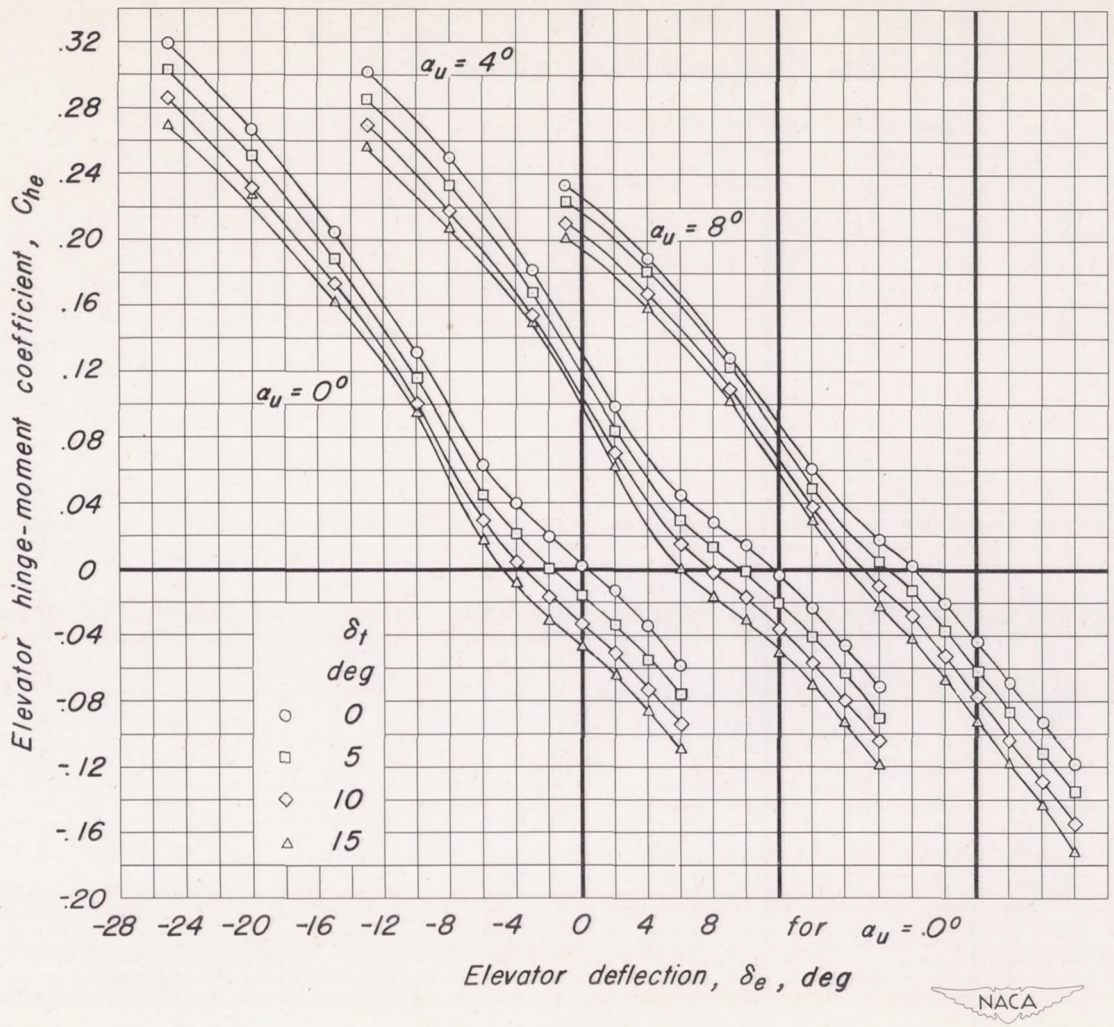

(d) M, 0.85.

Figure 7.– Continued.

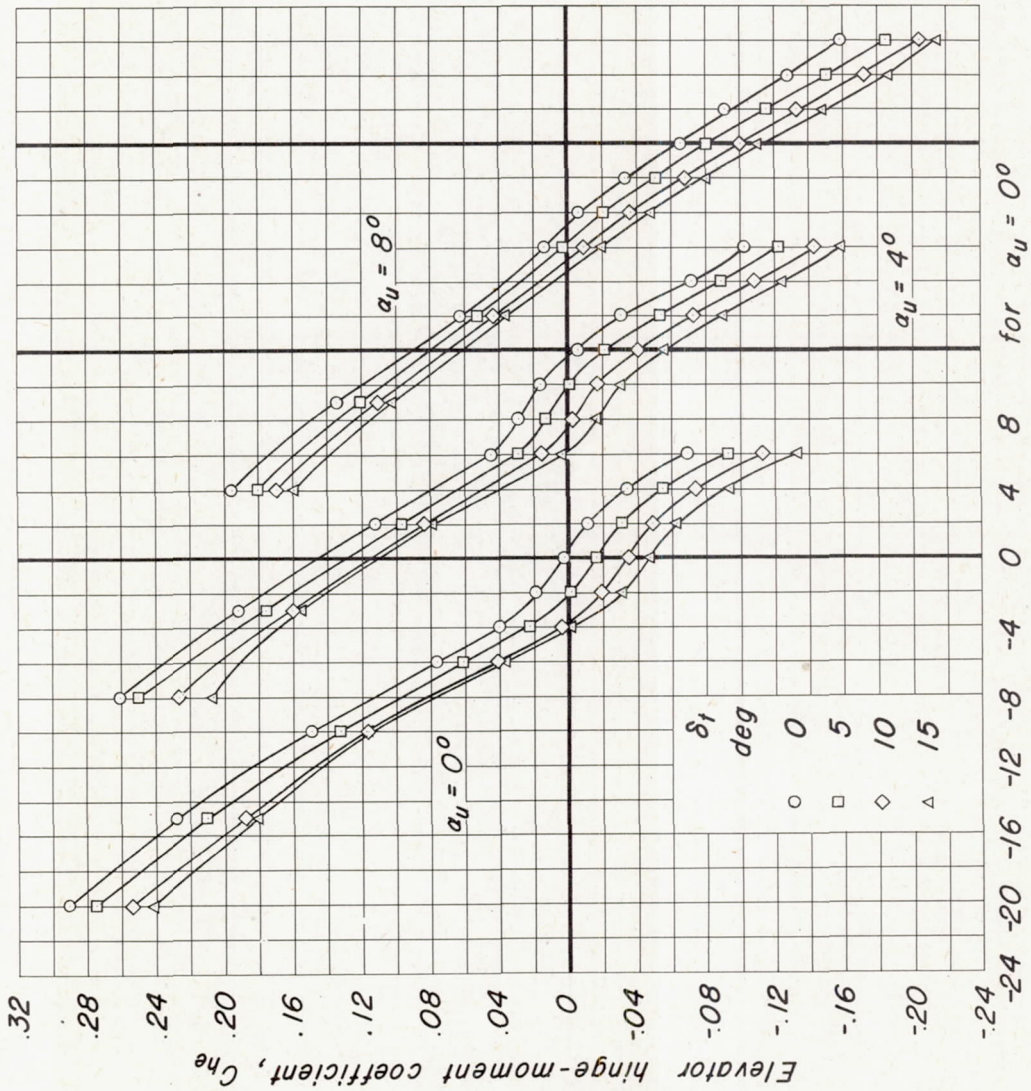

(e) M, 0.90.

Figure 7.– Continued.

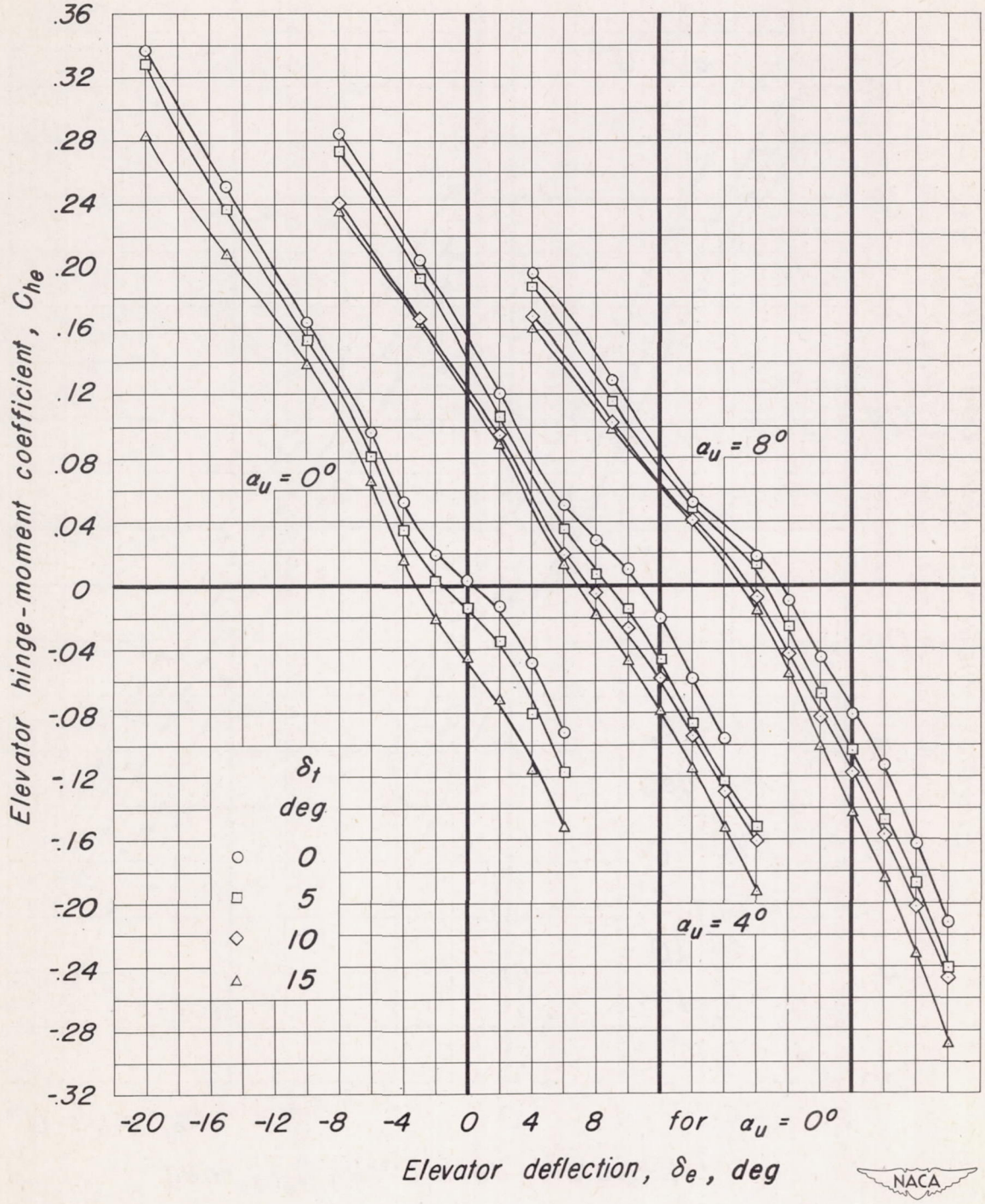

(f) M, 0.93.

Figure 7.– Continued.

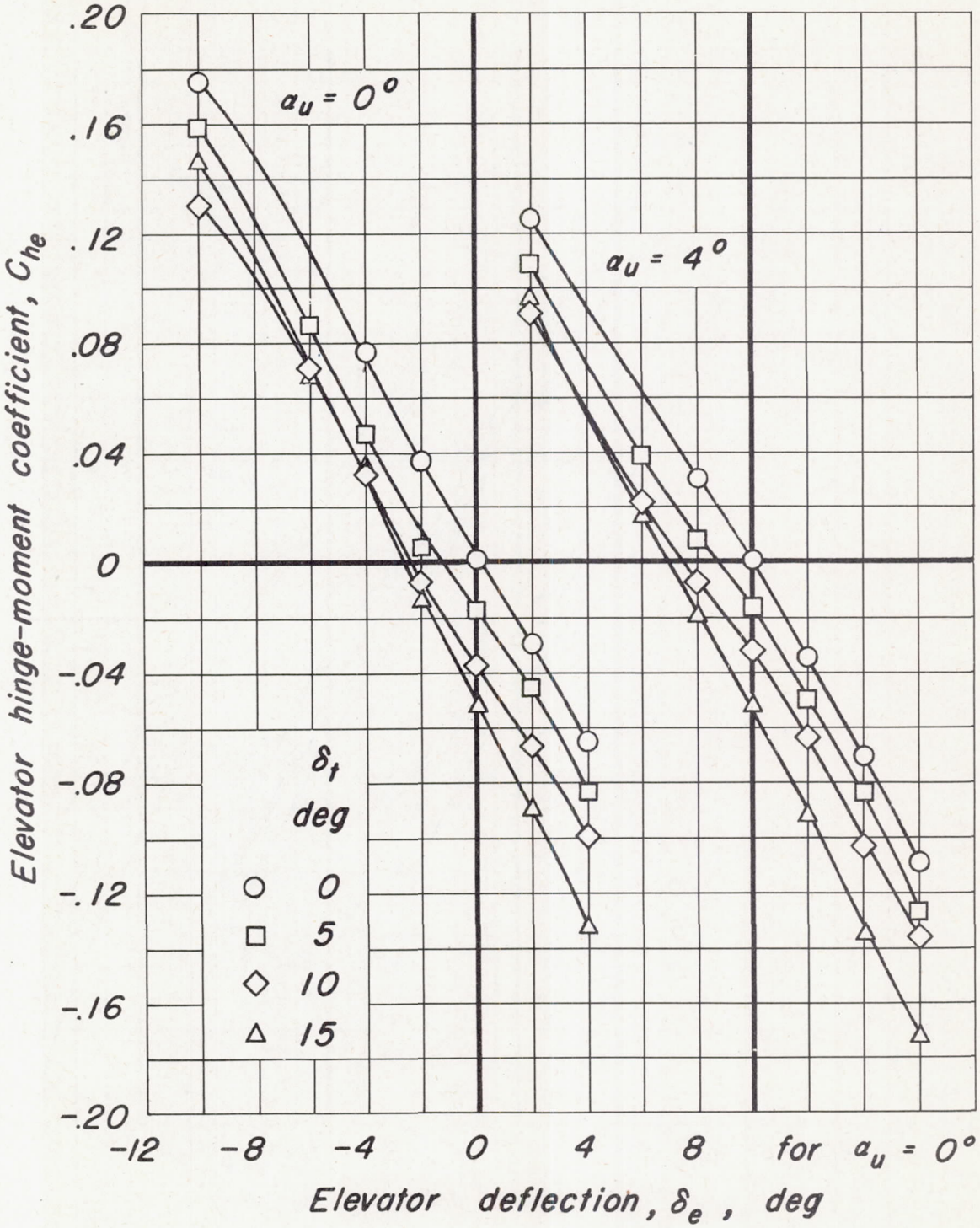

(g) M, 0.94.

Figure 7.—Concluded.

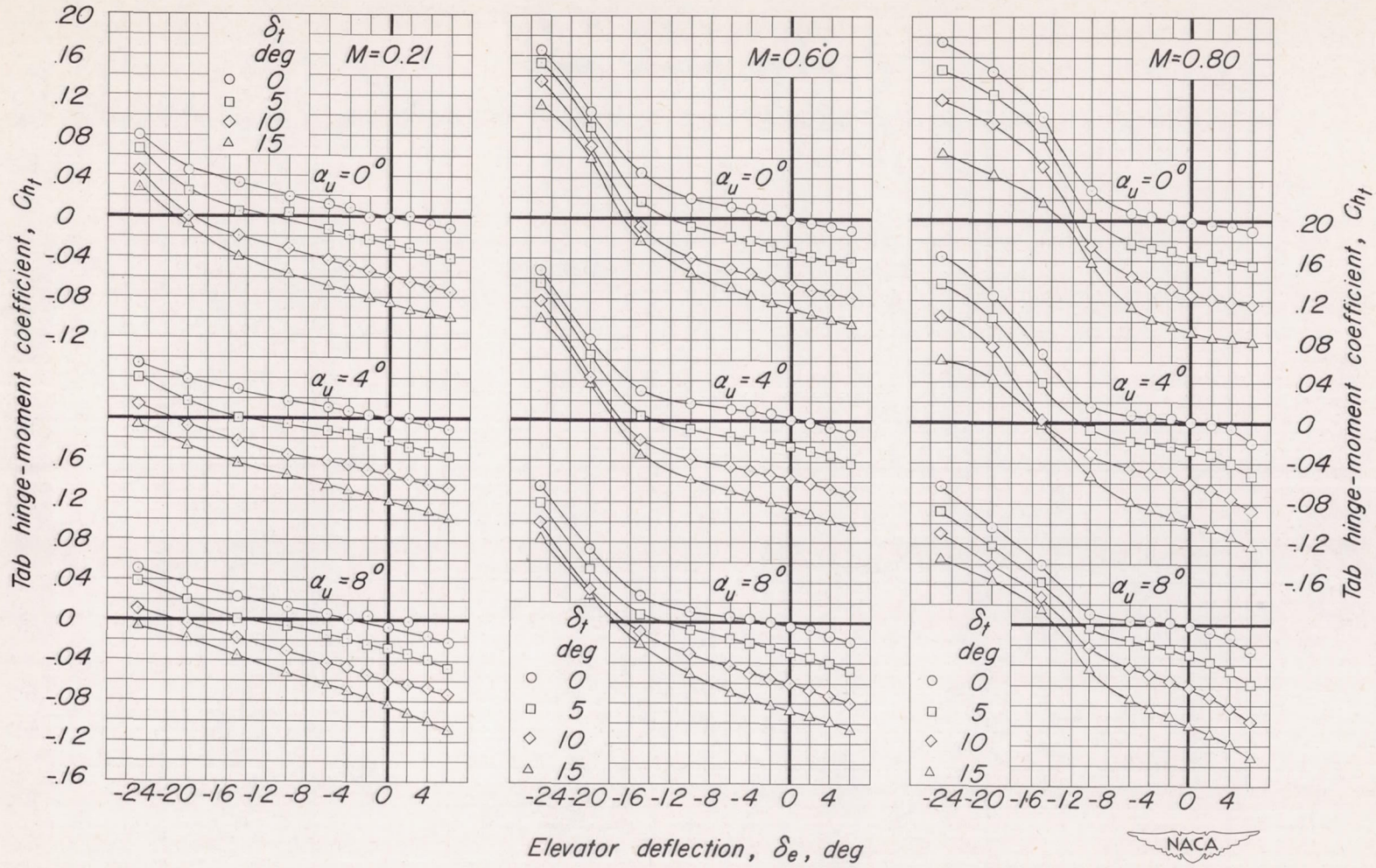

(a) M, 0.21 to M, 0.80.

Figure 8.– The variation of tab hinge-moment coefficient with elevator deflection. R, 2,000,000.

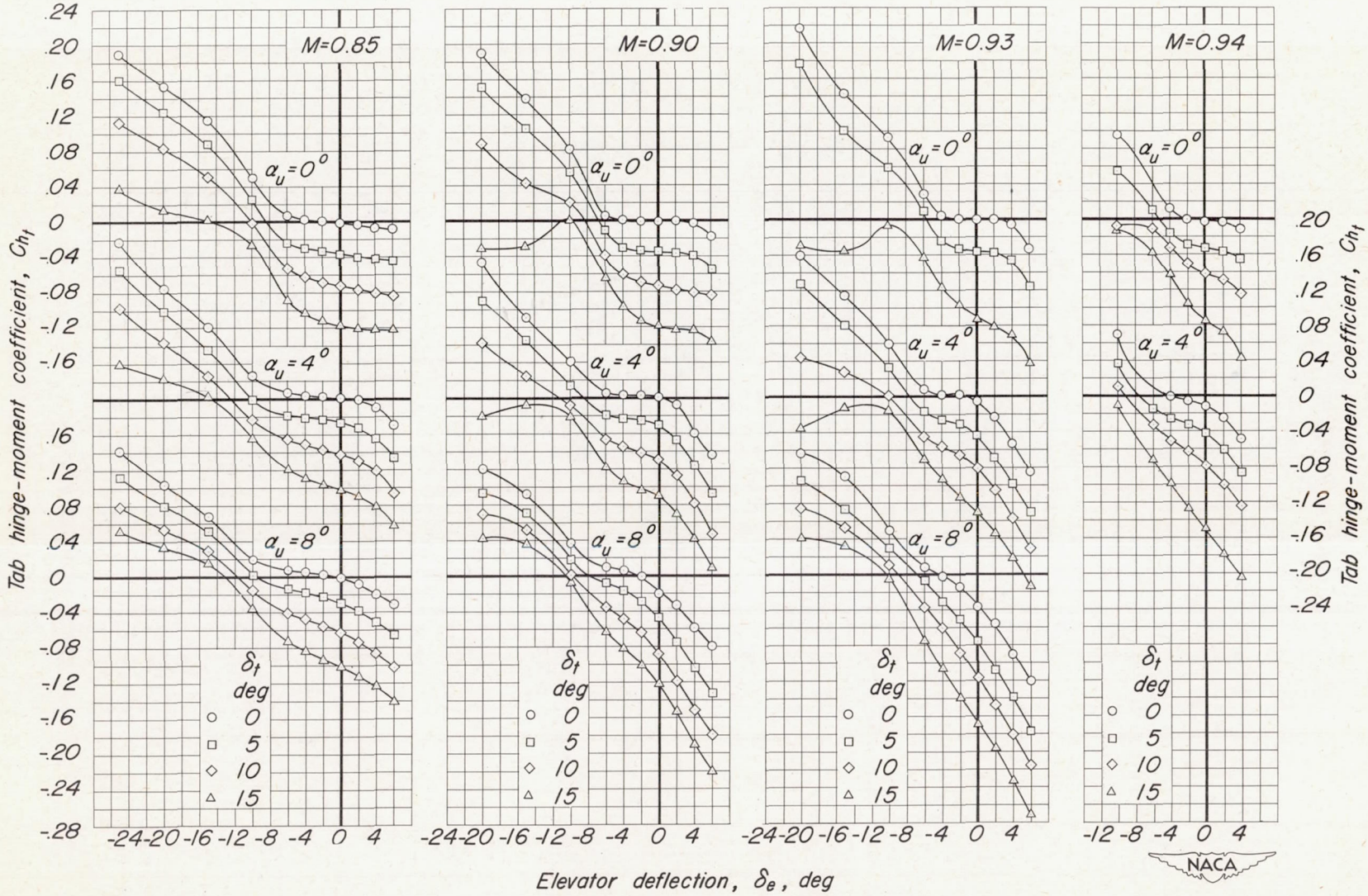

(b) M, 0.85 to M, 0.94.

Figure 8.– Concluded.

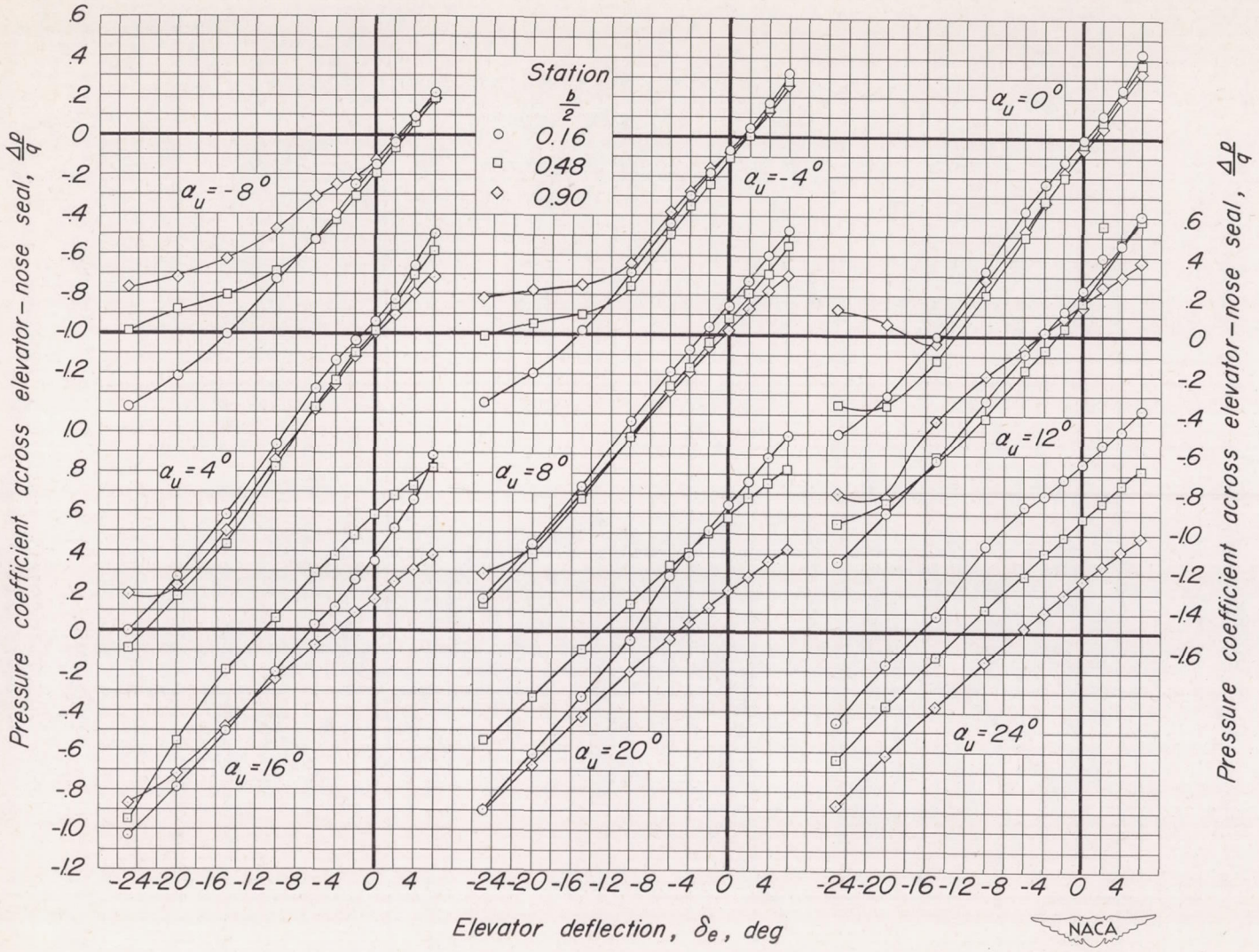

(a) M, 0.21.

Figure 9.– The variation of pressure coefficient across the elevator-nose seal with elevator deflection. δ_t, 0°; R, 2,000,000.

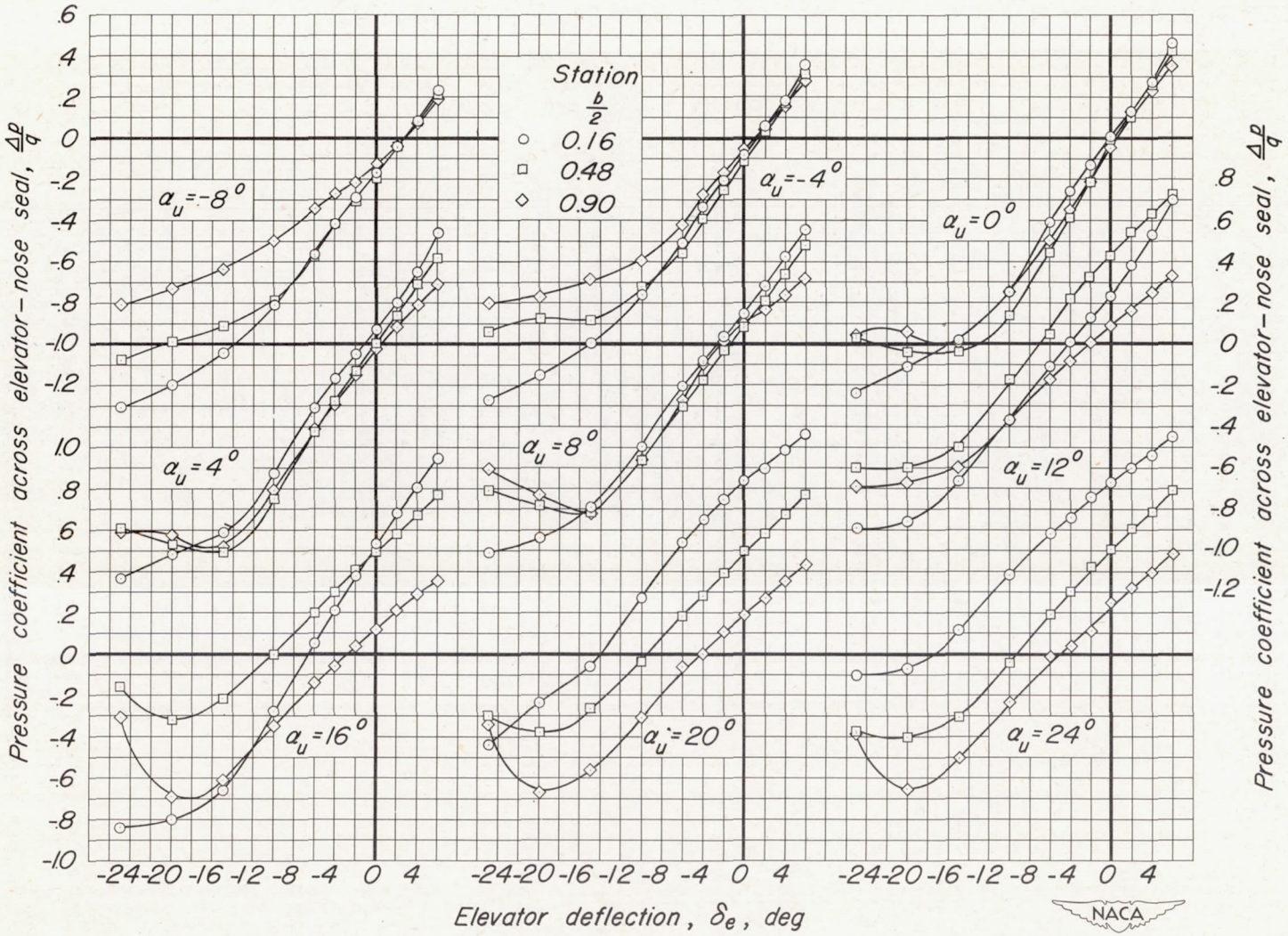

(b) M, 0.60.

Figure 9.– Continued.

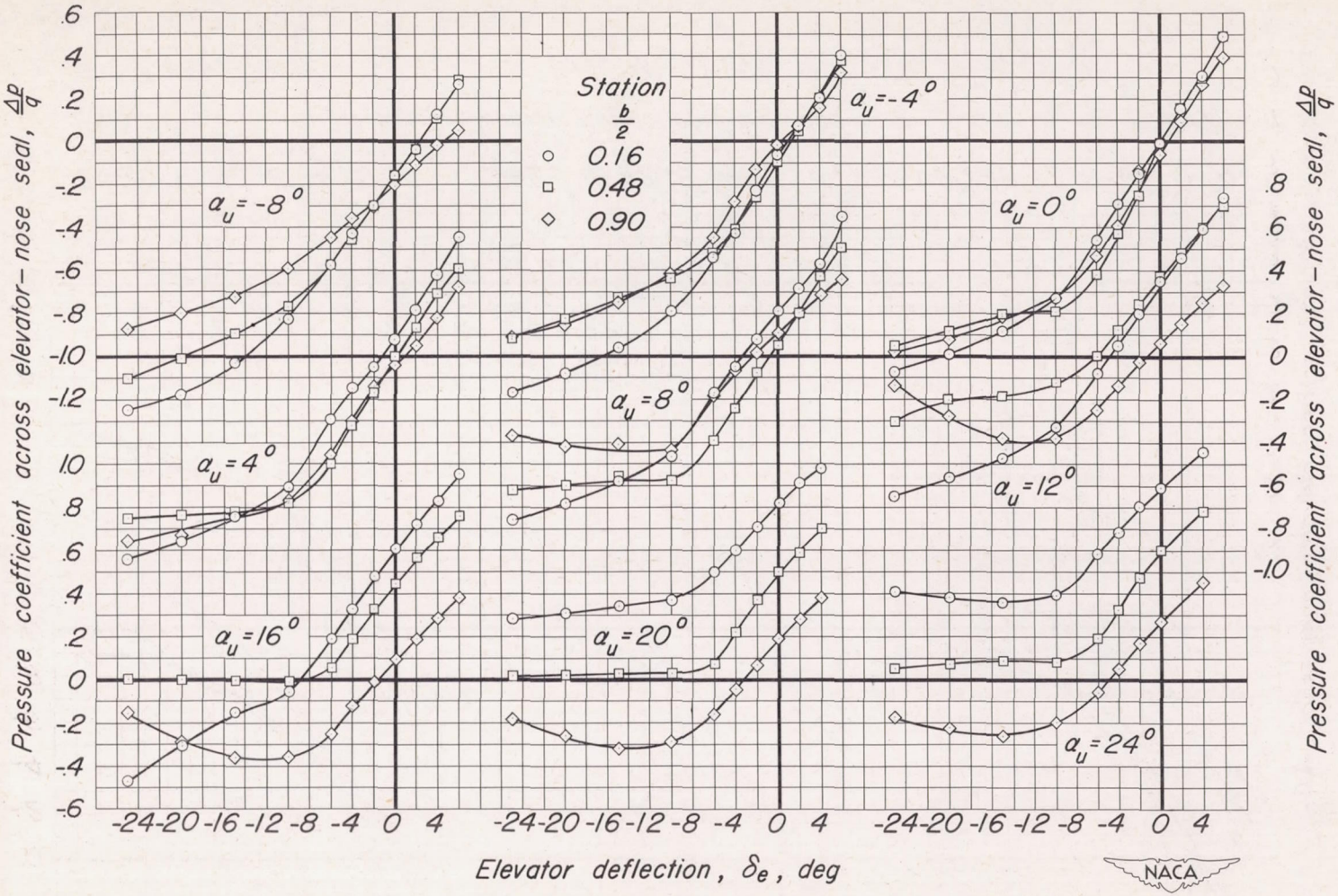

(c) M, 0.80.

Figure 9.– Continued.

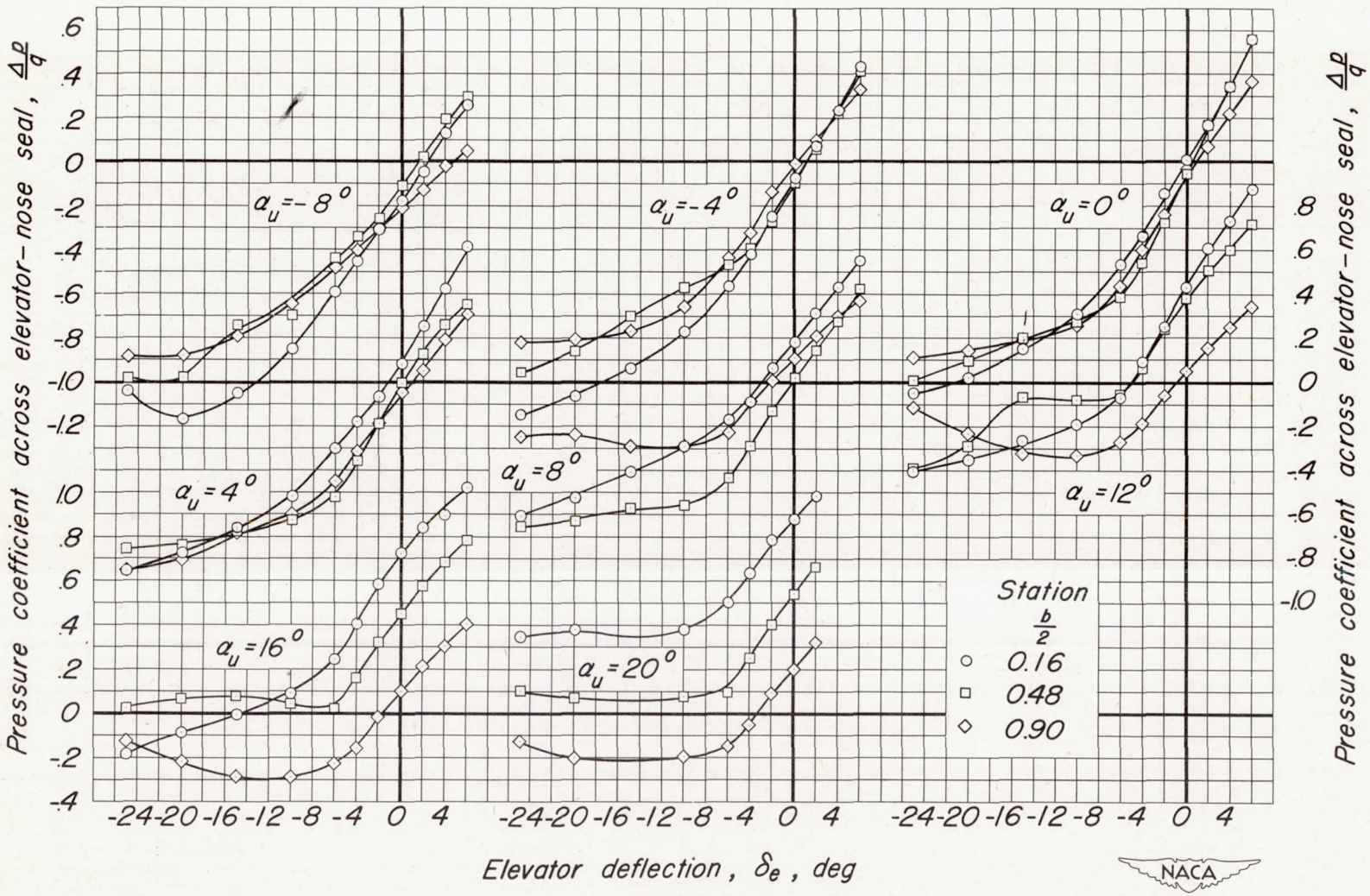

(d) M, 0.85.

Figure 9.– Continued.

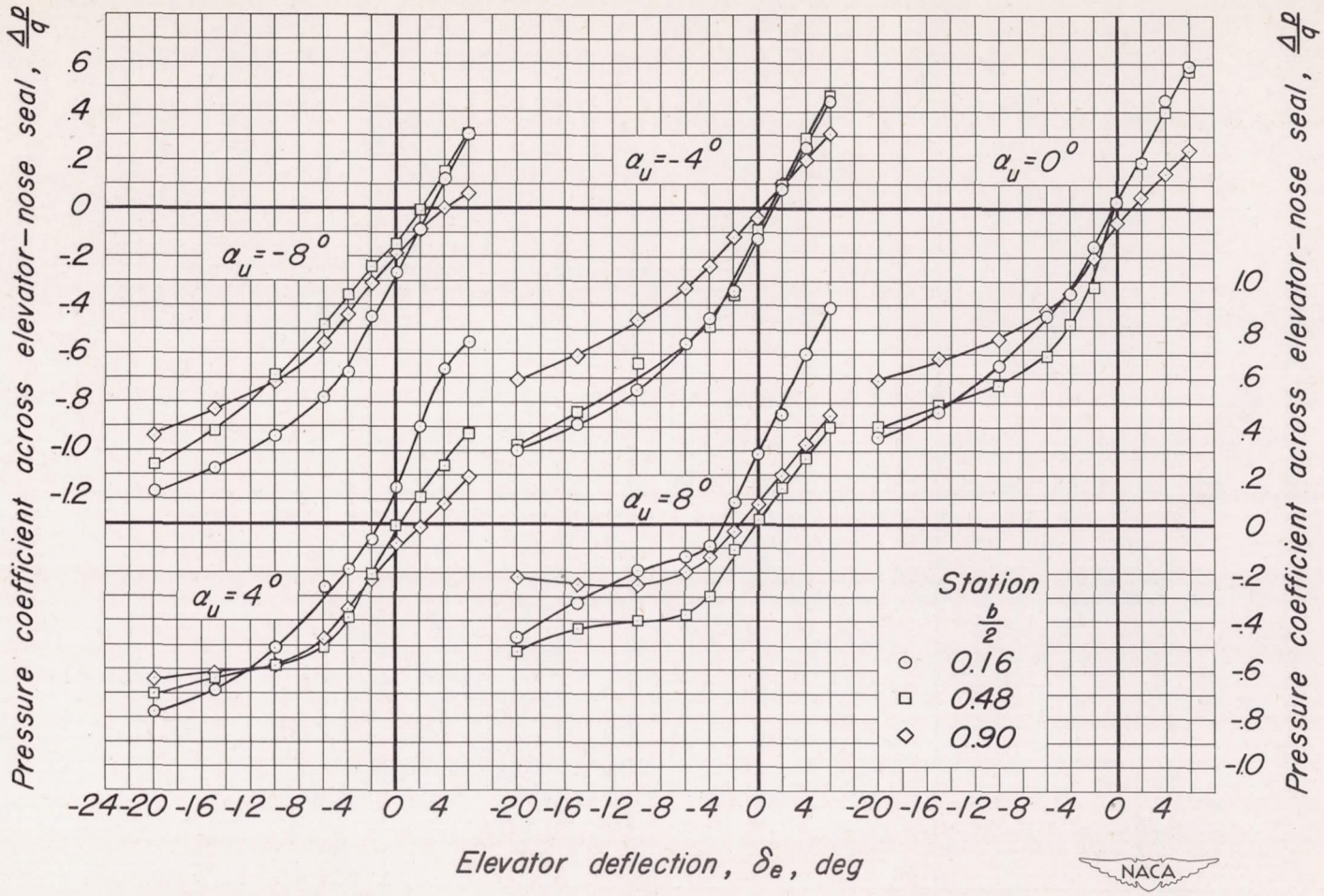

(e) M, 0.90.

Figure 9.—Continued.

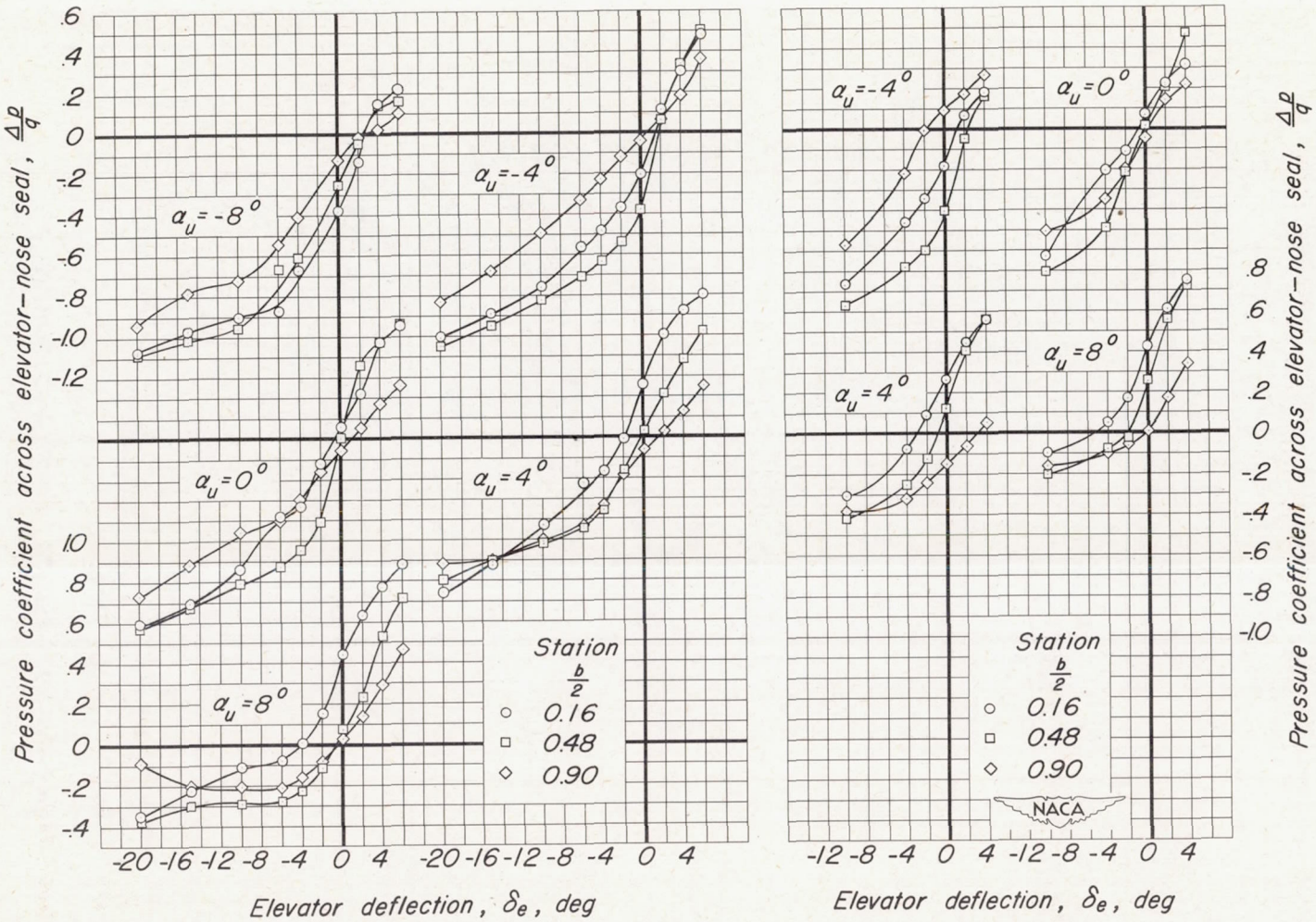

(f) M, 0.93.

(g) M, 0.94.

Figure 9.– Concluded.

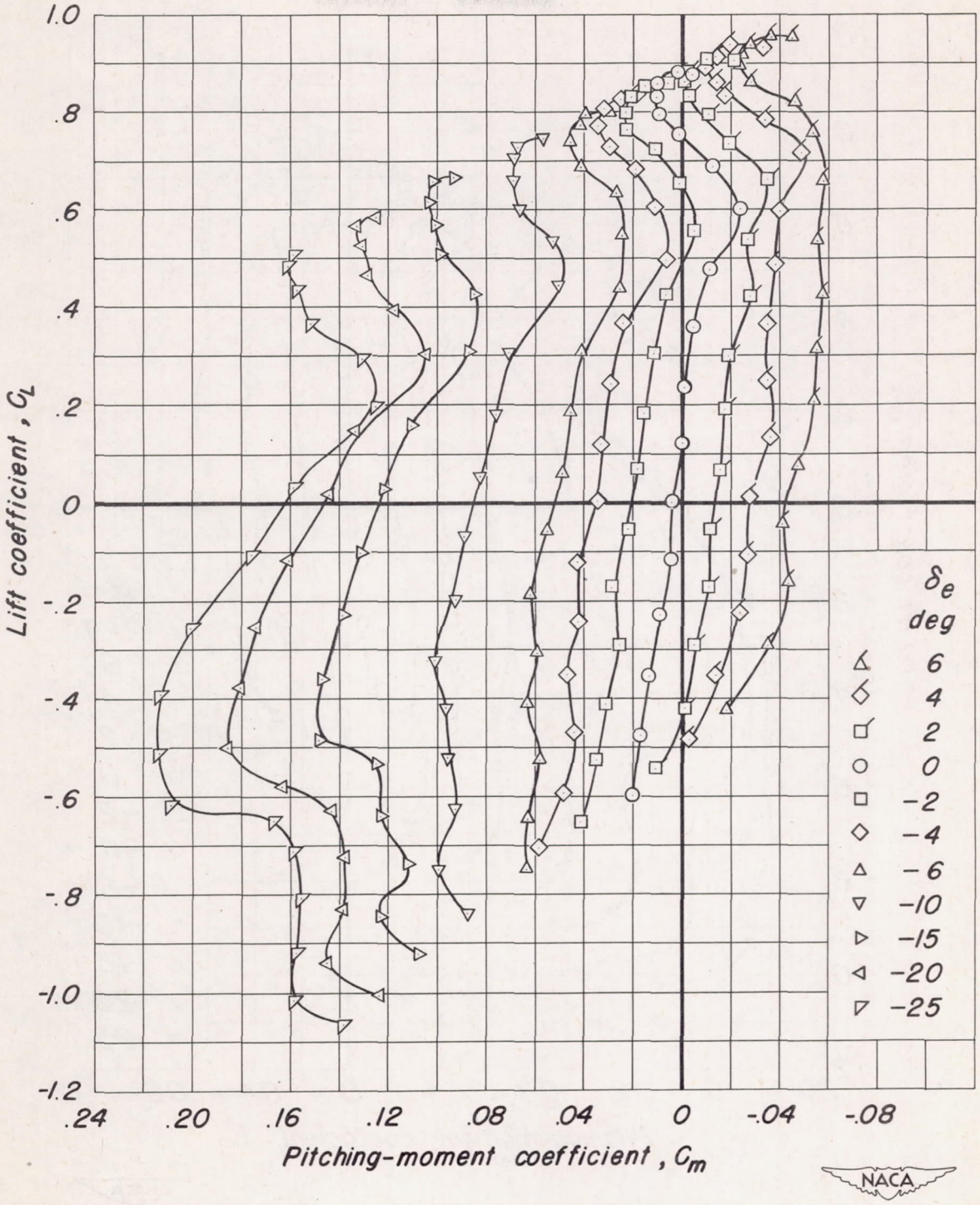

(a) M, 0.21.

Figure 10.– The variation of lift coefficient with pitching-moment coefficient. δ_t, 0°; R, 2,000,000.

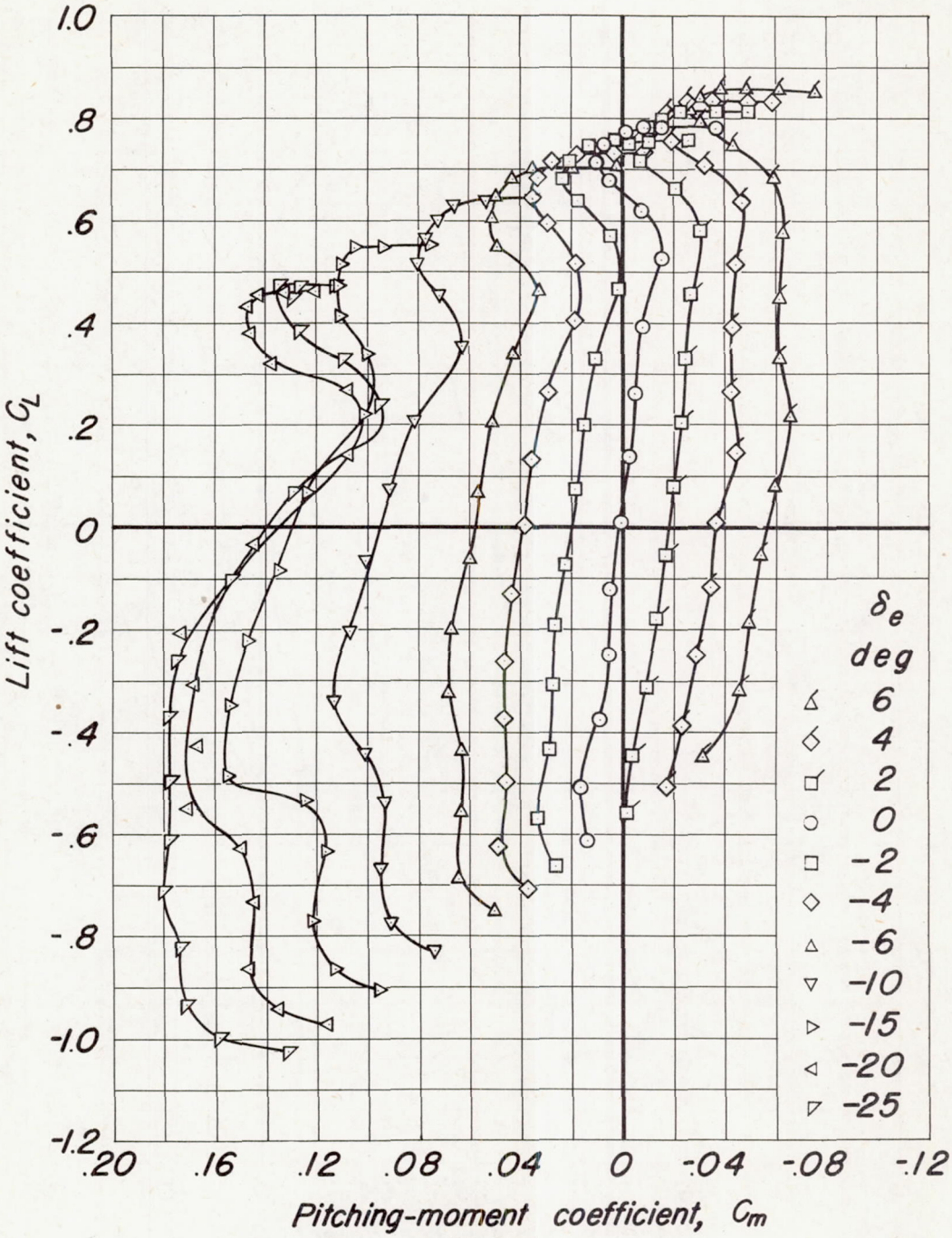

(b) M, 0.60.

Figure 10.— Continued.

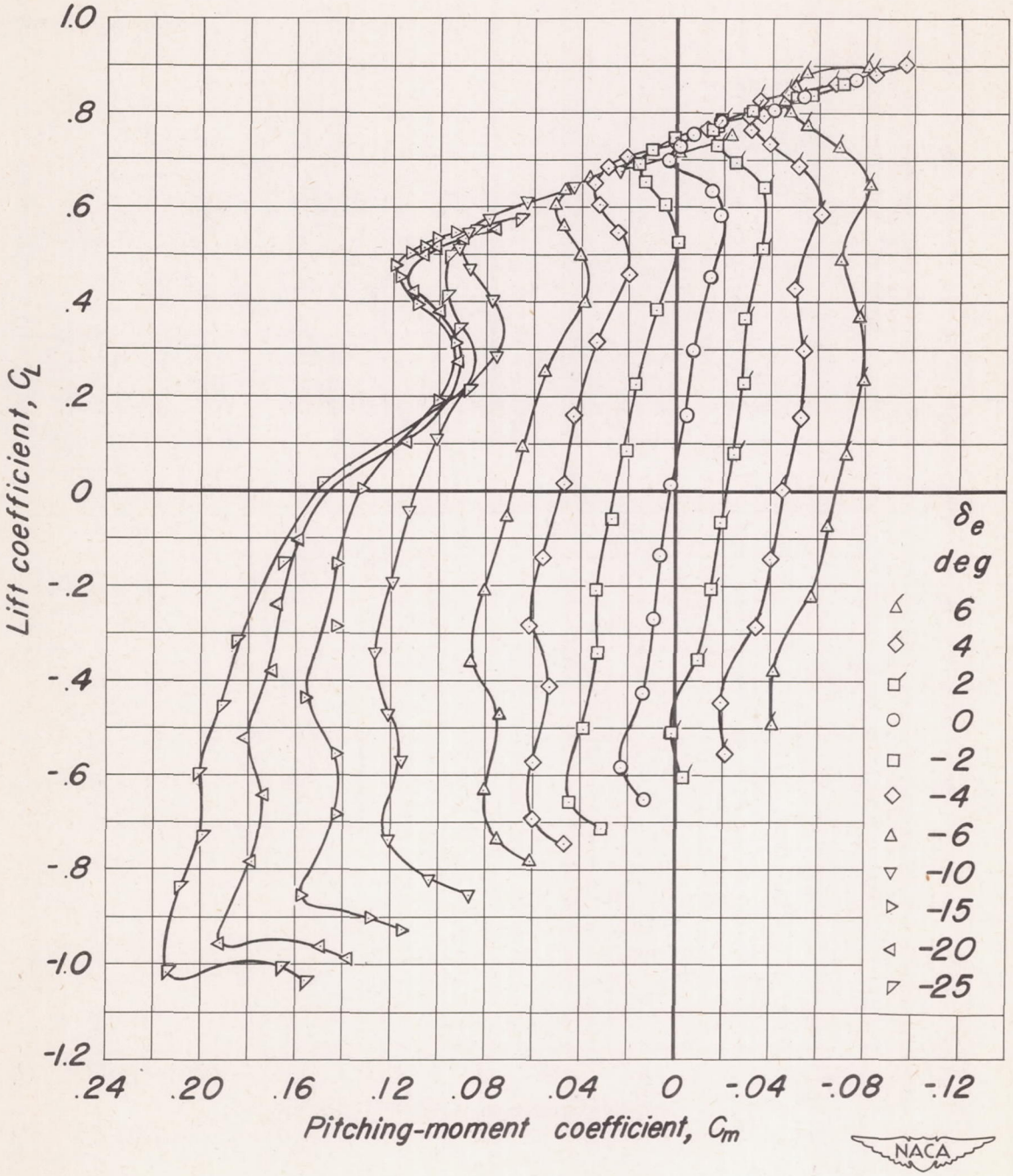

(c) M, 0.80.

Figure 10.— Continued.

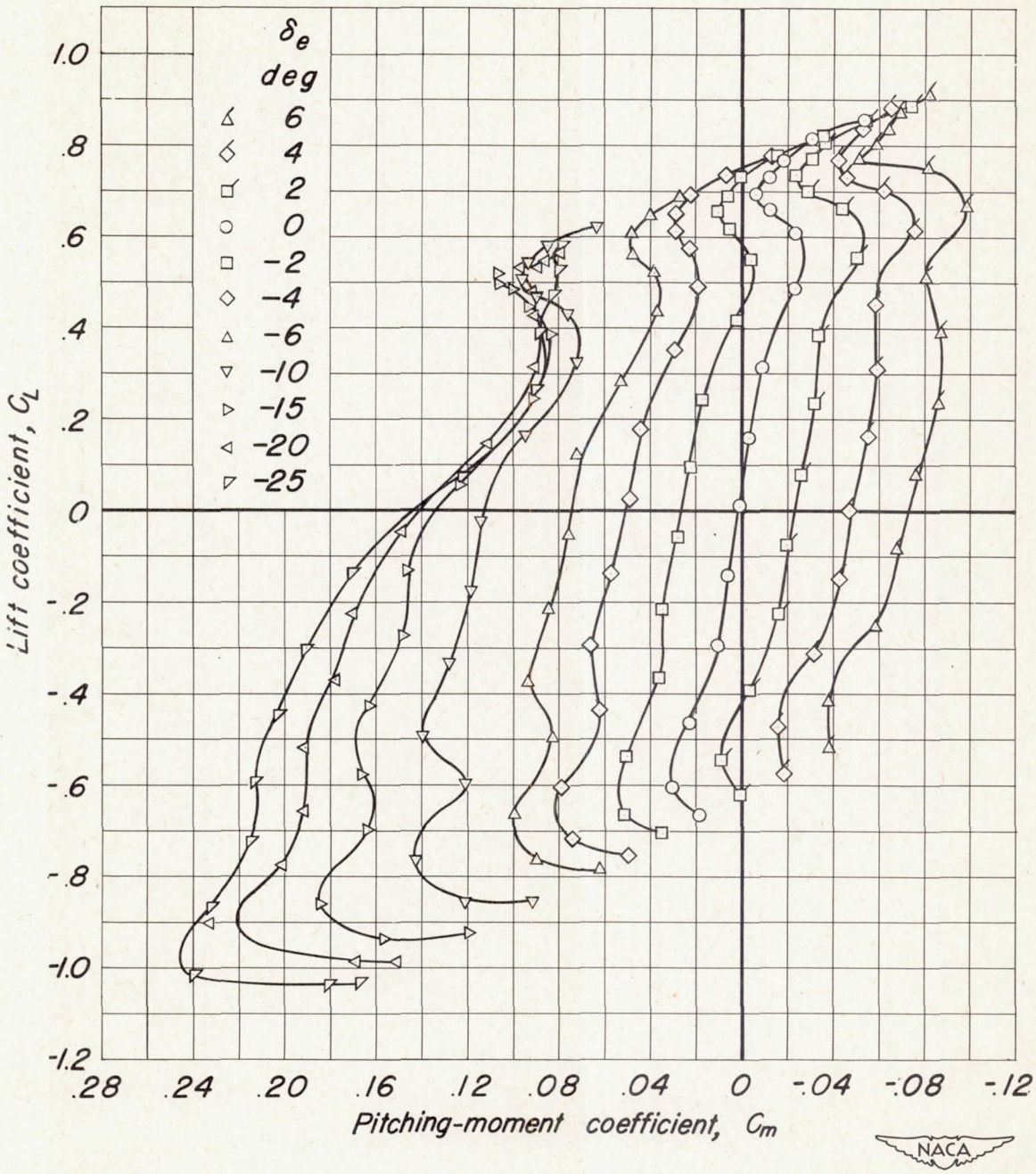

(d) M, 0.85.

Figure 10.— Continued.

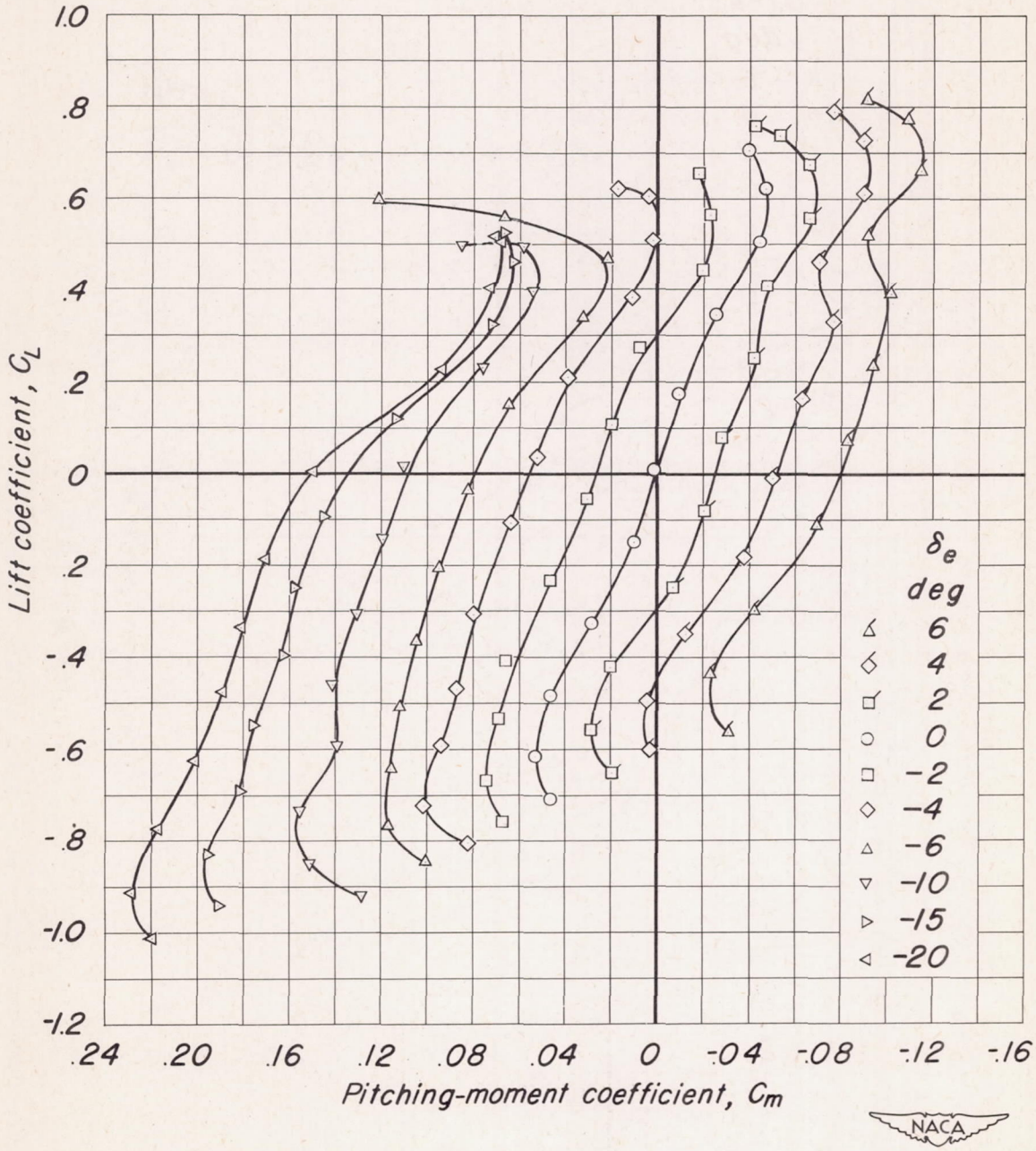

(e) M, 0.90.

Figure 10.— Continued.

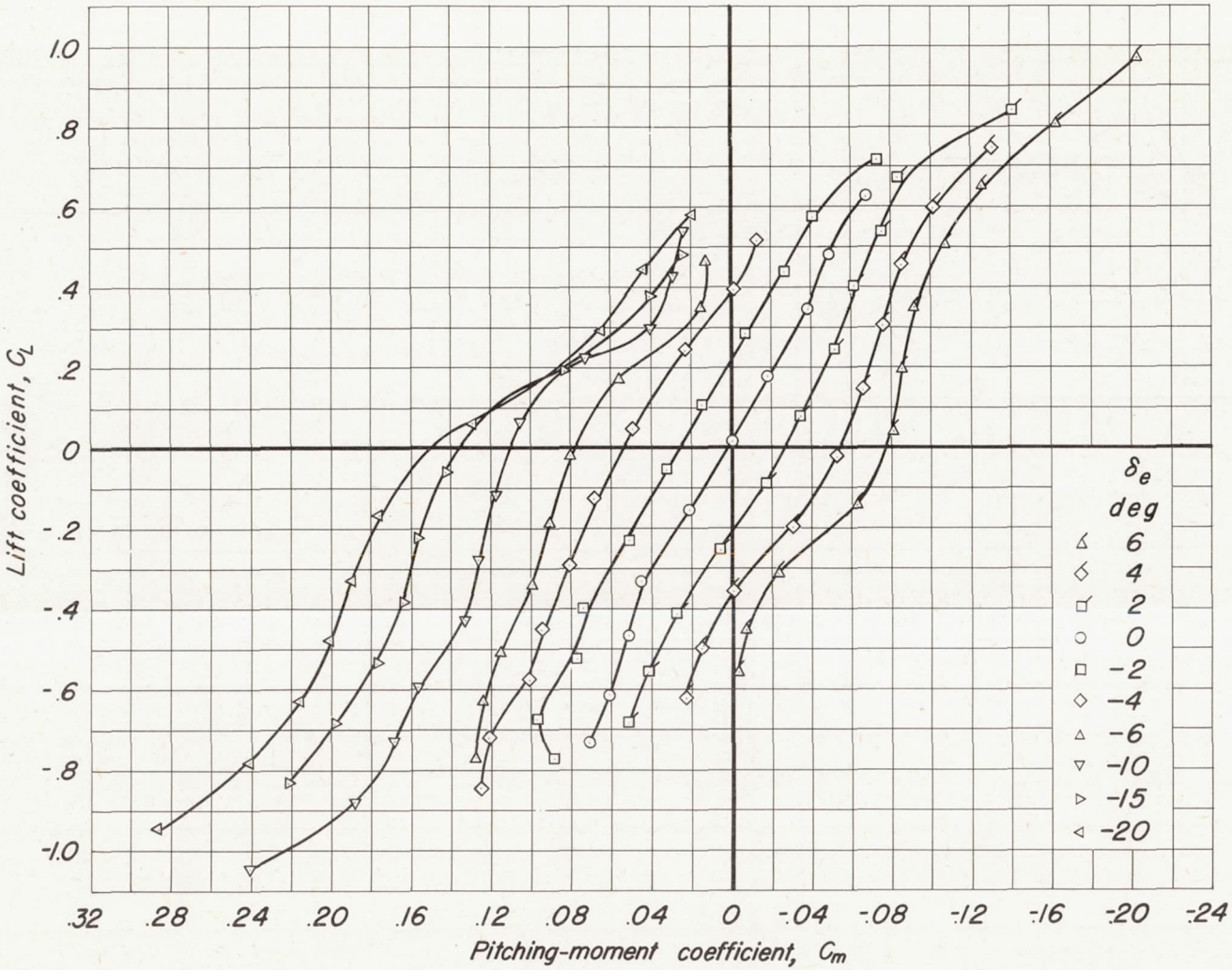

(f) M, 0.93.

Figure 10.— Continued.

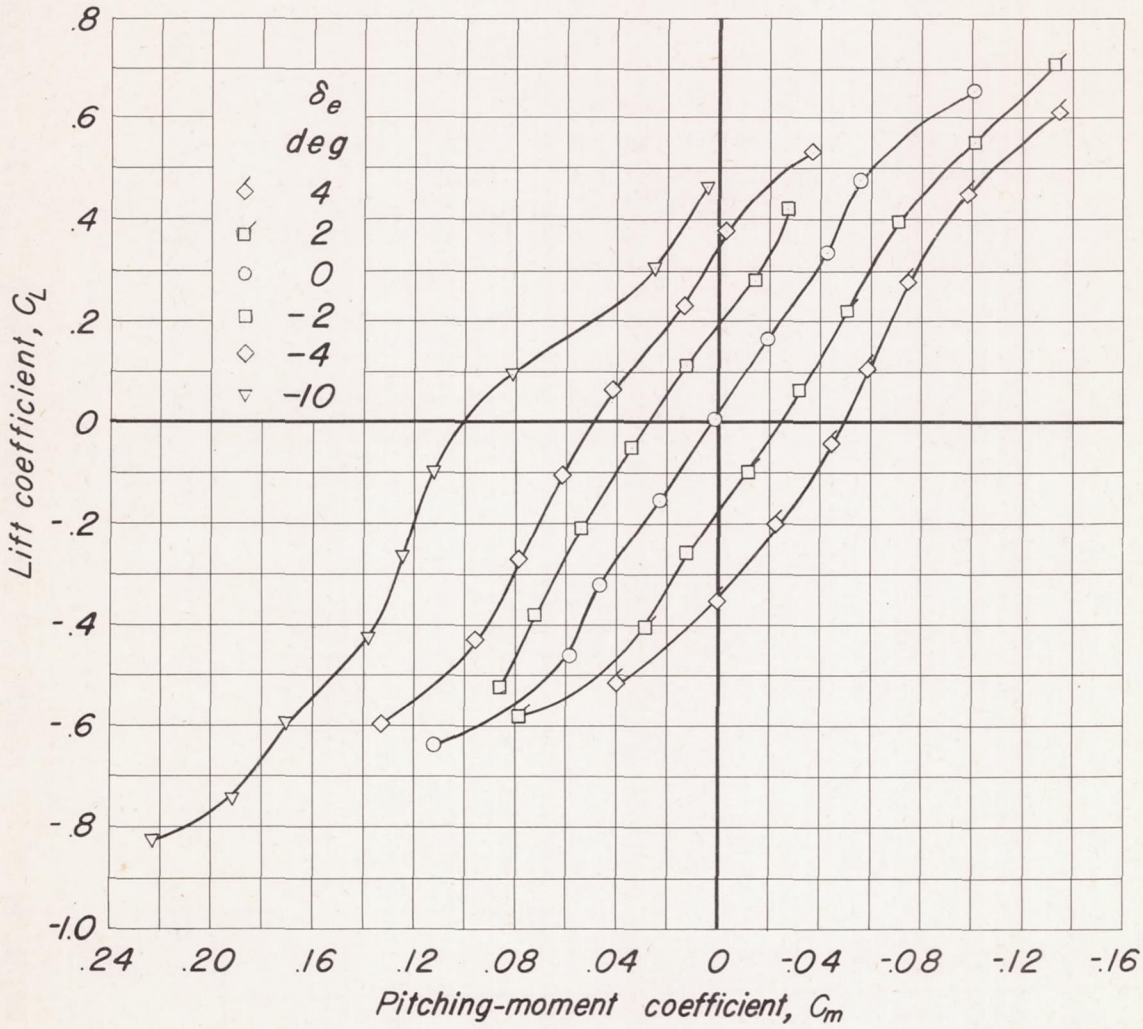

(g) M, 0.94.

Figure 10.— Concluded.

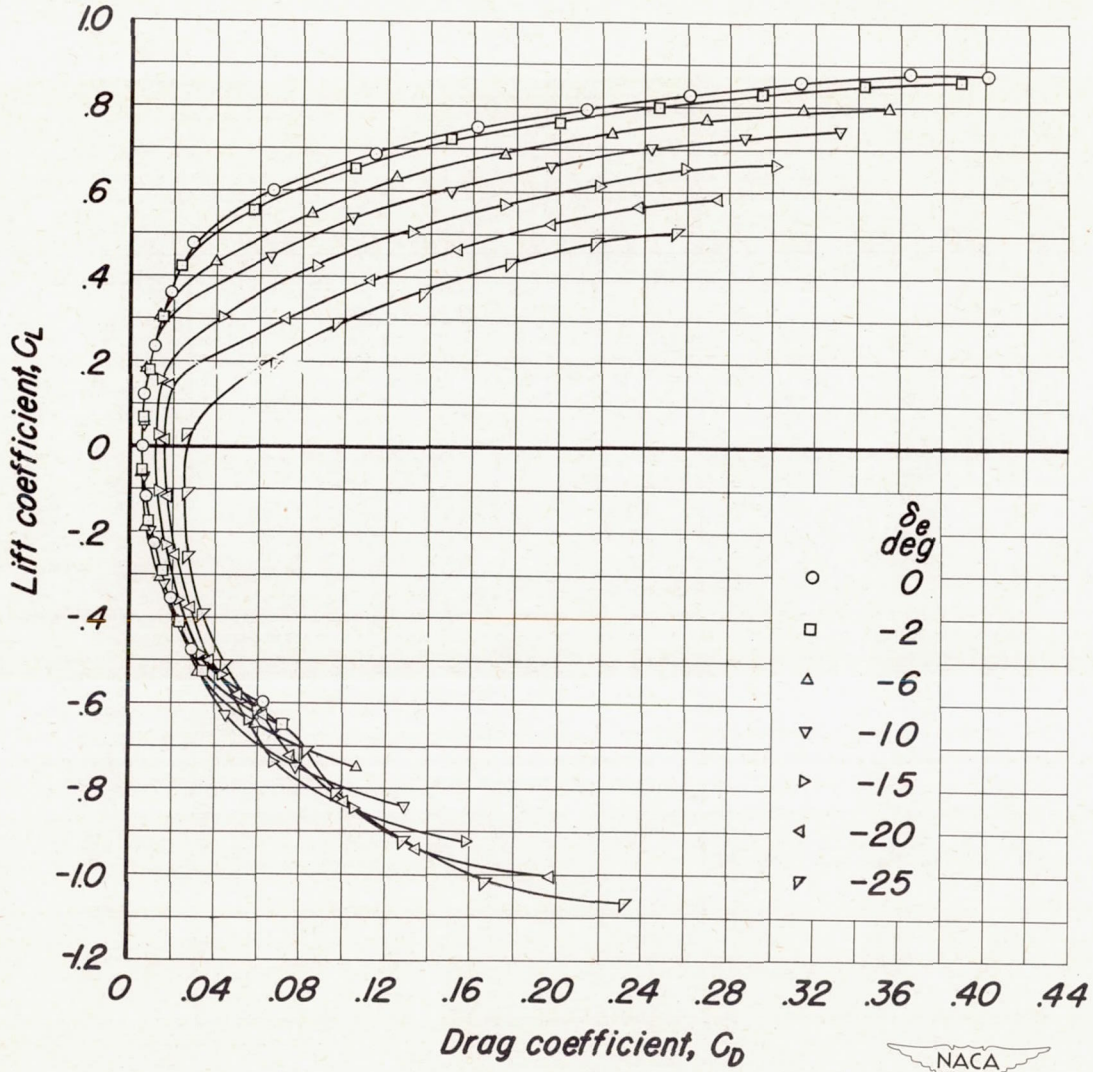

(a) M, 0.21.

Figure 11.– The variation of lift coefficient with drag coefficient. δ_f, 0°; R, 2,000,000.

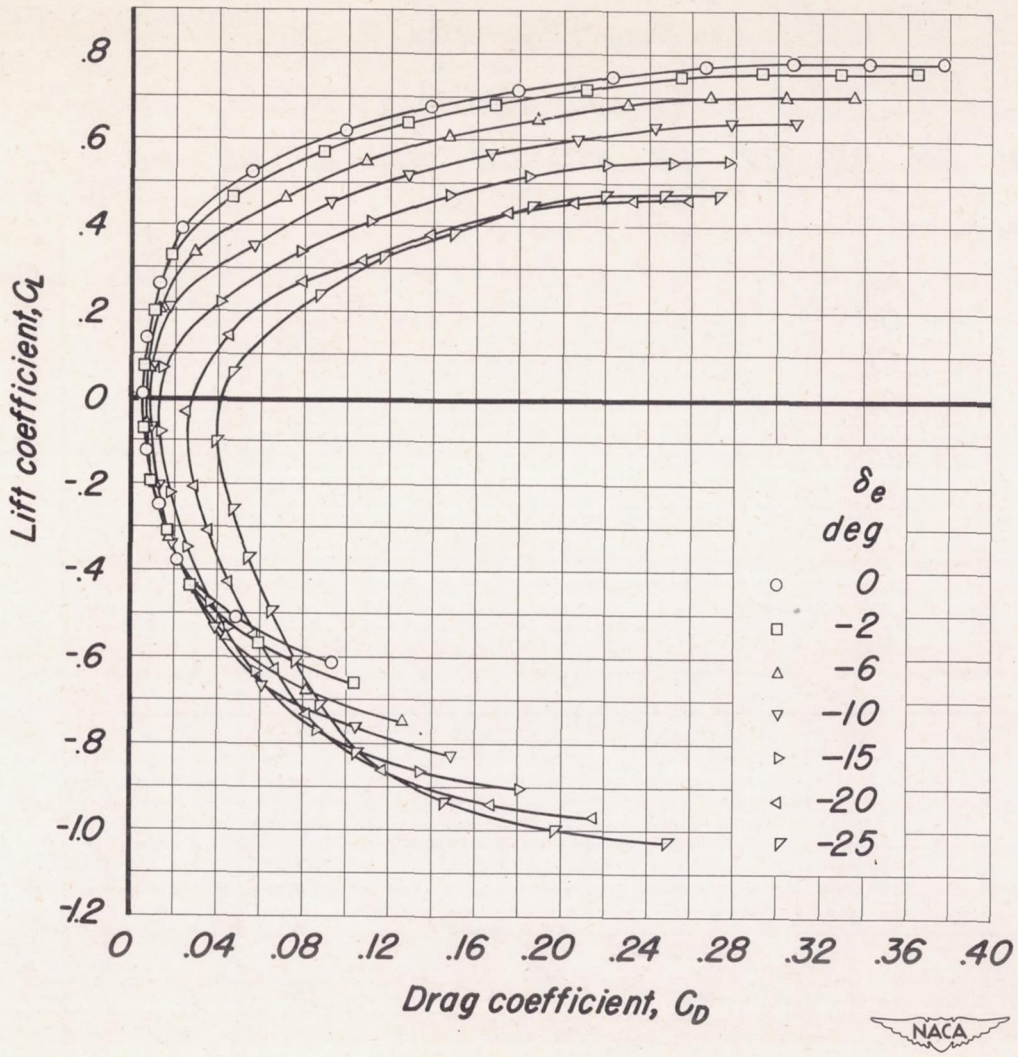

(b) M, 0.60.

Figure 11.—Continued.

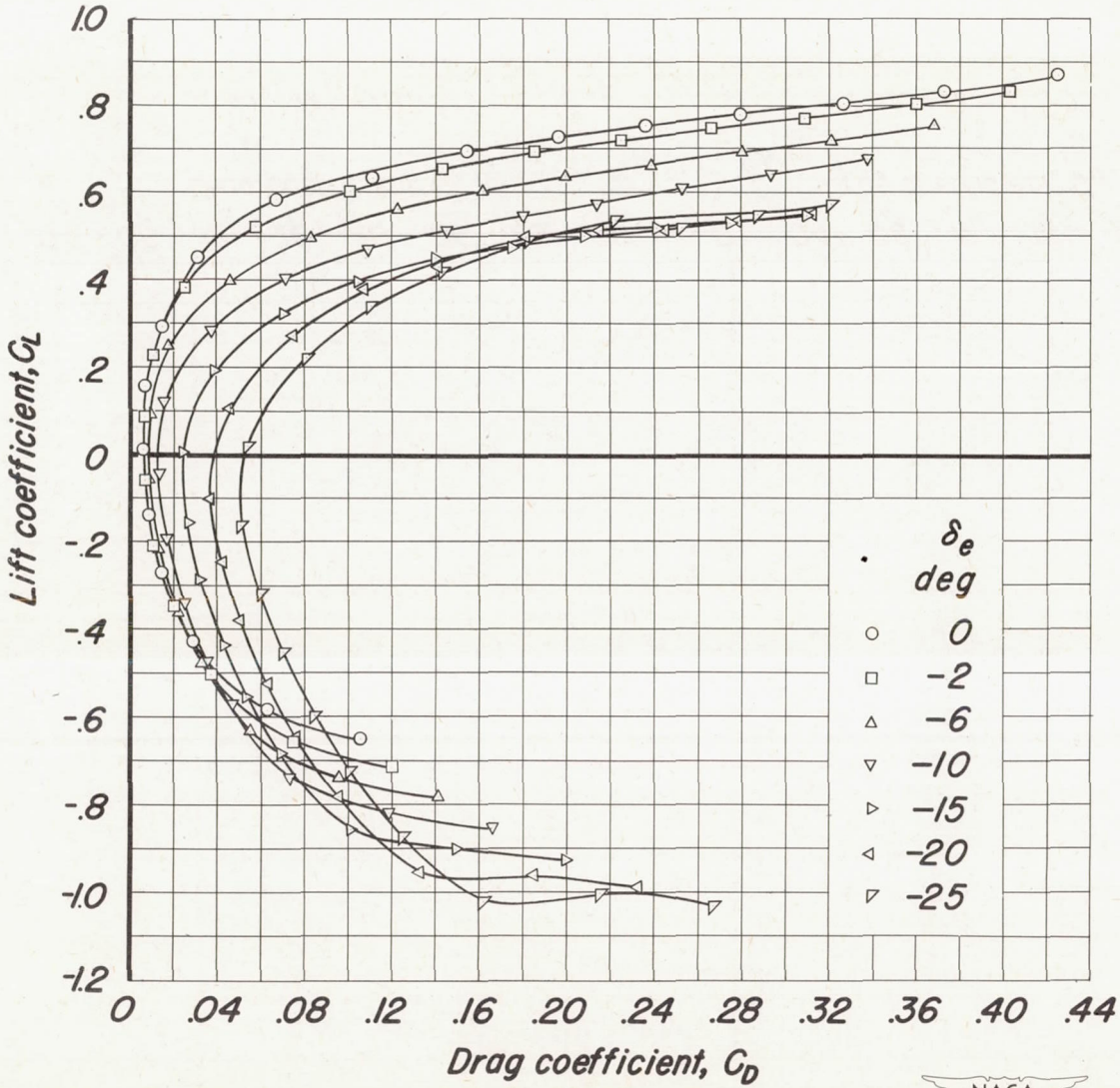

(c) M, 0.80.

Figure 11.—Continued.

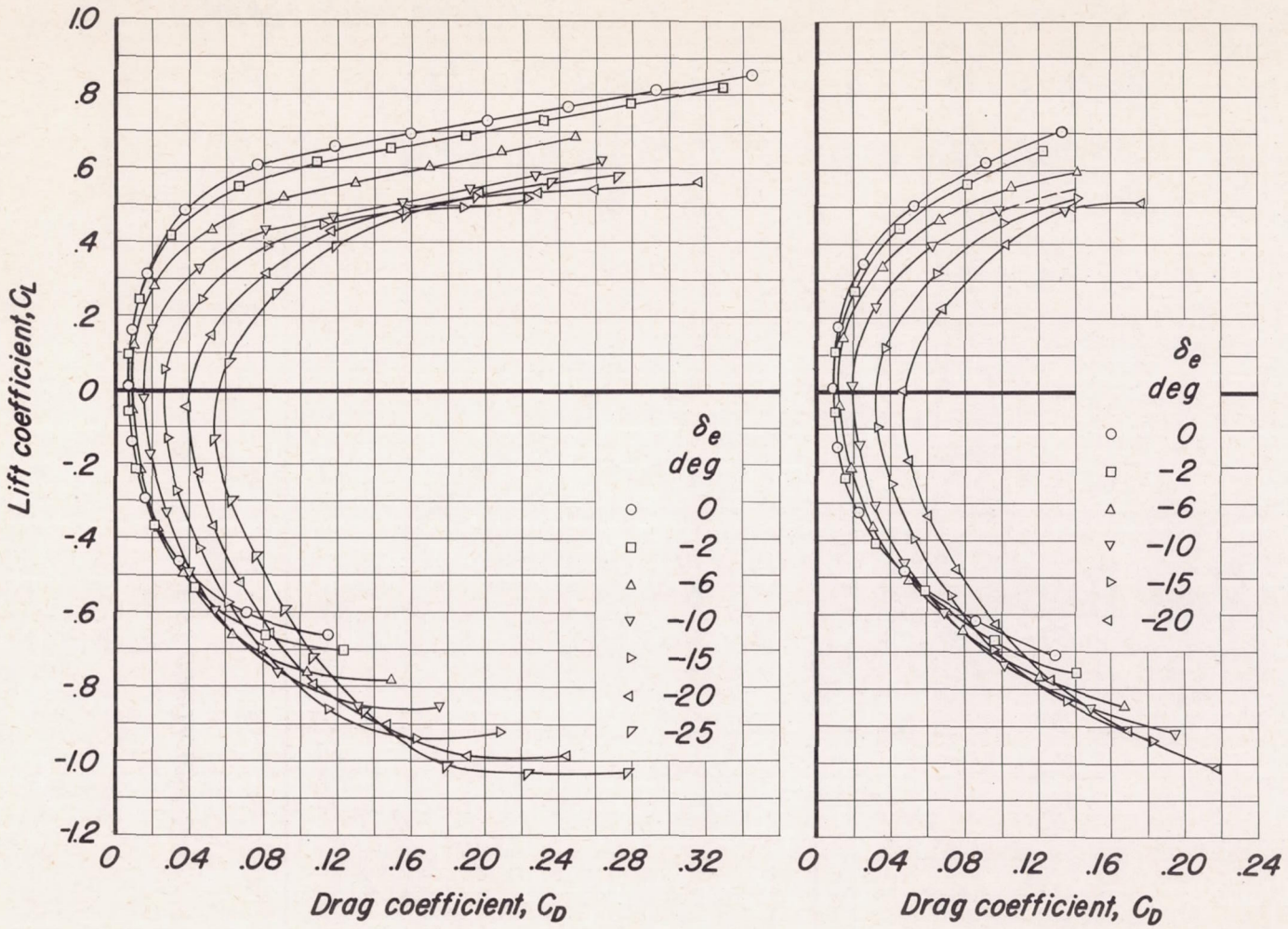

(d) M, 0.85.

(e) M, 0.90.

Figure 11.—Continued.

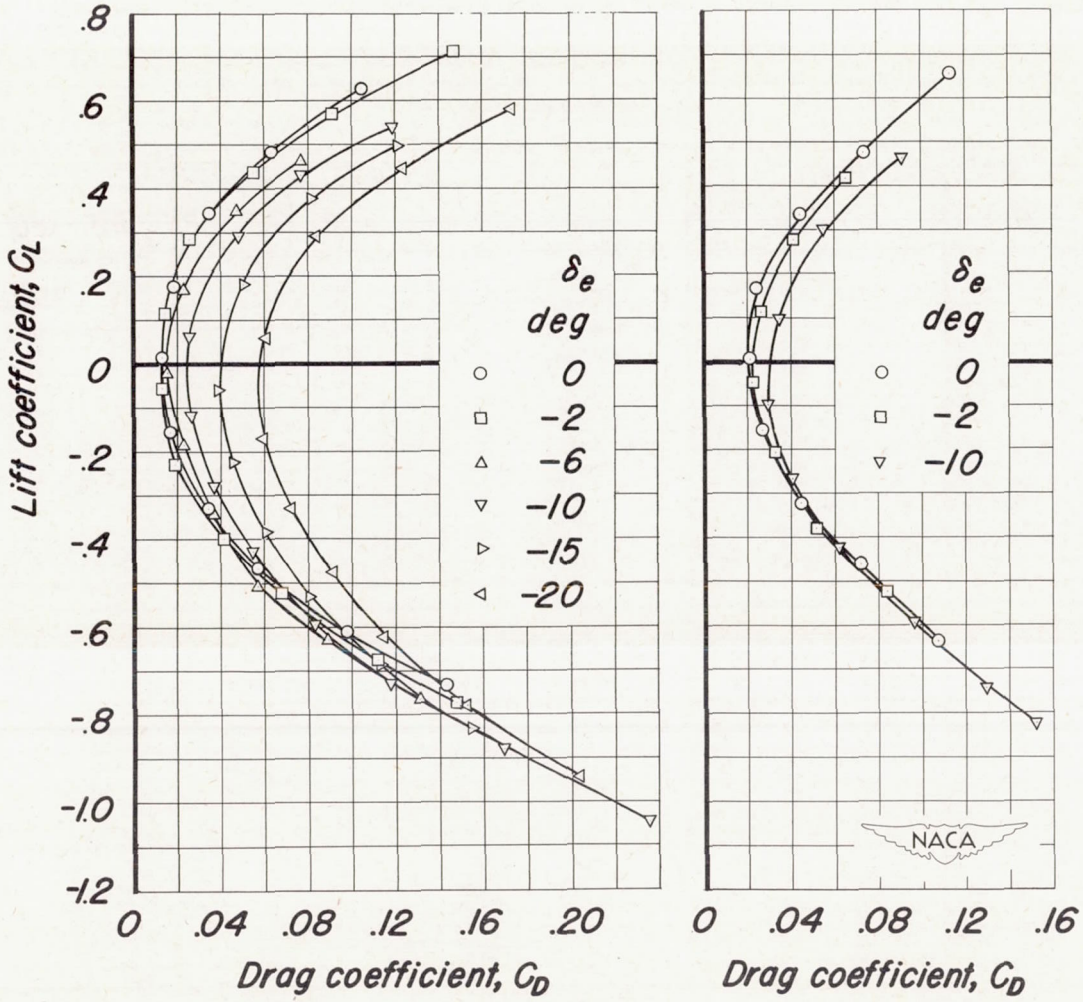

(f) M, 0.93.

(g) M, 0.94.

Figure 11.– Concluded.

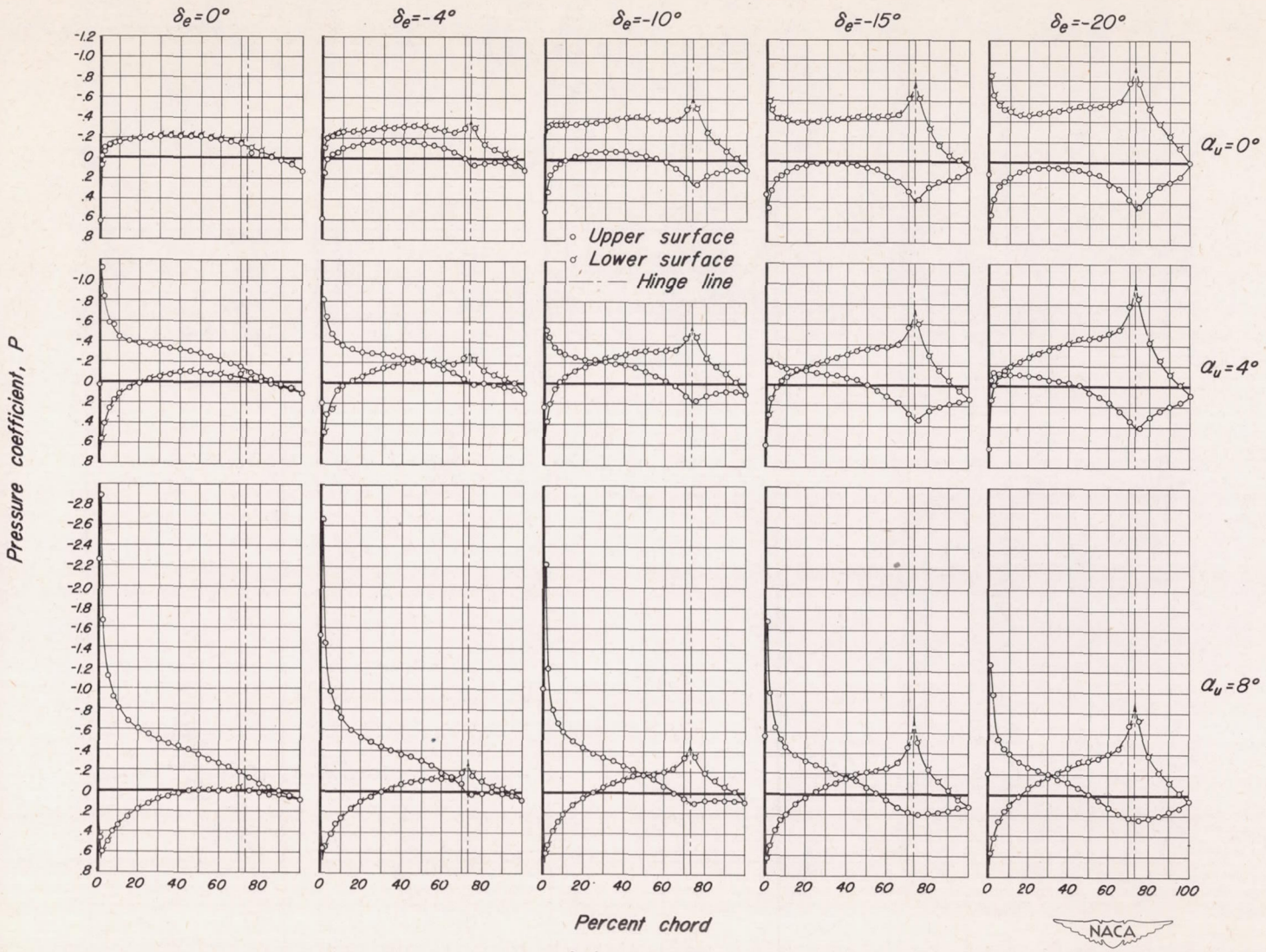

(a) M, 0.21.

Figure 12.– The streamwise distribution of pressure coefficient at 50 percent of the semispan. δ_f, 0°; R, 2,000,000.

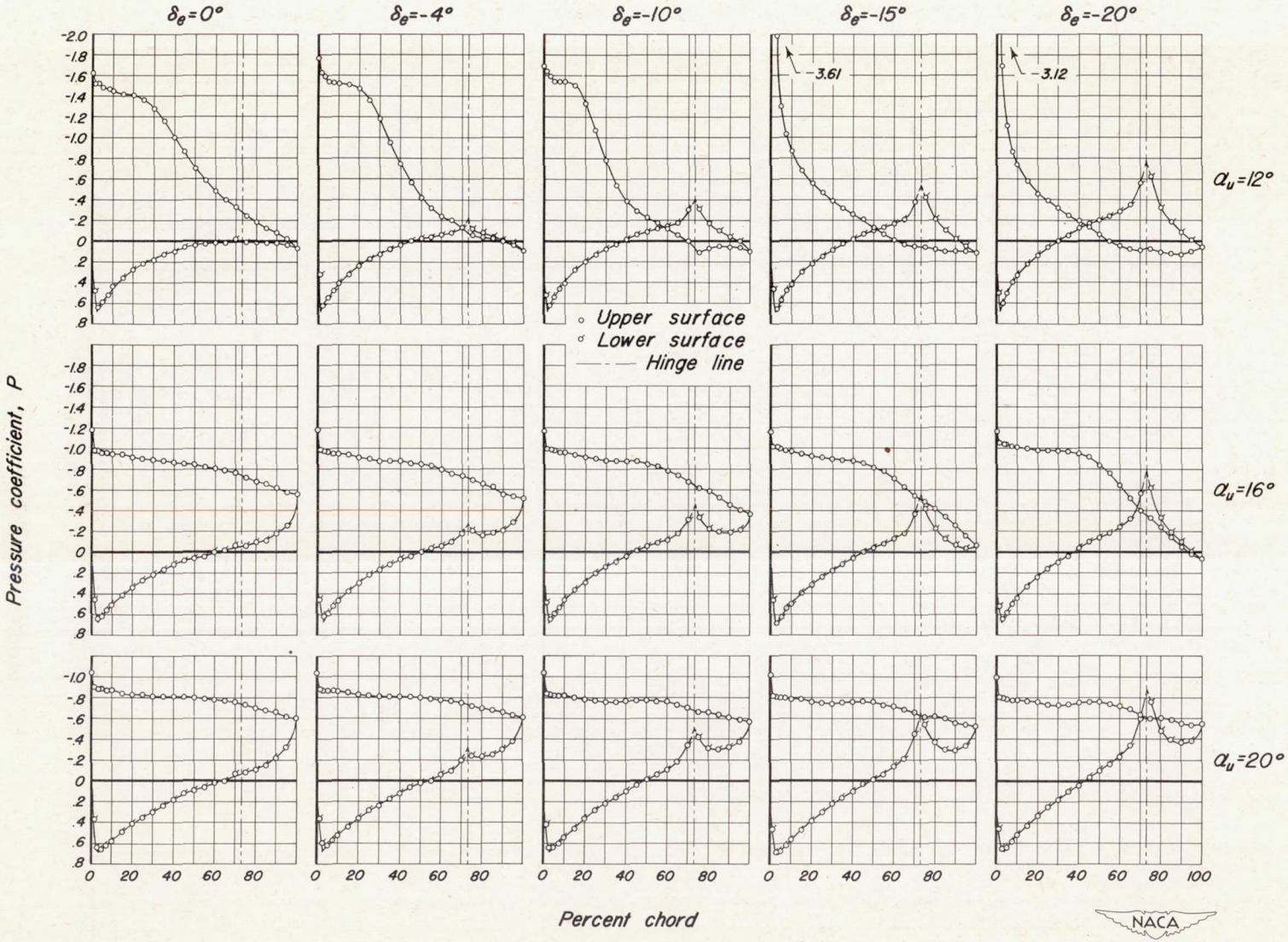

(b) M, 0.21, concluded.

Figure 12.—Continued.

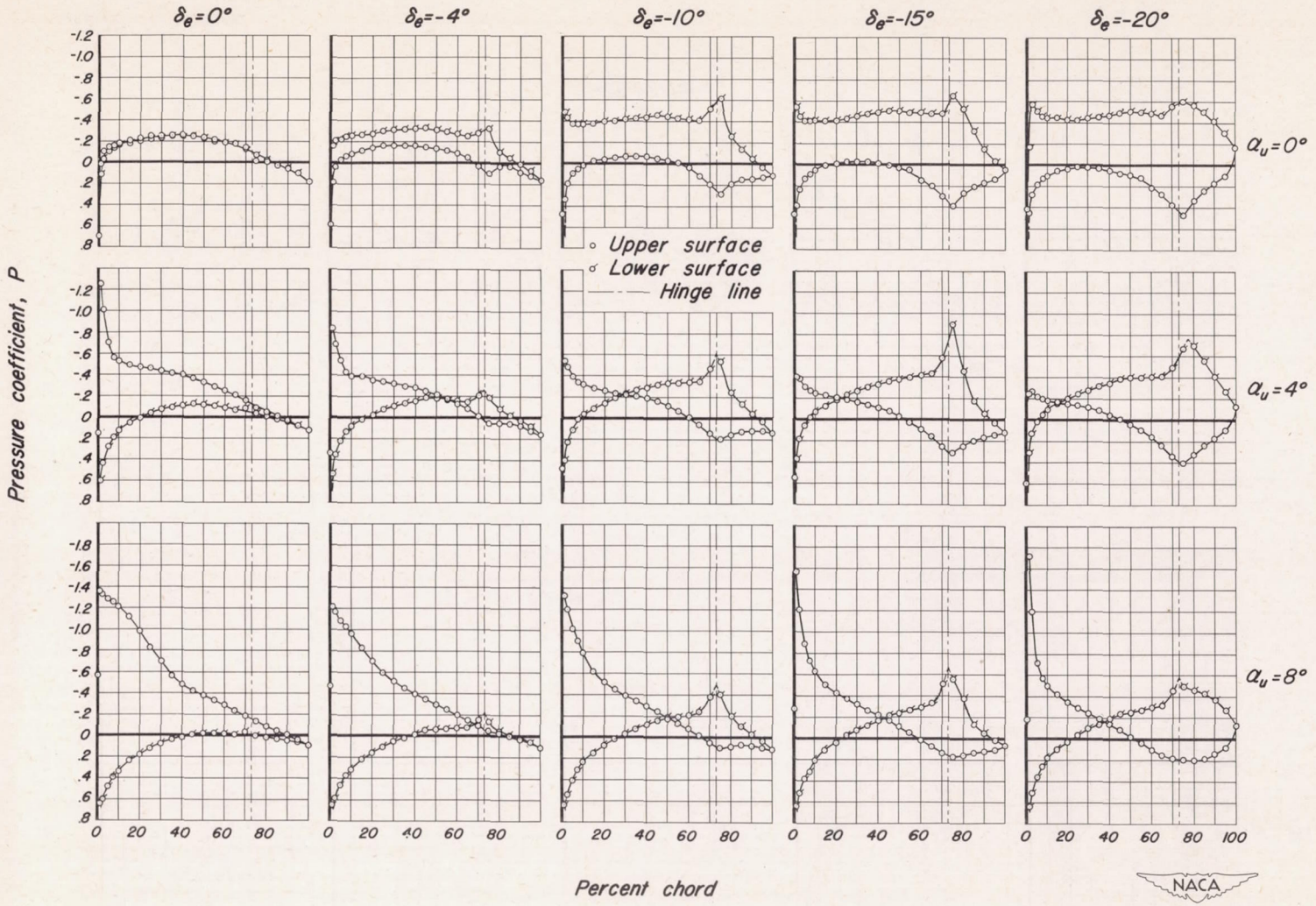

(c) M, 0.60.

Figure 12.—Continued.

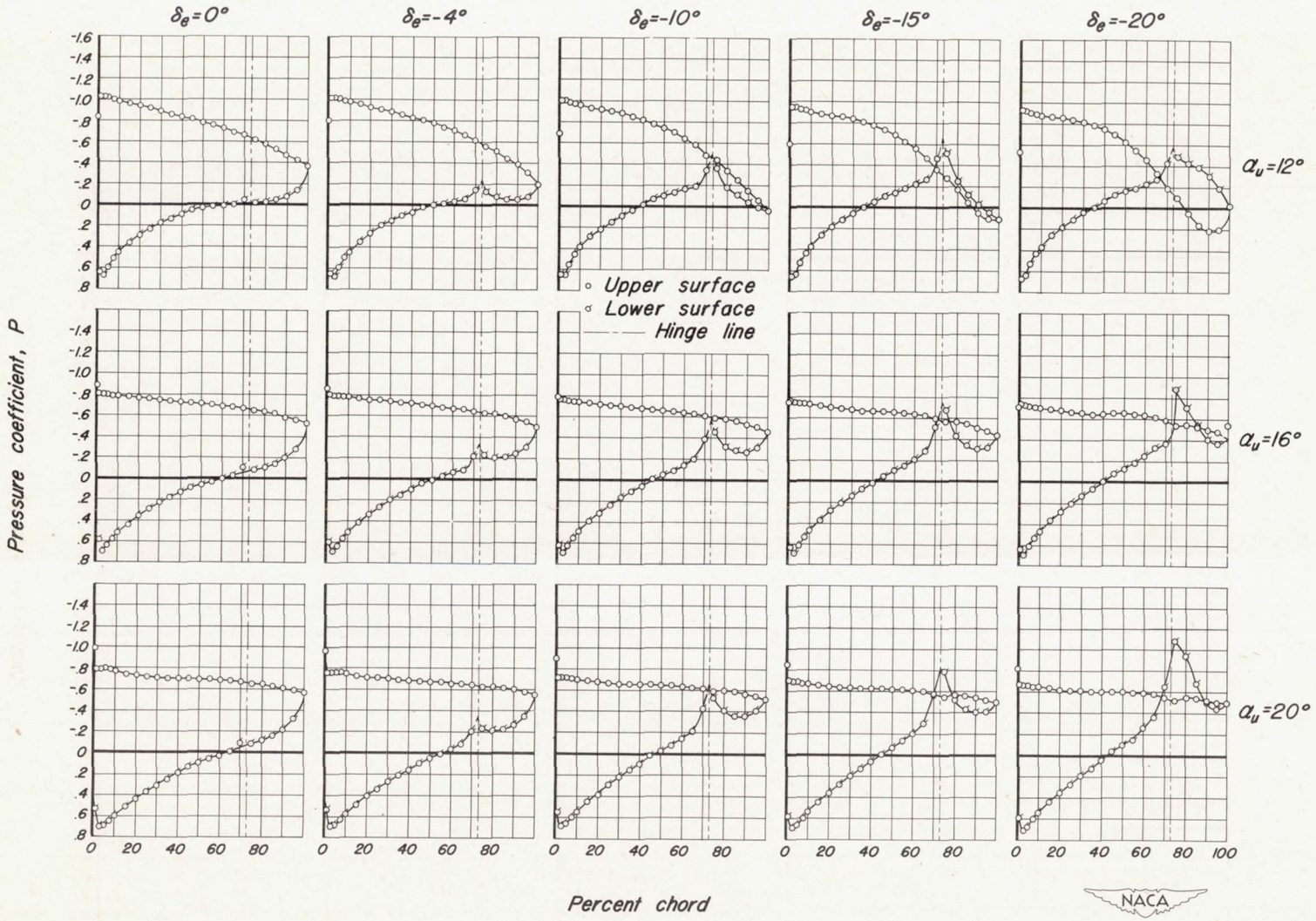

(d) M, 0.60, concluded.

Figure 12.—Continued.

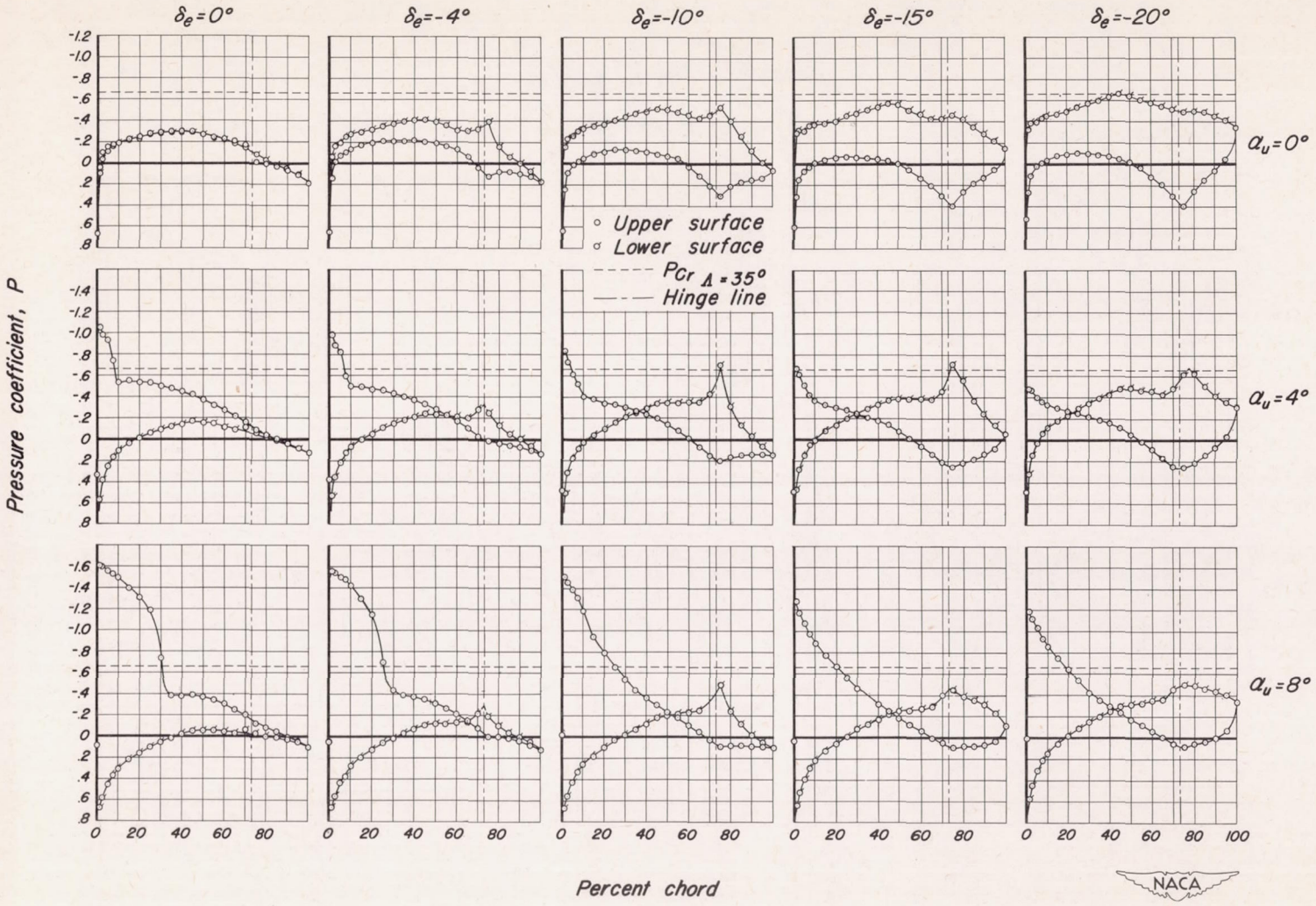

(e) M, 0.80.

Figure 12.—Continued.

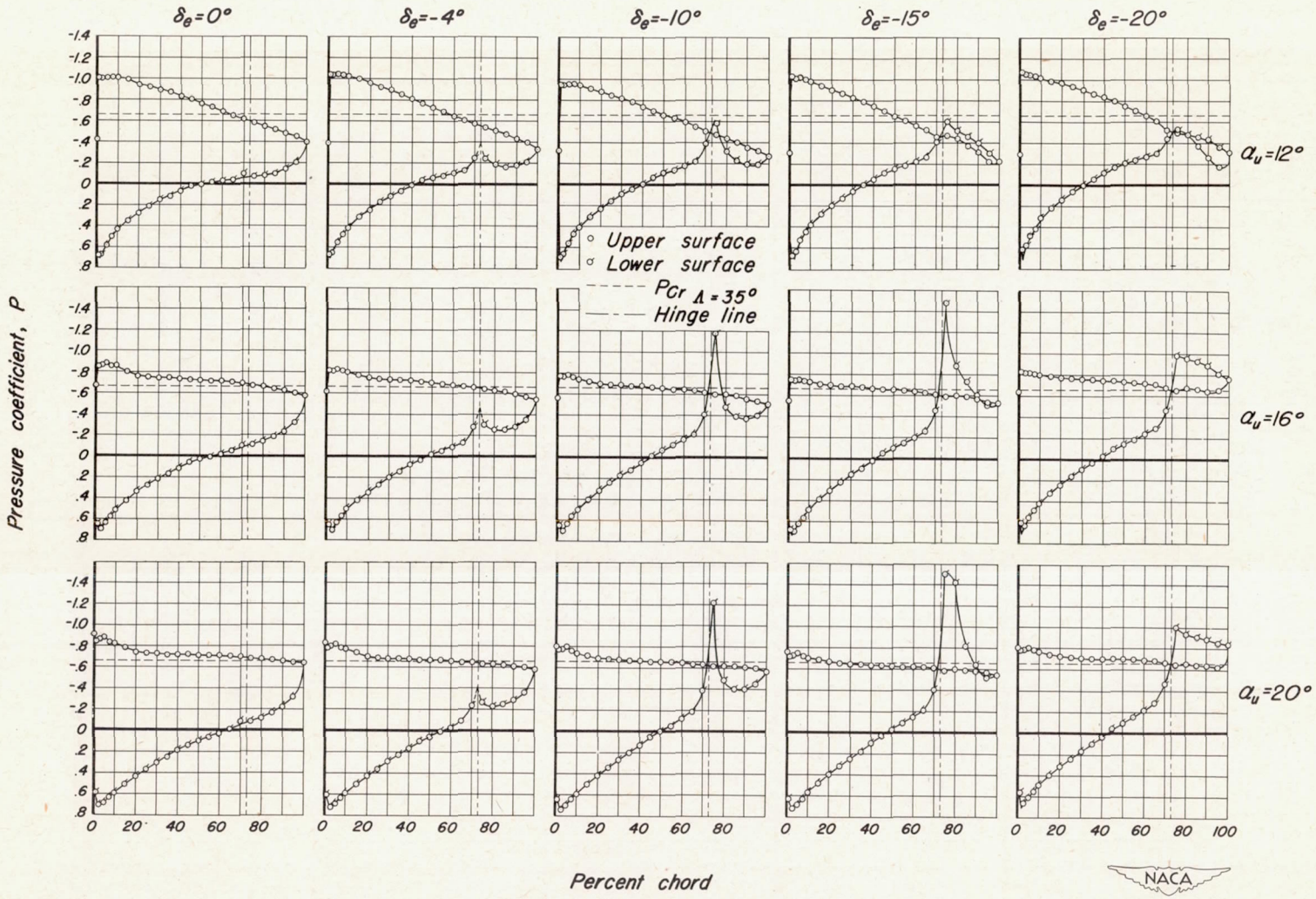

(f) M, 0.80, concluded.

Figure 12.—Continued.

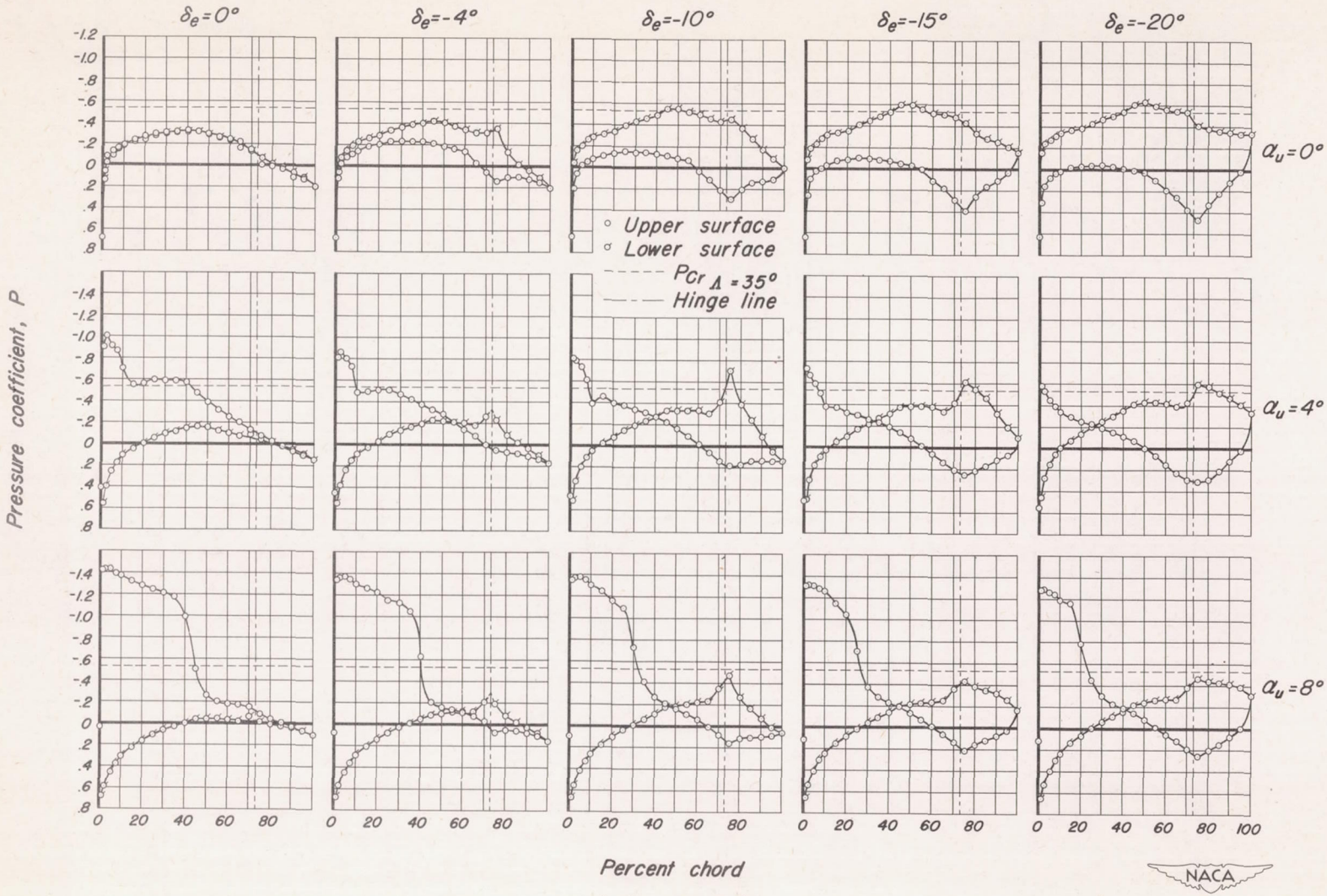

(g) M, 0.85.

Figure 12.—Continued.

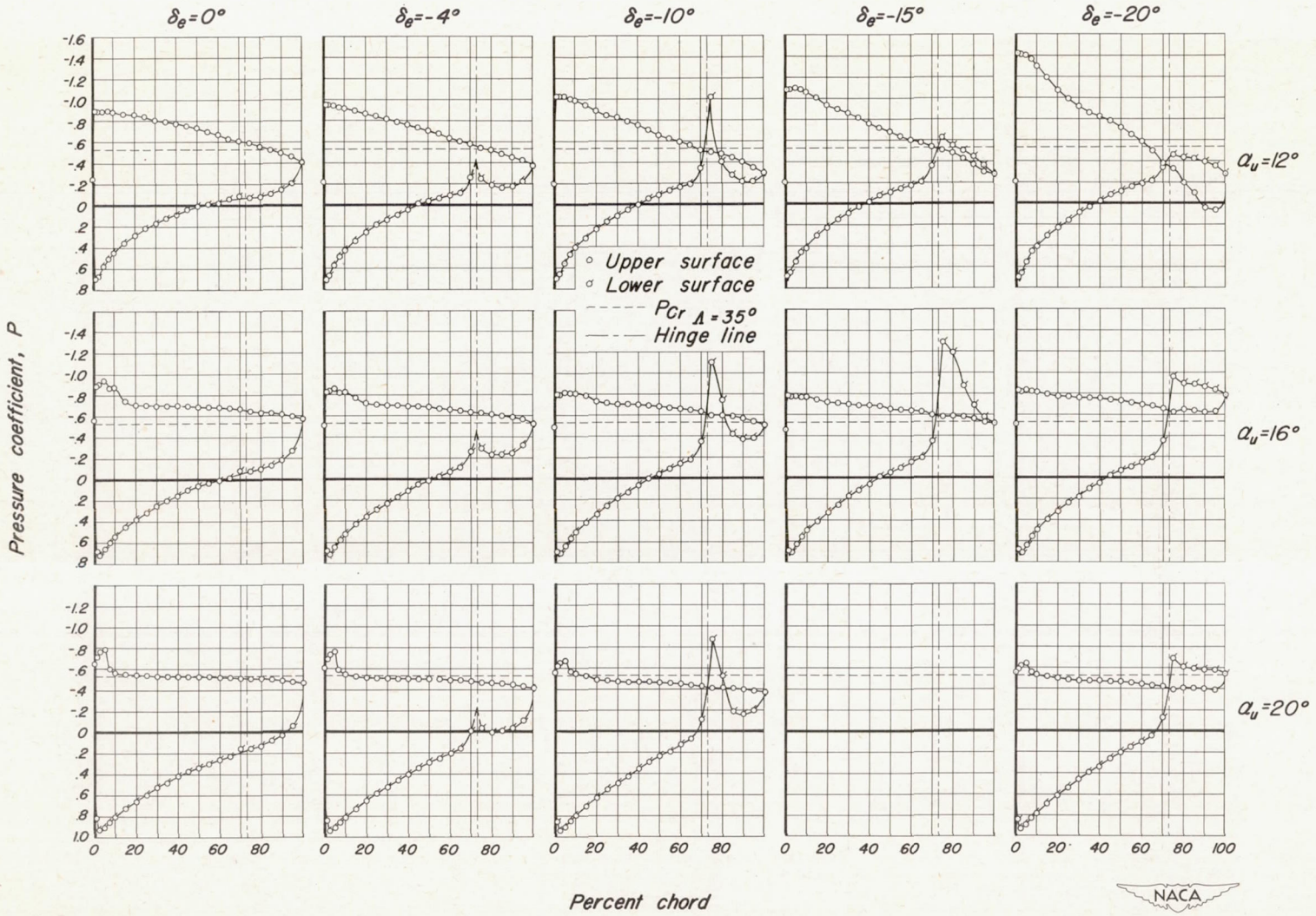

(h) M, 0.85, concluded.

Figure 12.—Continued.

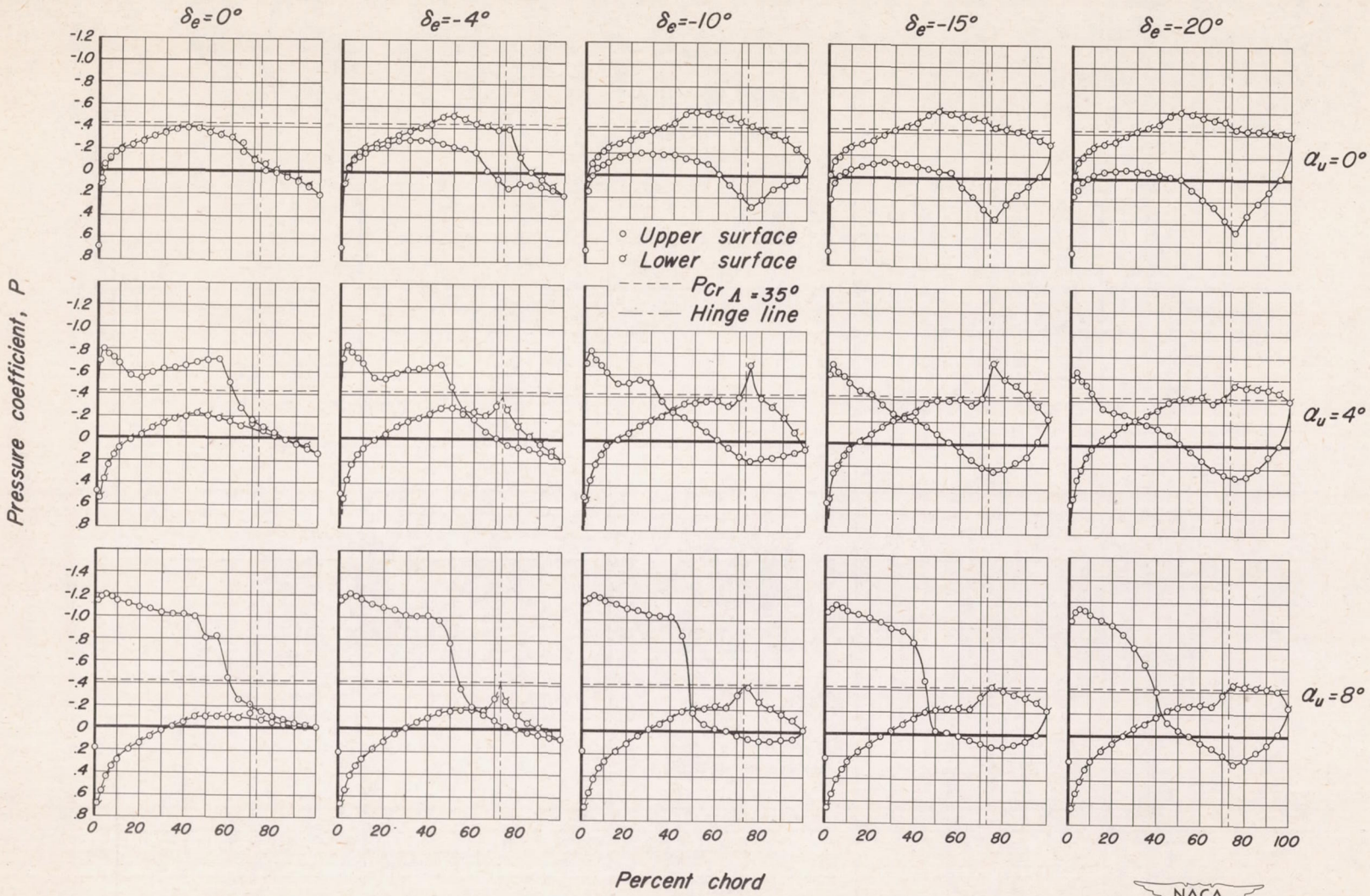

(i) M, 0.90.

Figure 12.—Continued.

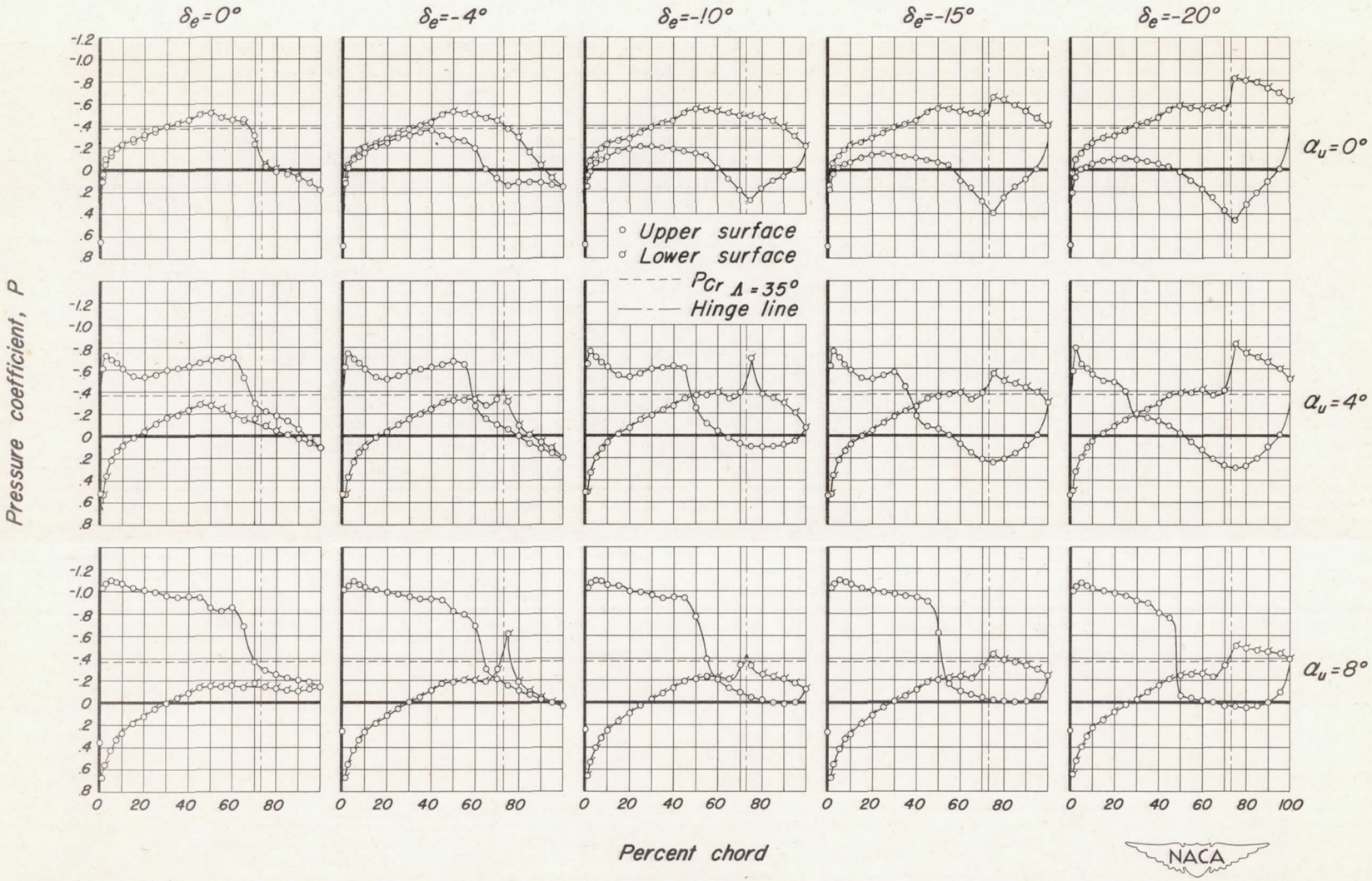

(j) M, 0.93.

Figure 12.—Continued.

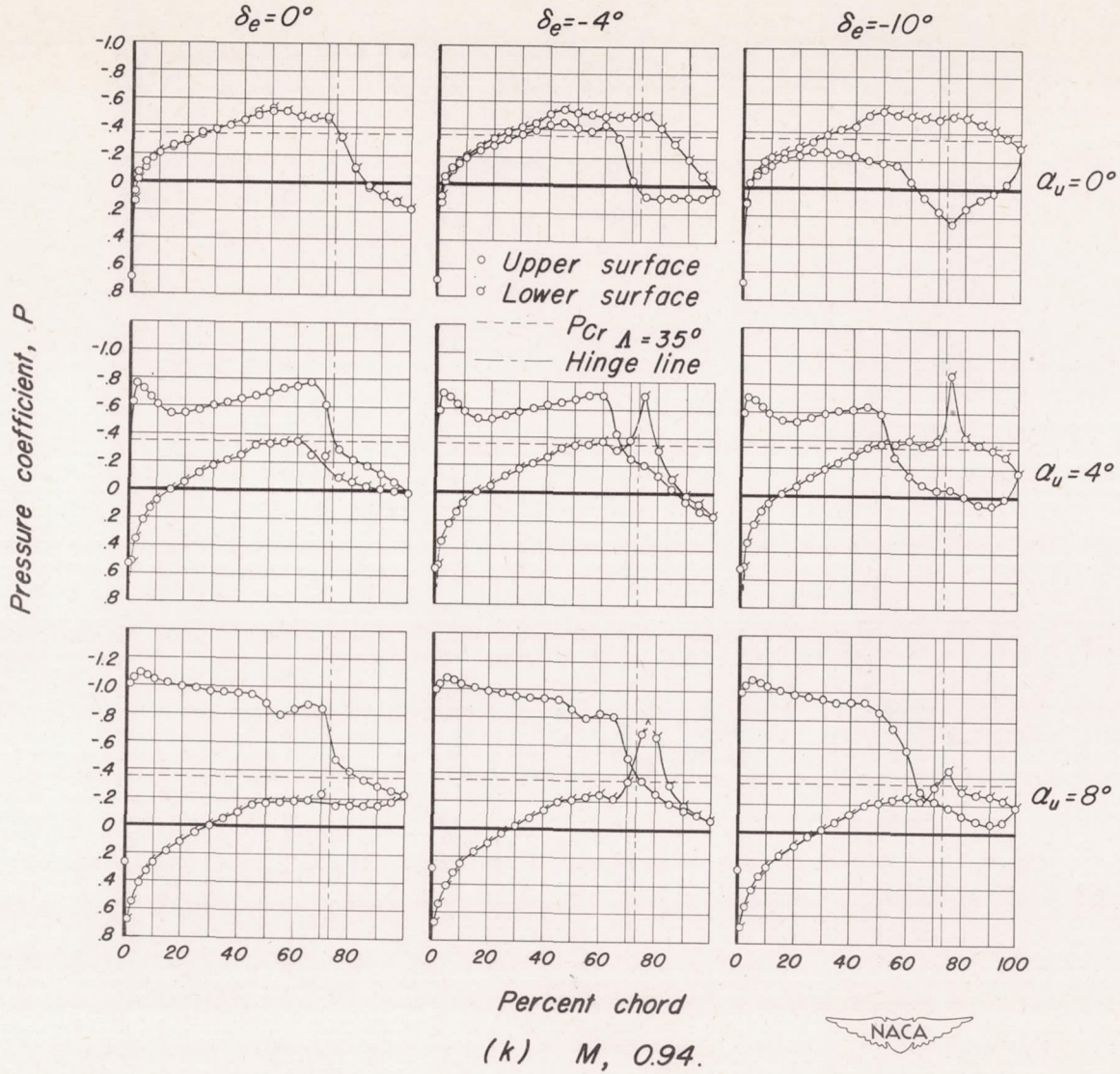

(k) M, 0.94.

Figure 12.— Concluded.

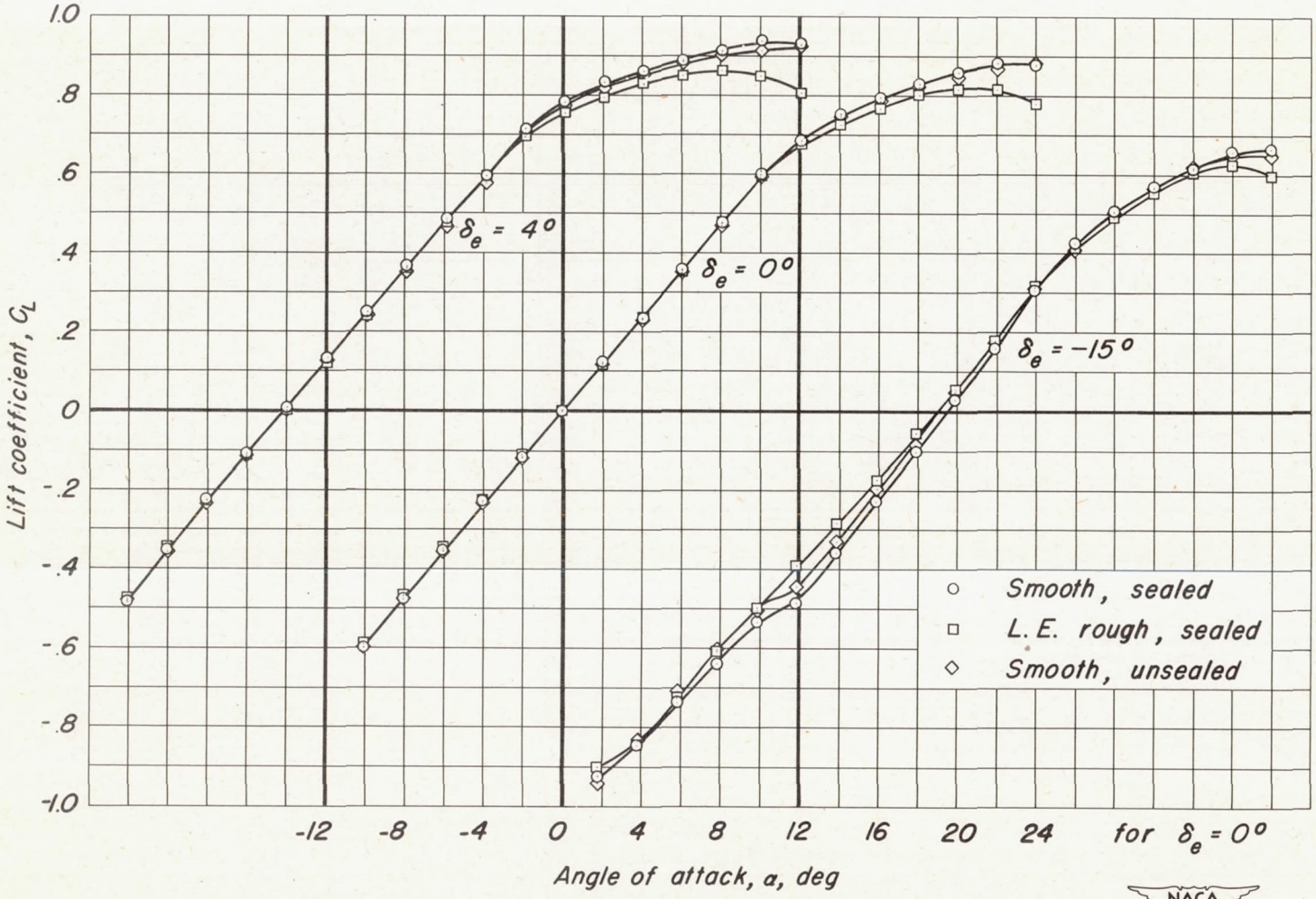

(a) M, 0.21.

Figure 13.– The independent effects of leading-edge roughness and removal of the elevator-nose seal on the variation of lift coefficient with angle of attack. δ_t, 0°; R, 2,000,000.

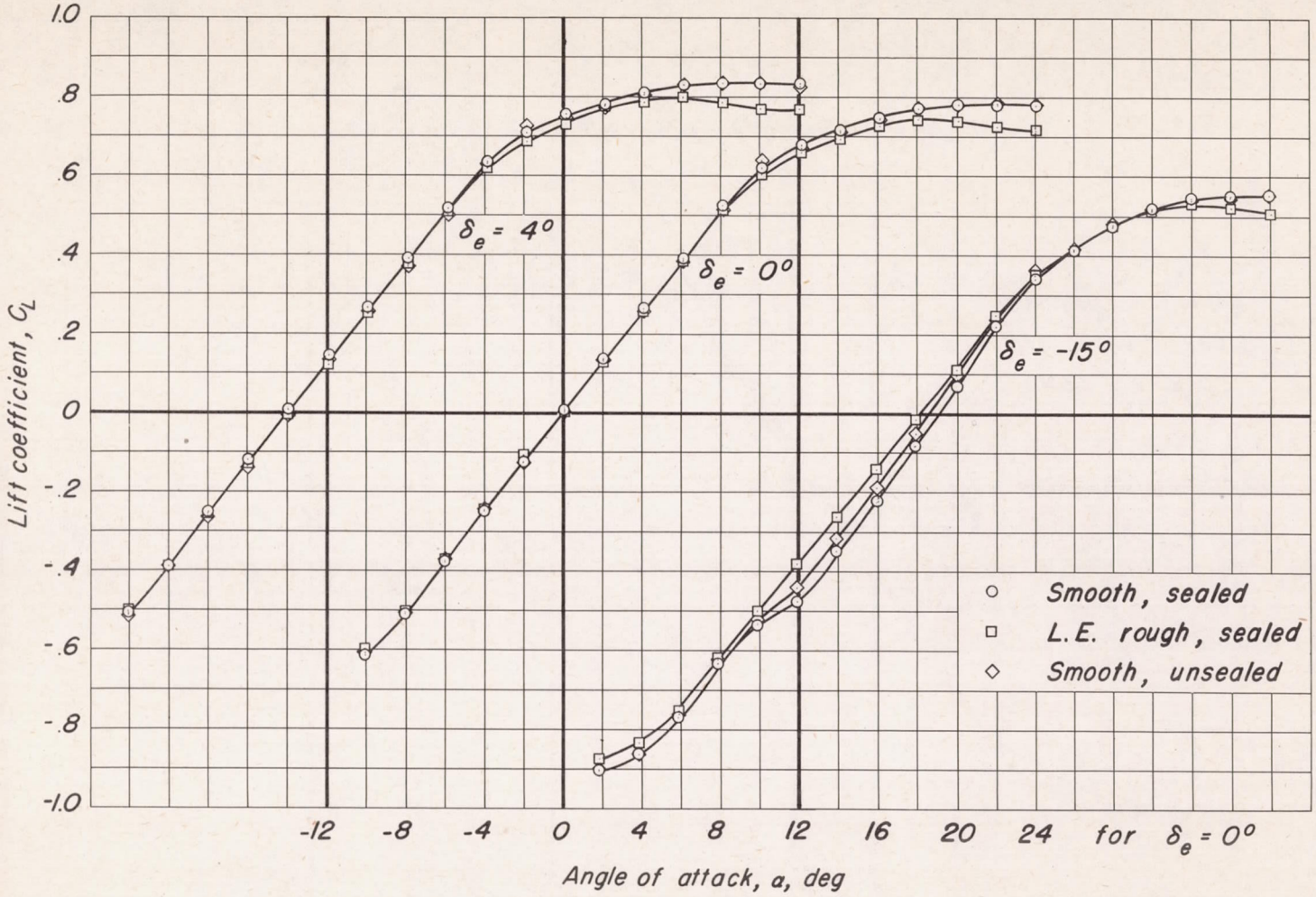

(b) M, 0.60.

Figure 13.– Continued.

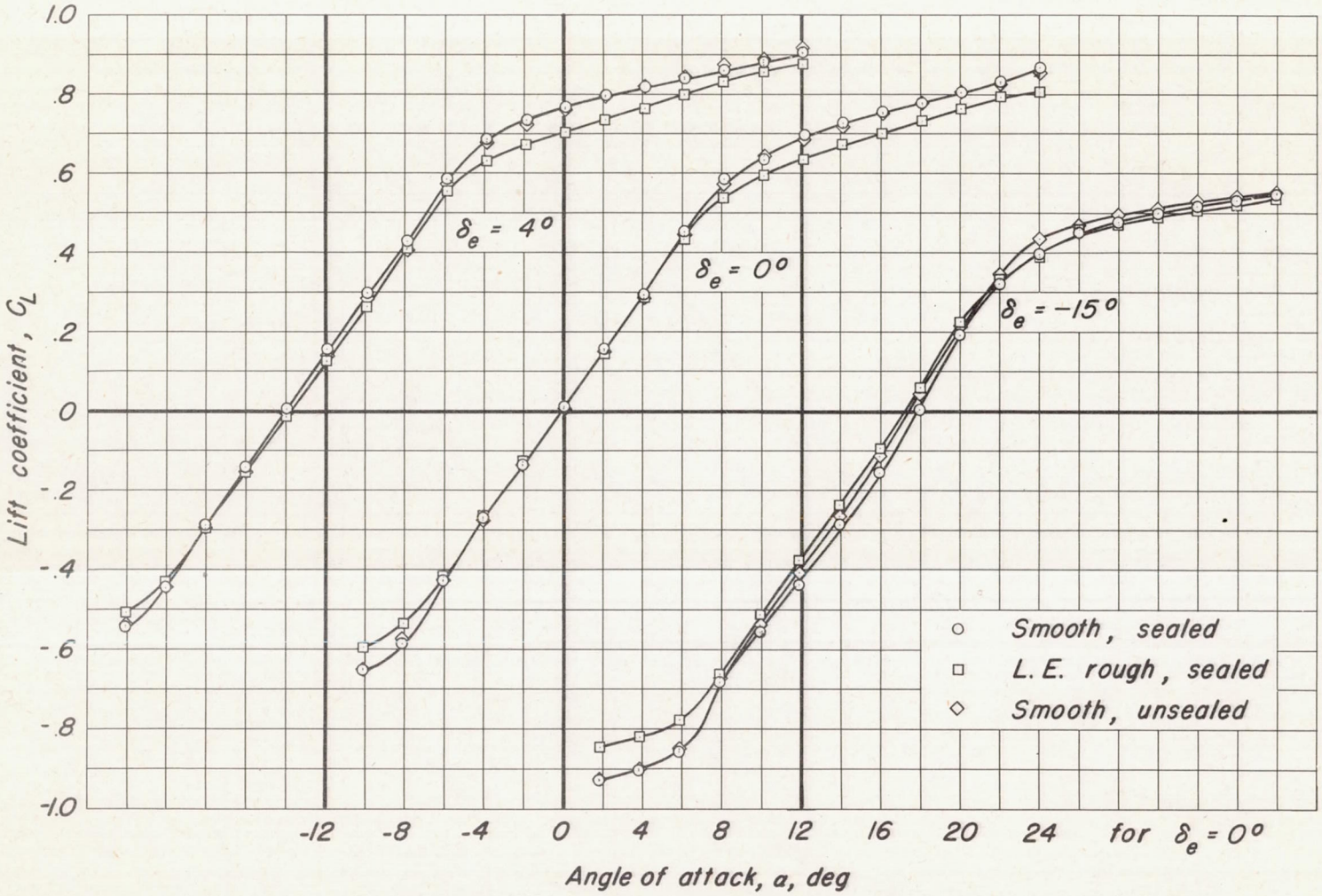

(c) M, 0.80.

Figure 13.– Continued.

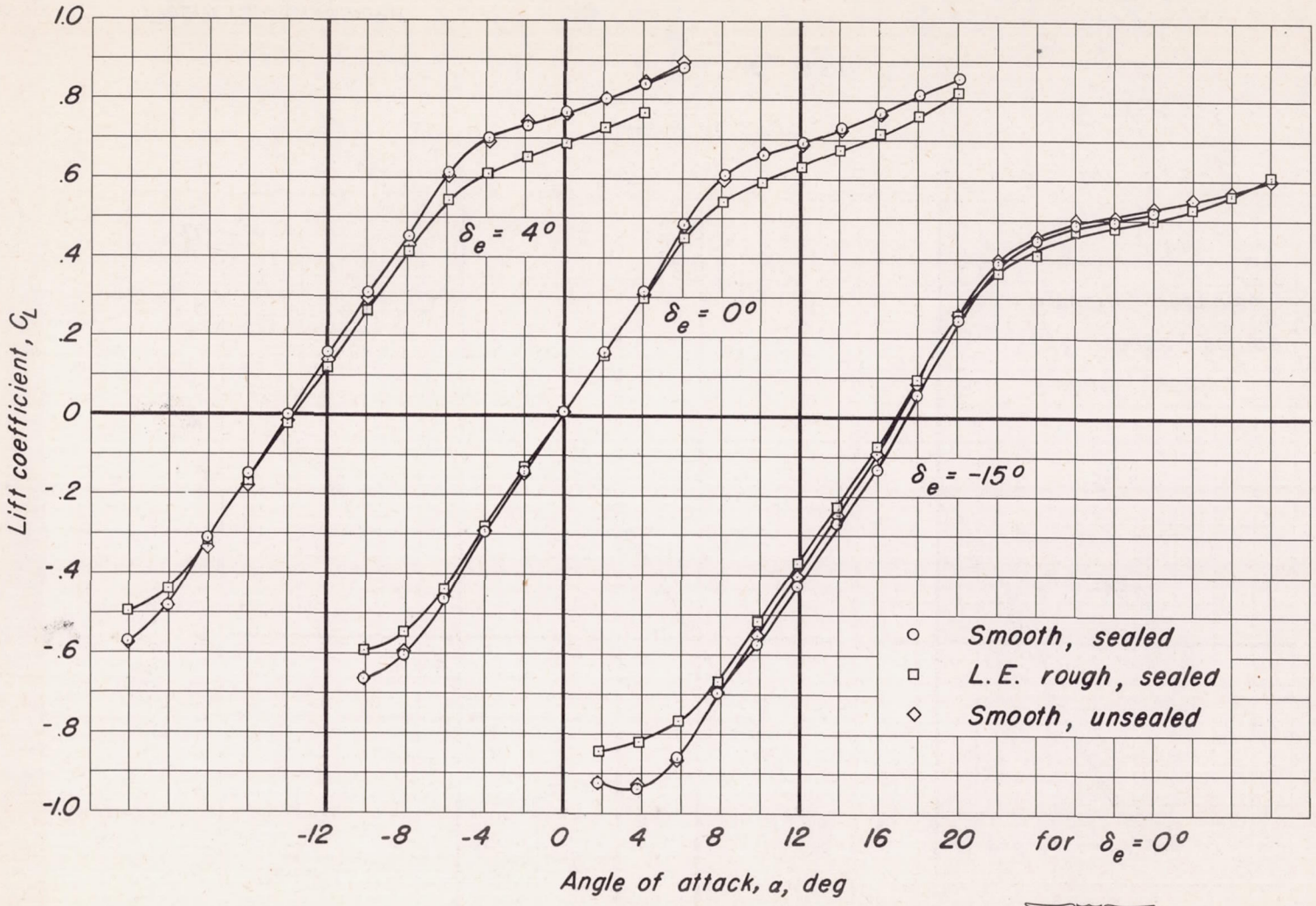

(d) M, 0.85.

Figure 13.– Continued.

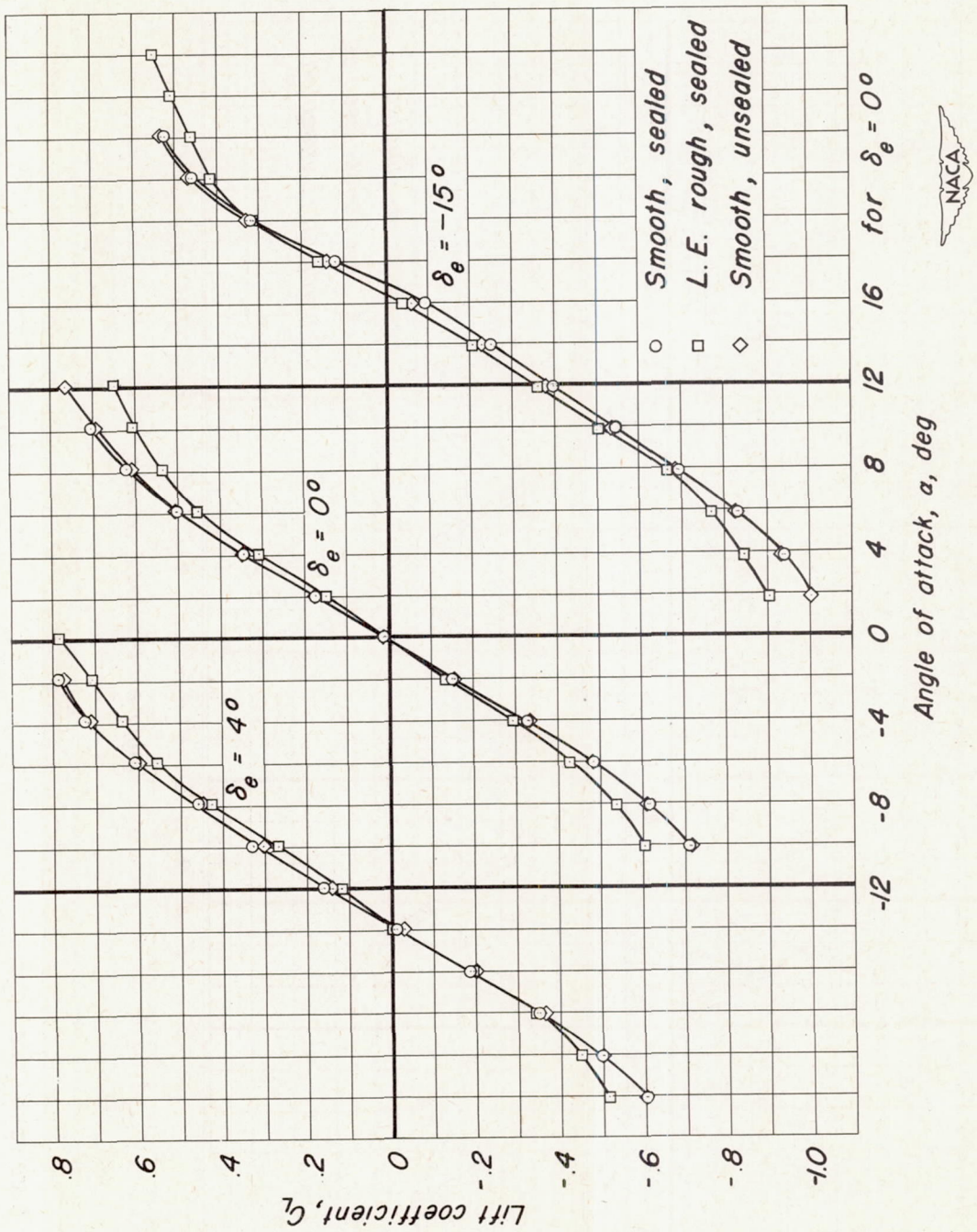

(e) M, 0.90.

Figure 13.– Continued.

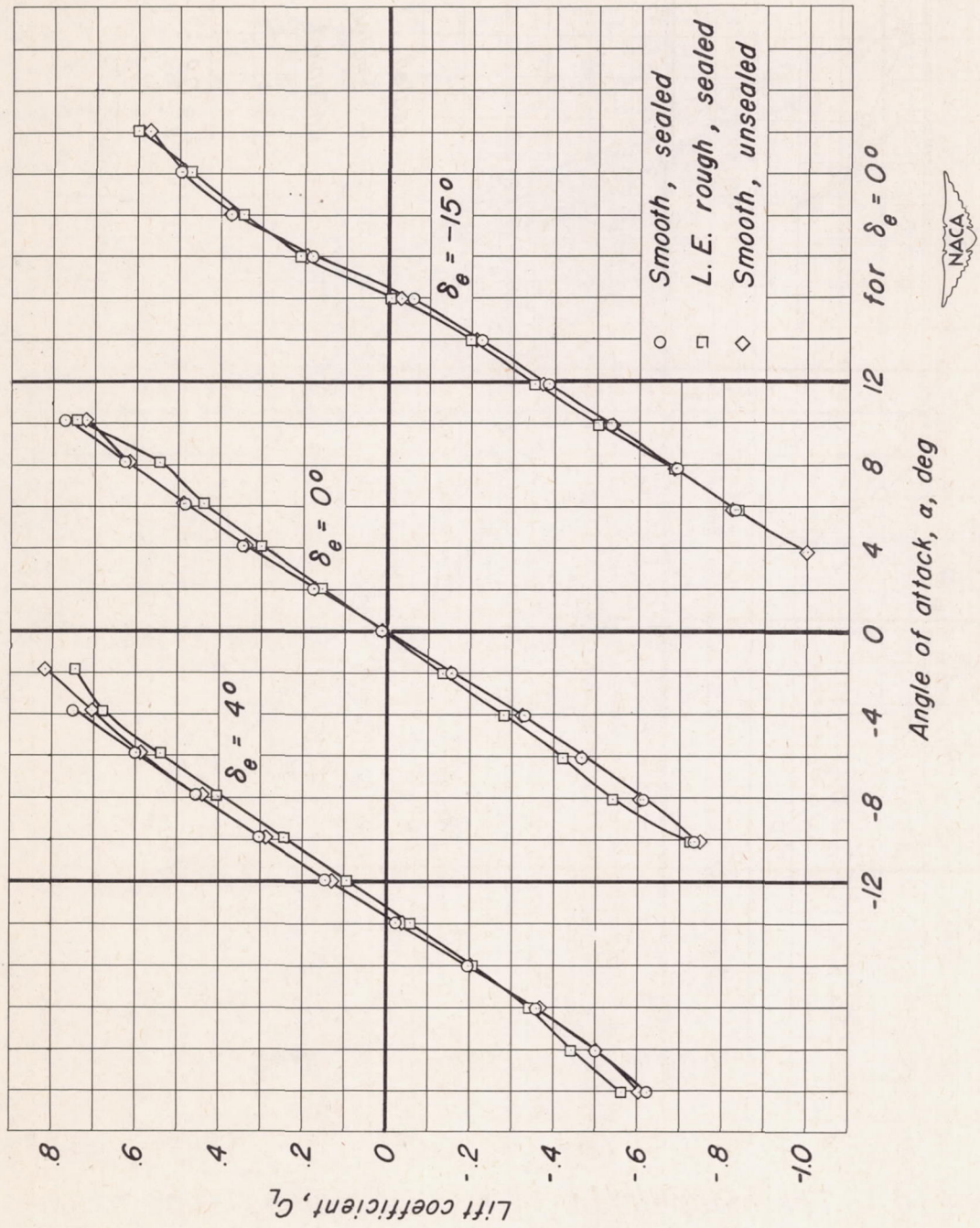

(f) M, 0.93.

Figure 13.– Concluded.

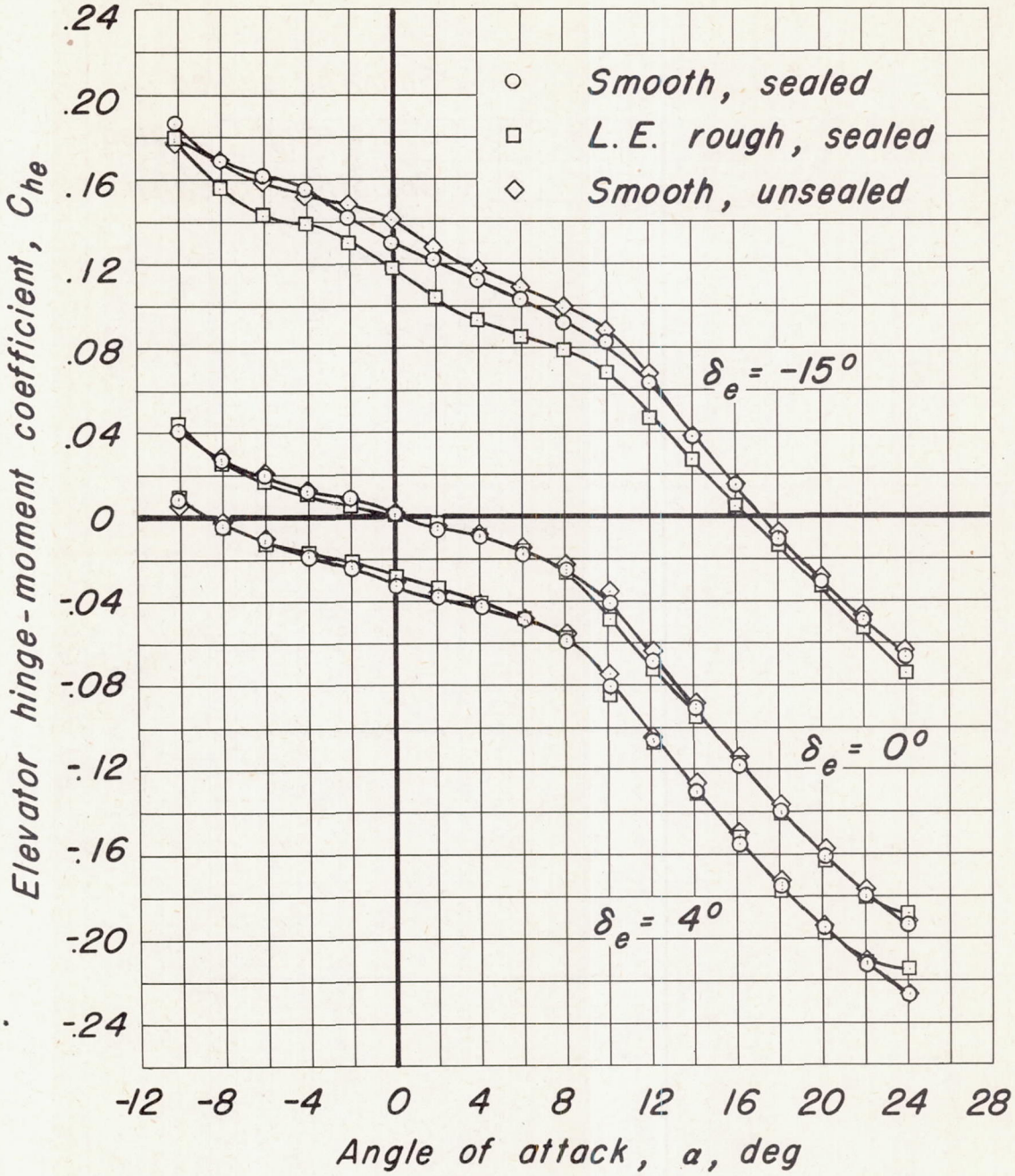

(a) M, 0.21.

Figure 14.– The independent effects of leading-edge roughness and removal of the elevator-nose seal on the variation of elevator hinge-moment coefficient with angle of attack. δ_t, 0°; R, 2,000,000.

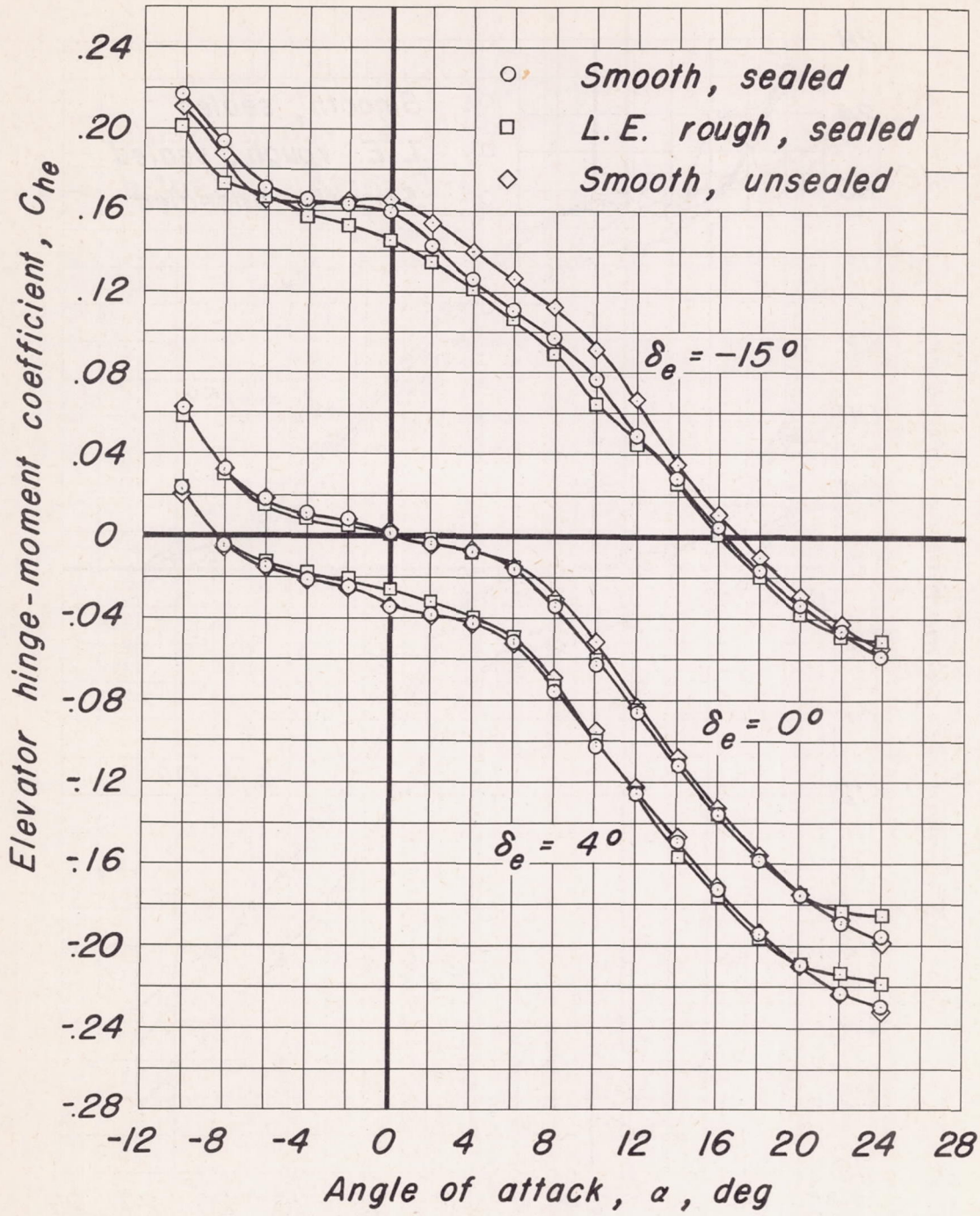

(b) M, 0.60.

Figure 14.– Continued.

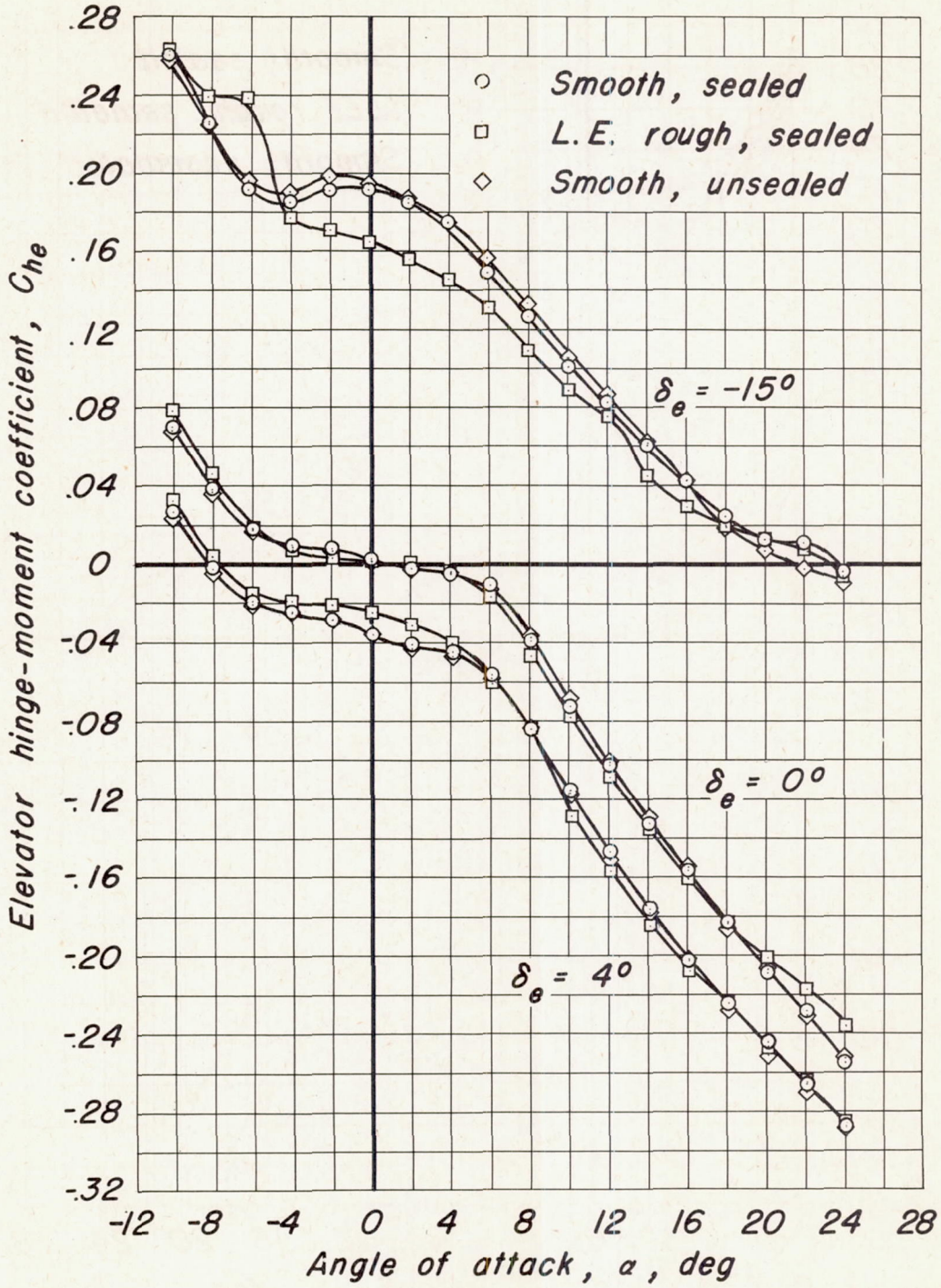

(c) M, 0.80.

Figure 14.– Continued.

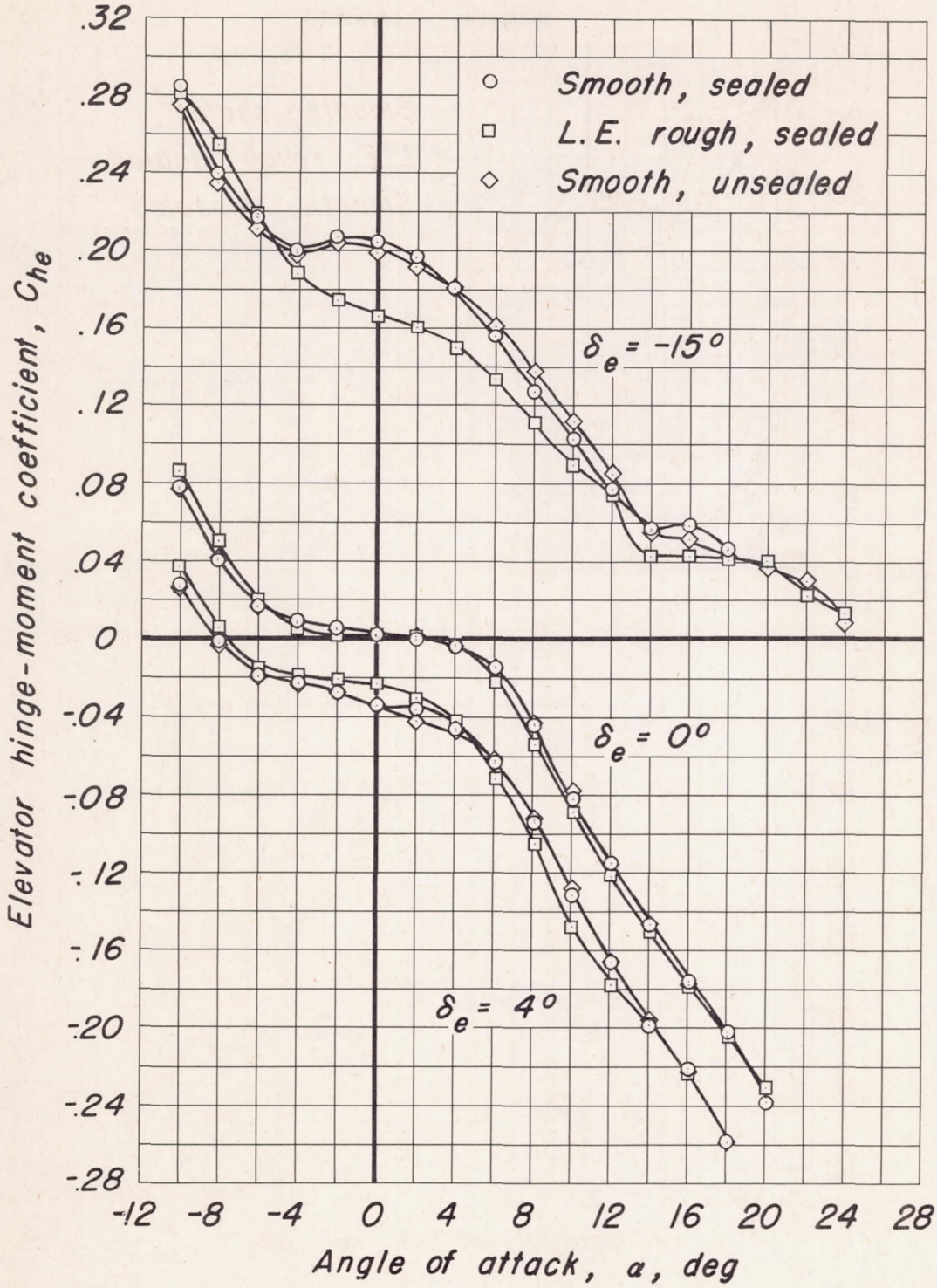

(d) M, 0.85.

Figure 14.– Continued.

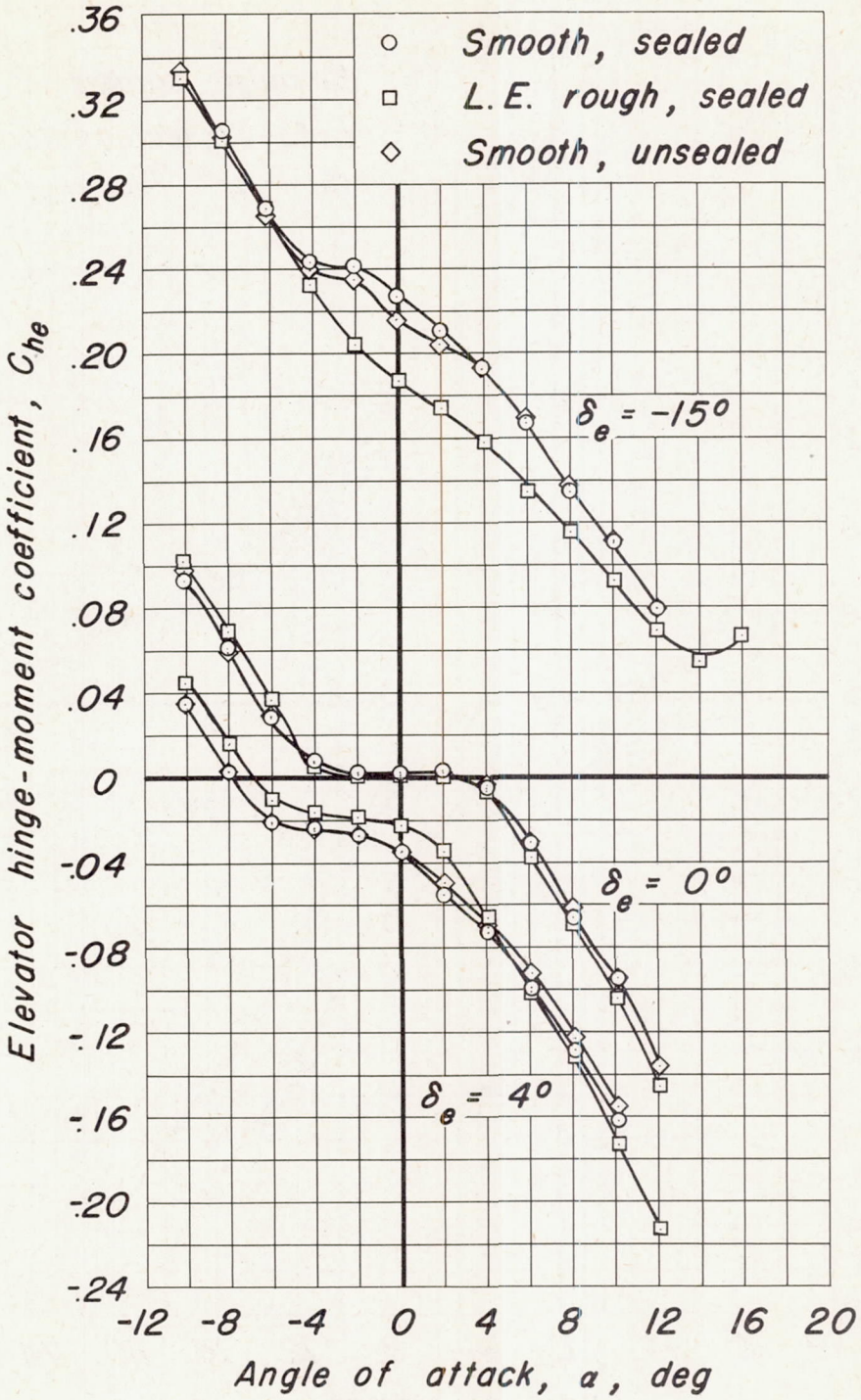

(e) M, 0.90.

Figure 14.– Continued.

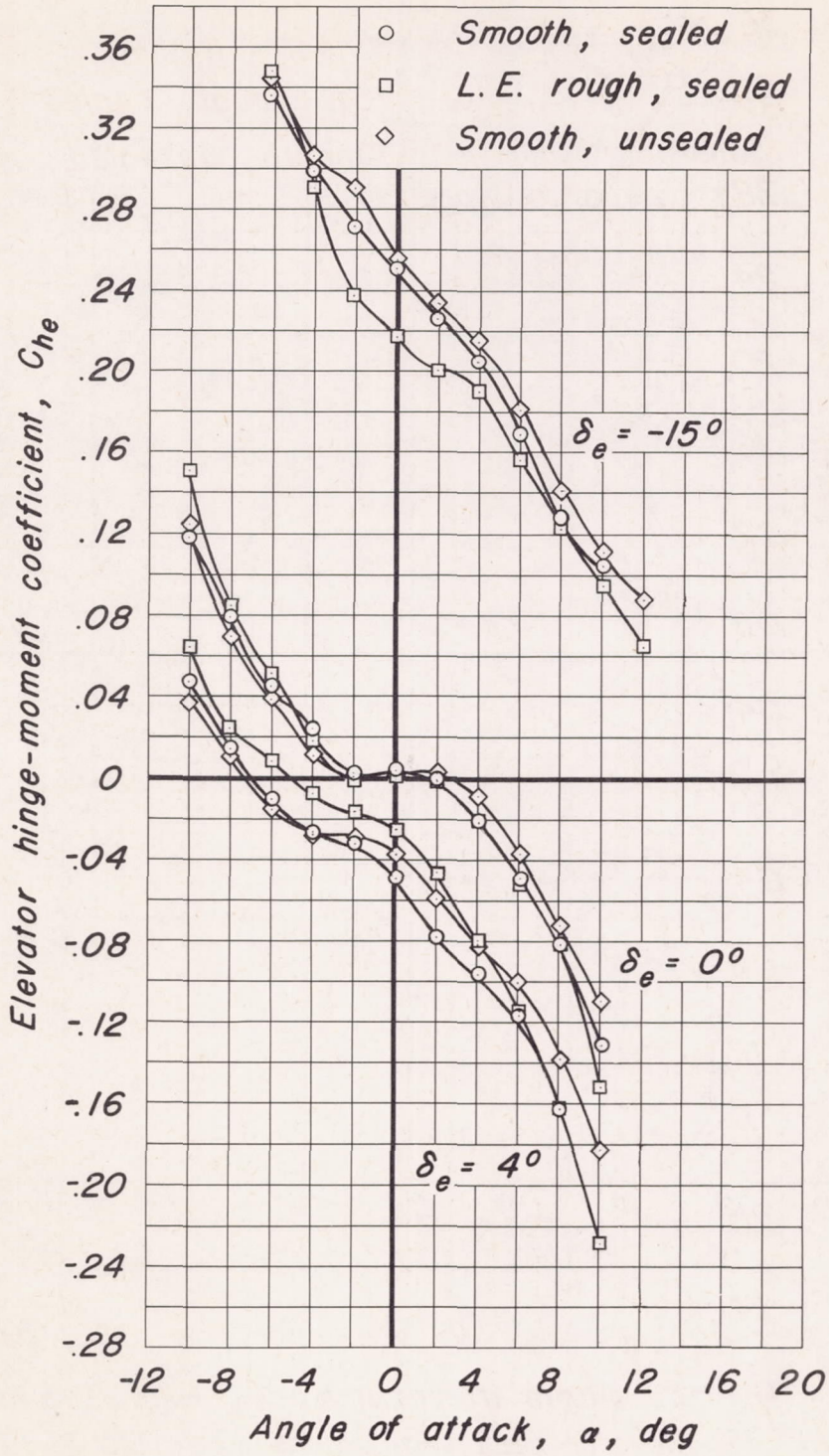

(f) M, 0.93.

Figure 14.– Concluded.

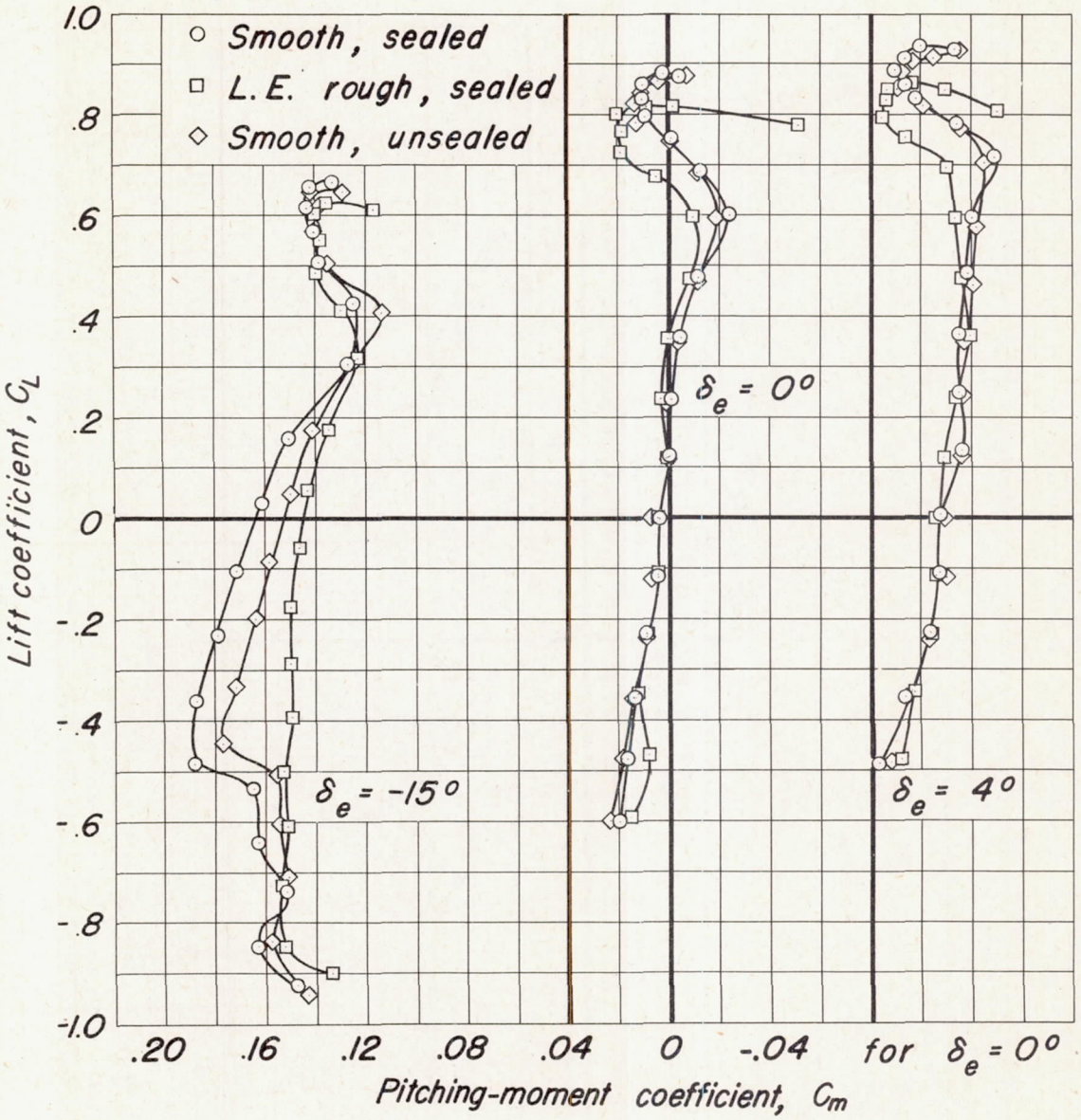

(a) M, 0.21.

Figure 15.— The independent effects of leading-edge roughness and removal of the elevator-nose seal on the variation of lift coefficient with pitching-moment coefficient. δ_t, 0°; R, 2,000,000.

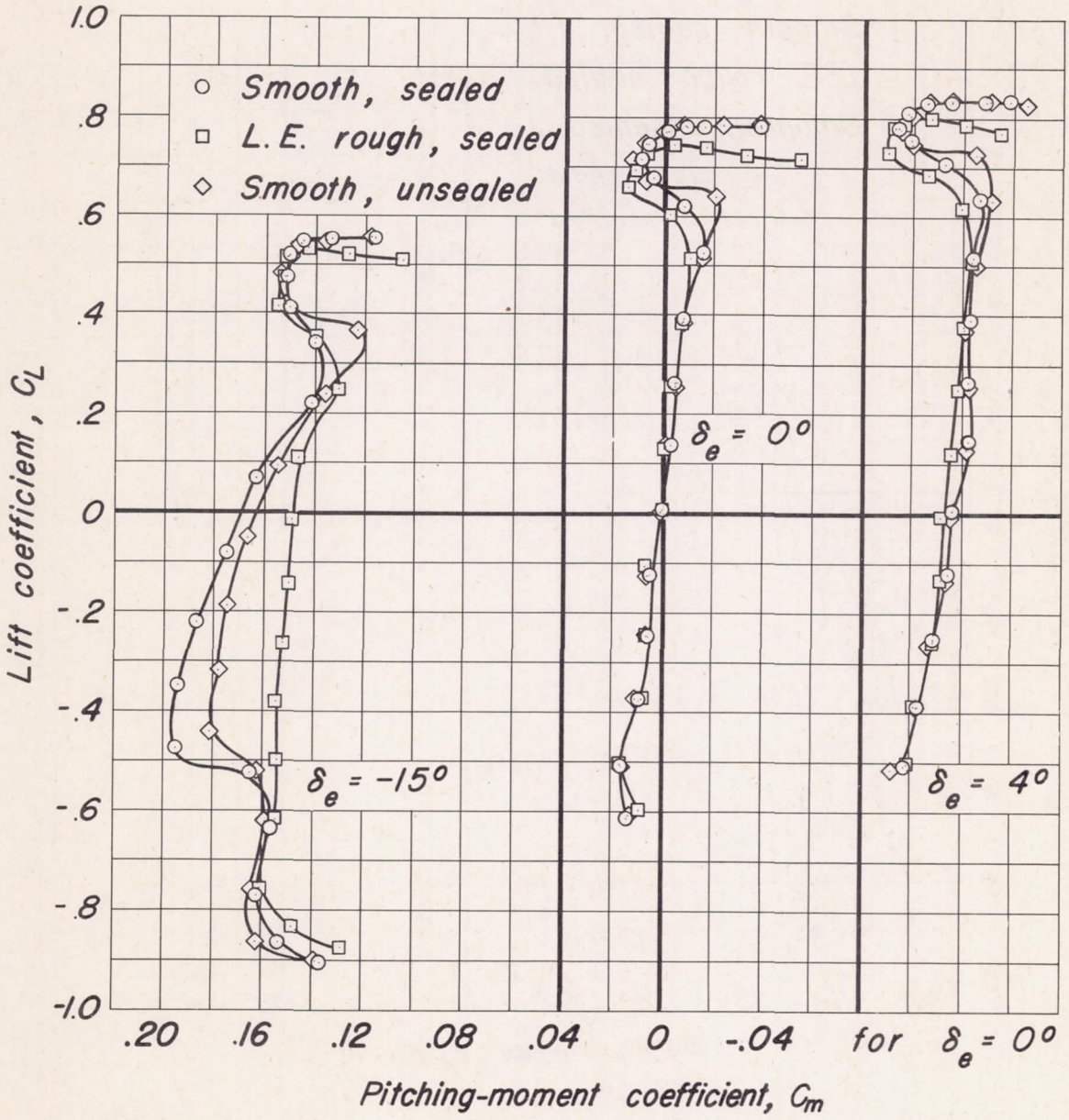

(b) M, 0.60.

Figure 15.—Continued.

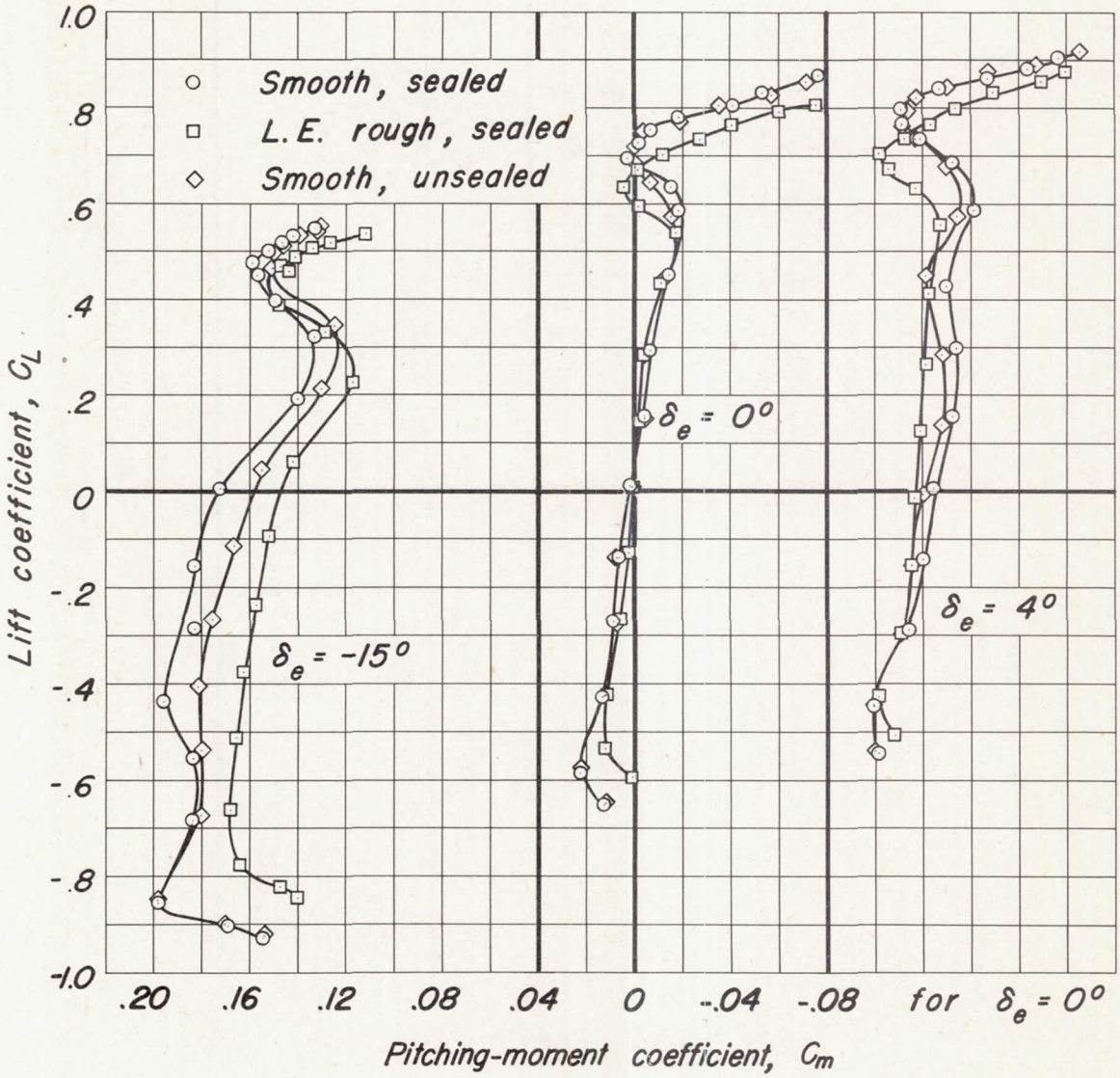

(c) M, 0.80.

Figure 15.—Continued.

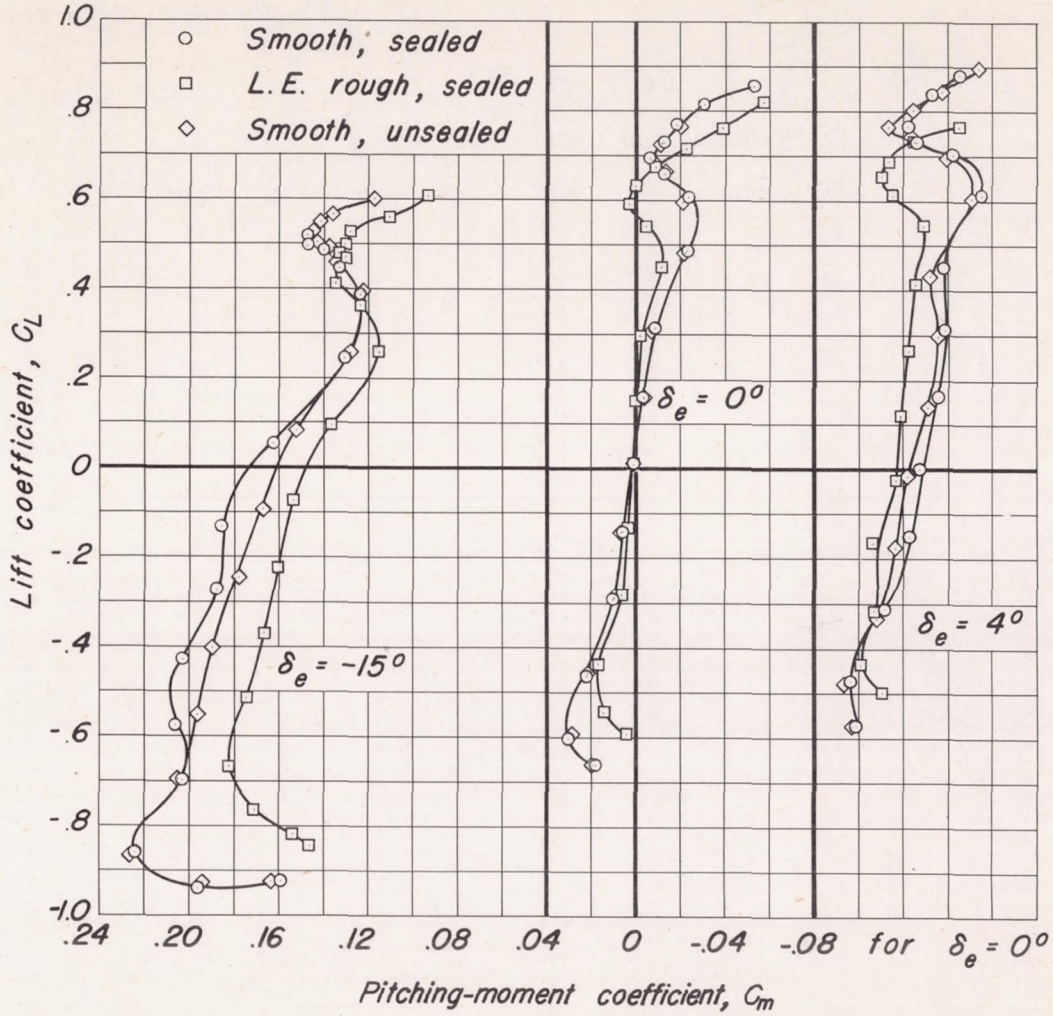

(d) M, 0.85.

Figure 15.—Continued.

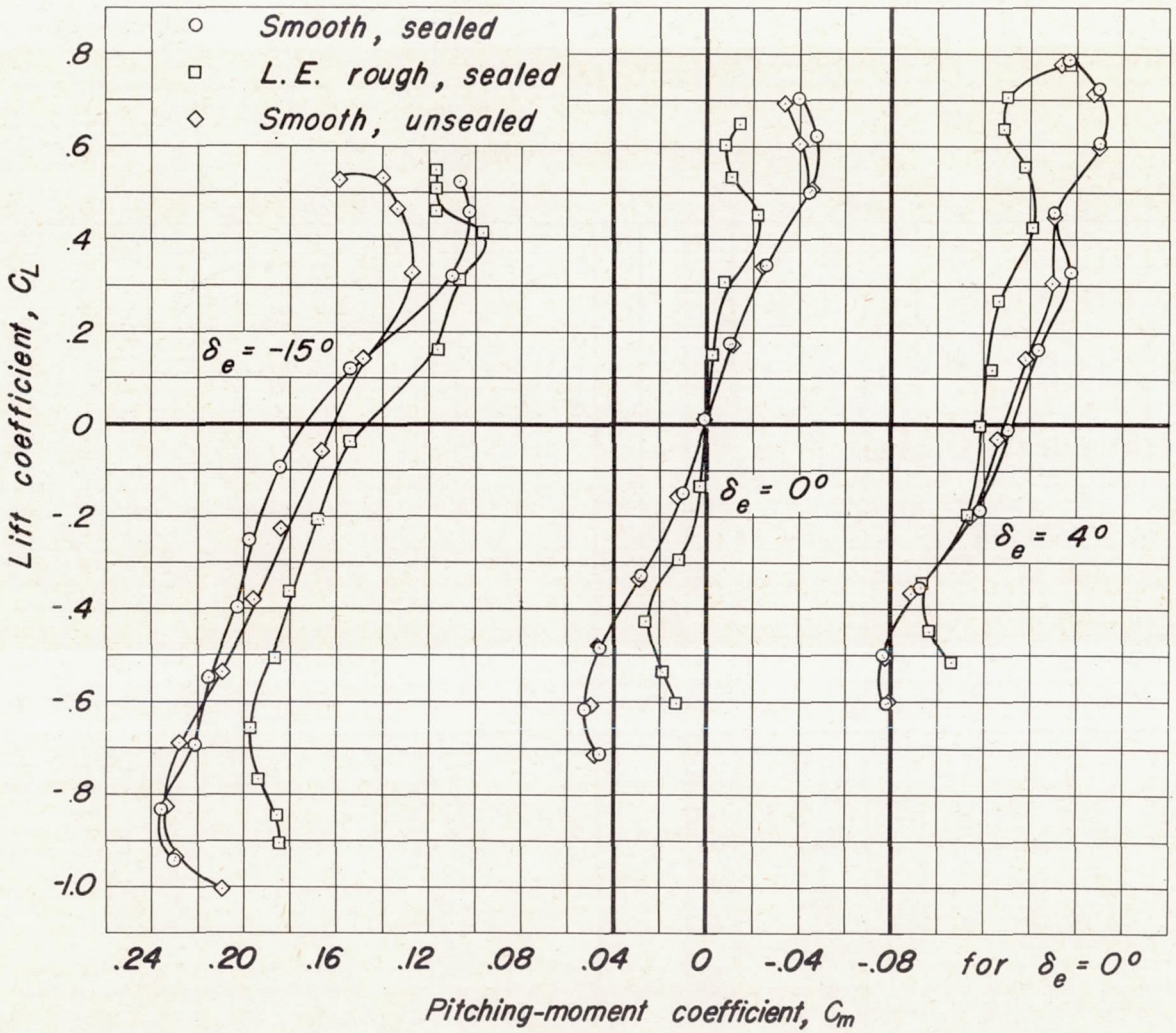

(e) M, 0.90.

Figure 15.—Continued.

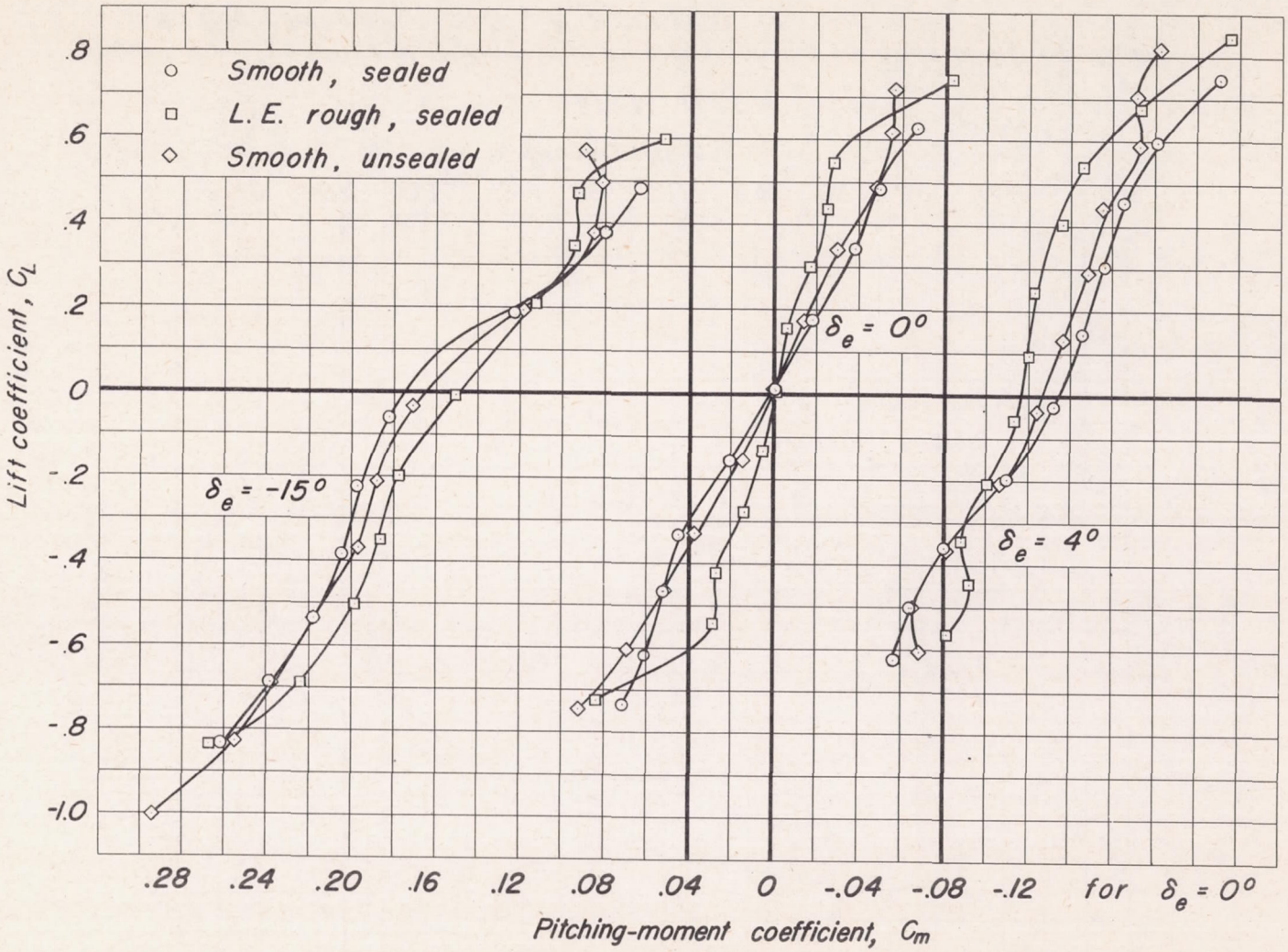

(f) M, 0.93.

Figure 15.—Concluded.

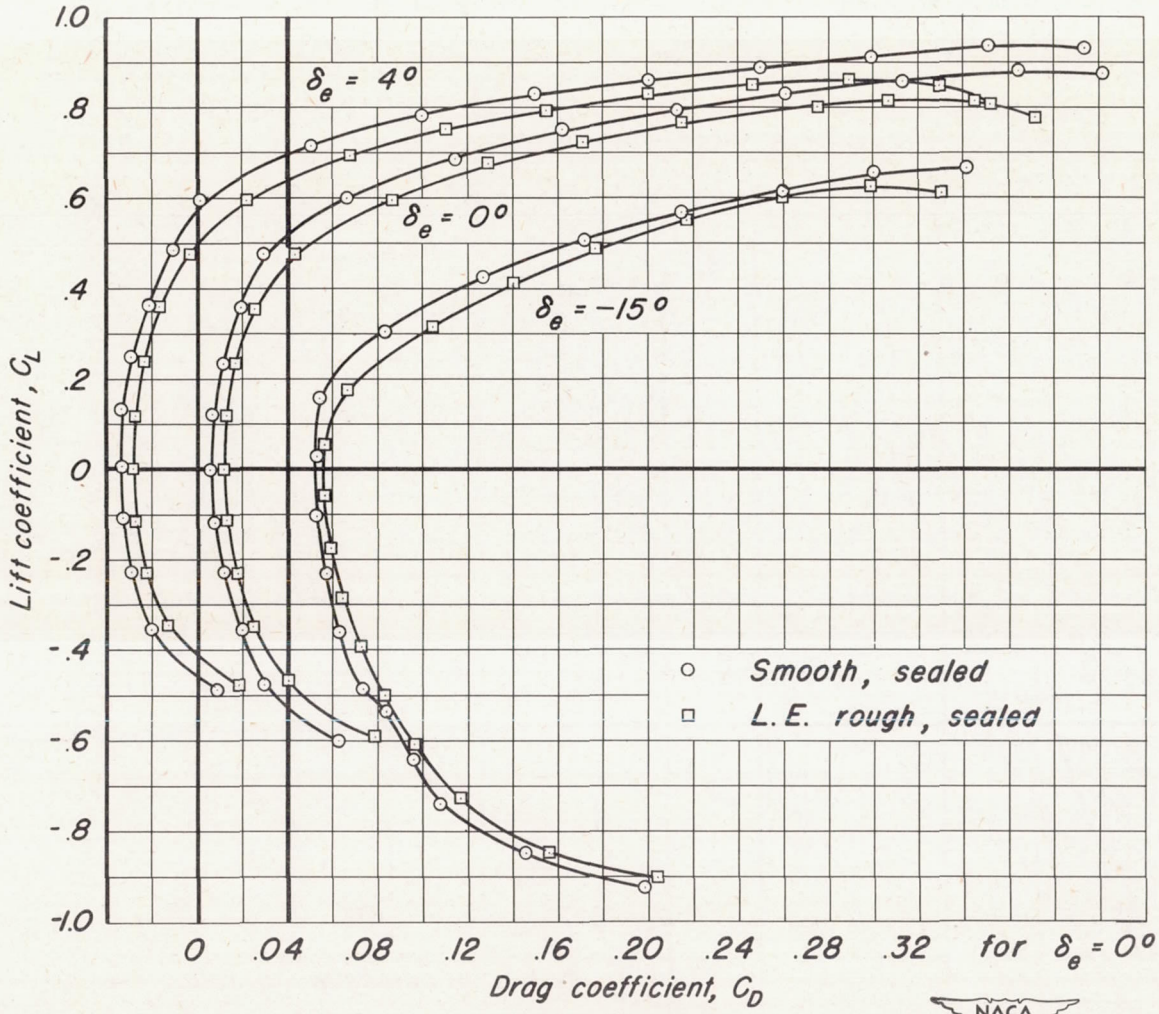

(a) M, 0.21.

Figure 16.— The effect of leading-edge roughness on the variation of lift coefficient with drag coefficient. δ_f, 0°; R, 2,000,000.

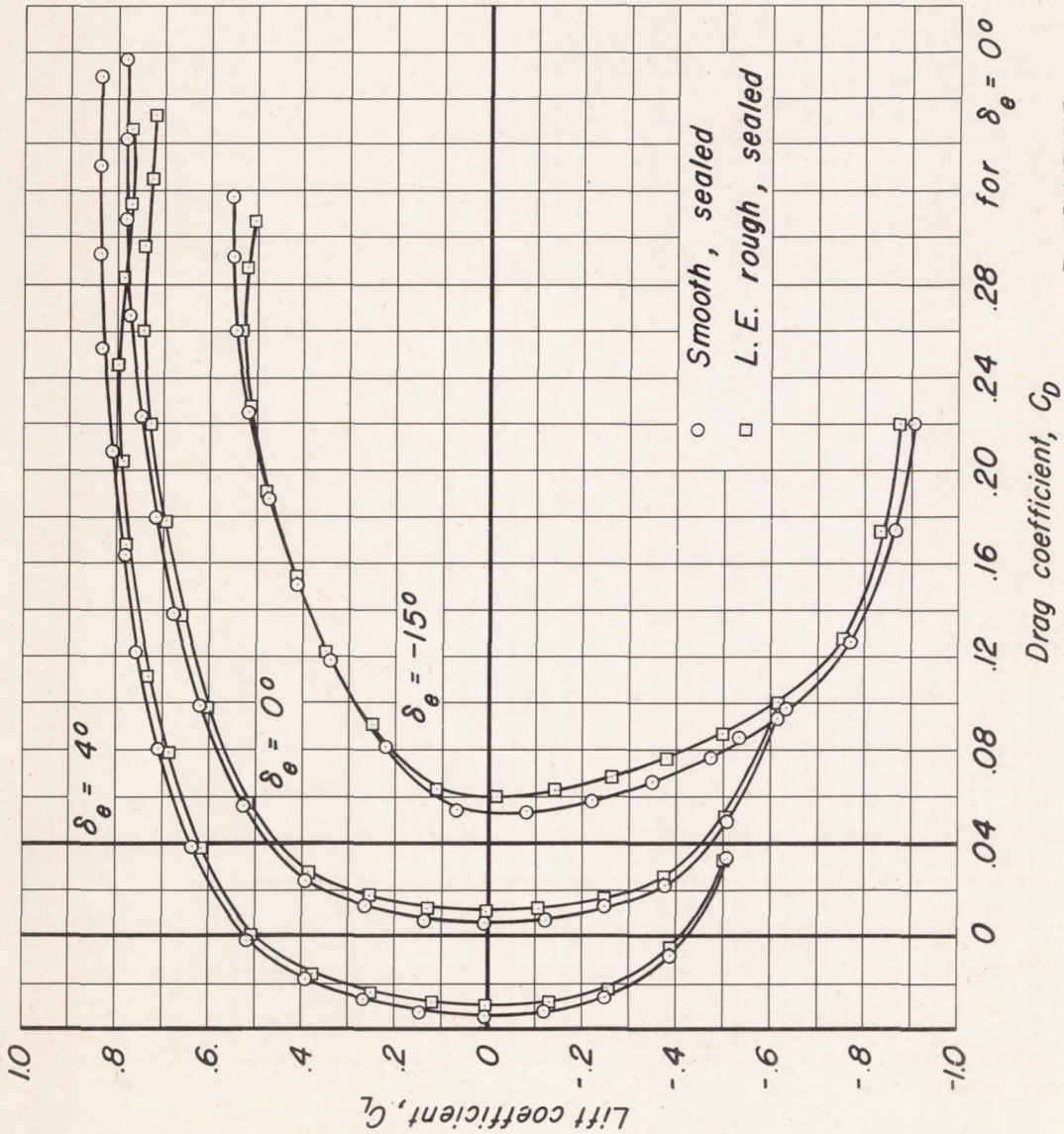

(b) M, 0.60.

Figure 16.— Continued.

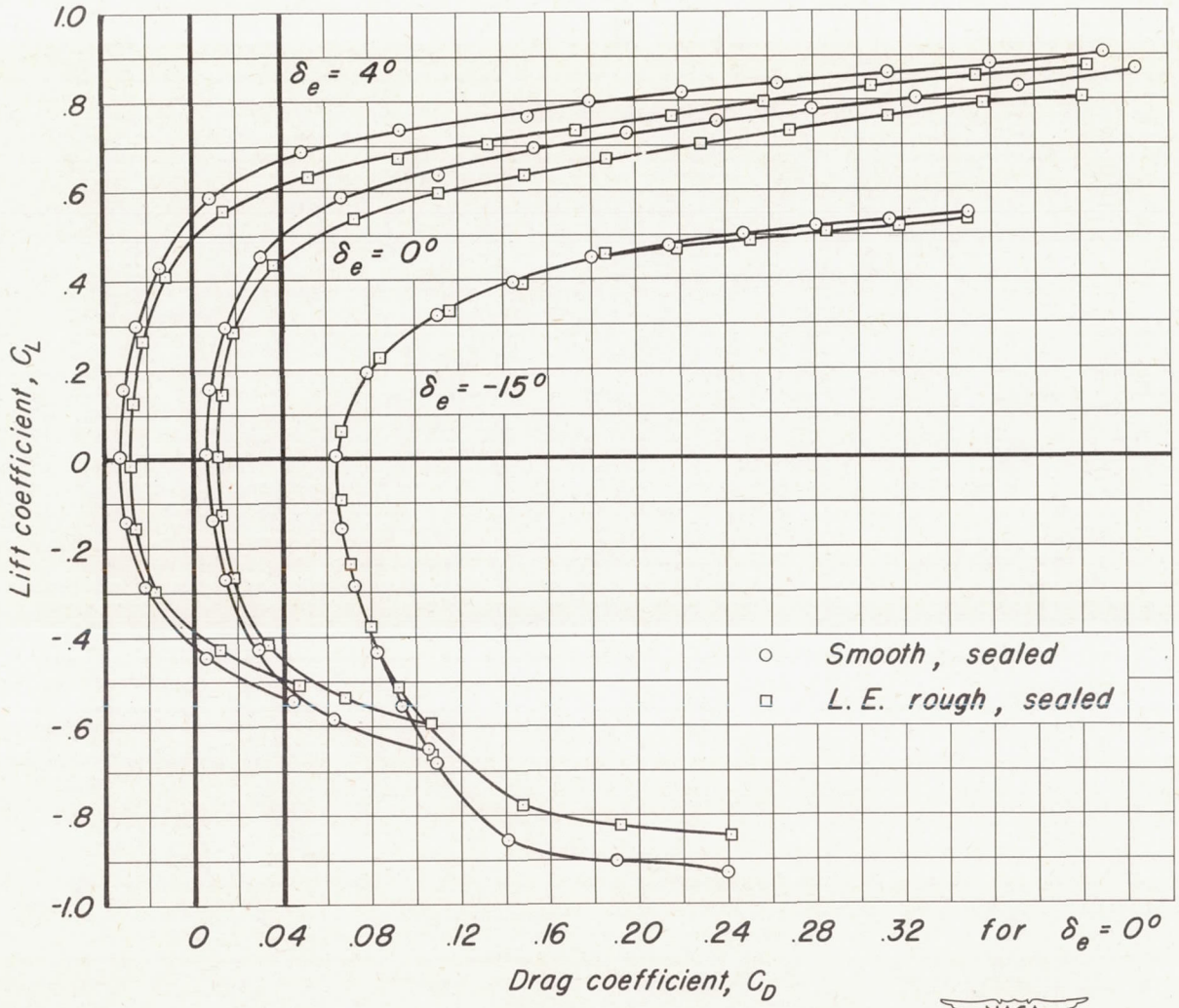

(c) M, 0.80.

Figure 16.— Continued.

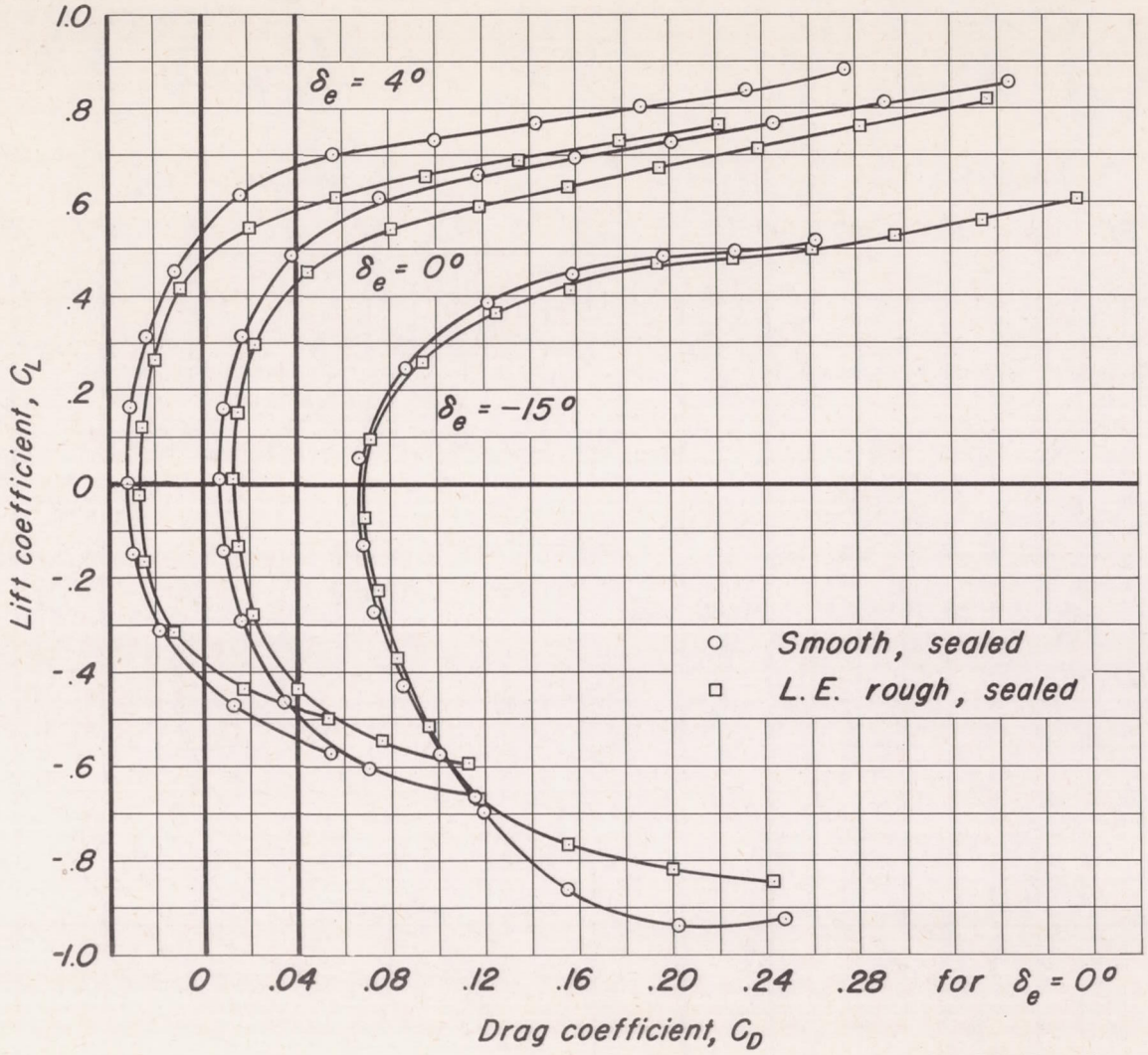

(d) M, 0.85.

Figure 16.— Continued.

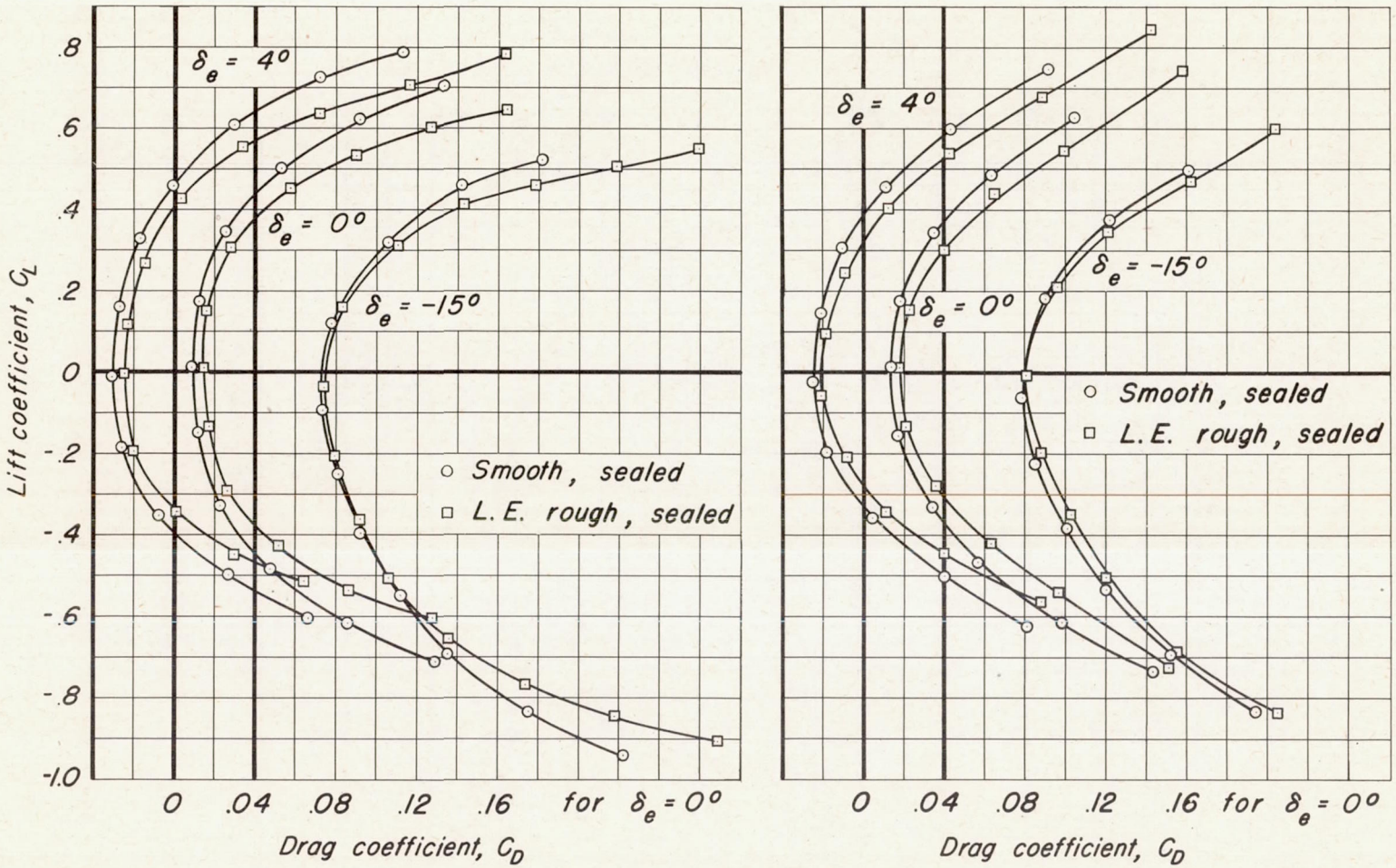

(e) M, 0.90.

(f) M, 0.93.

Figure 16.— Concluded.

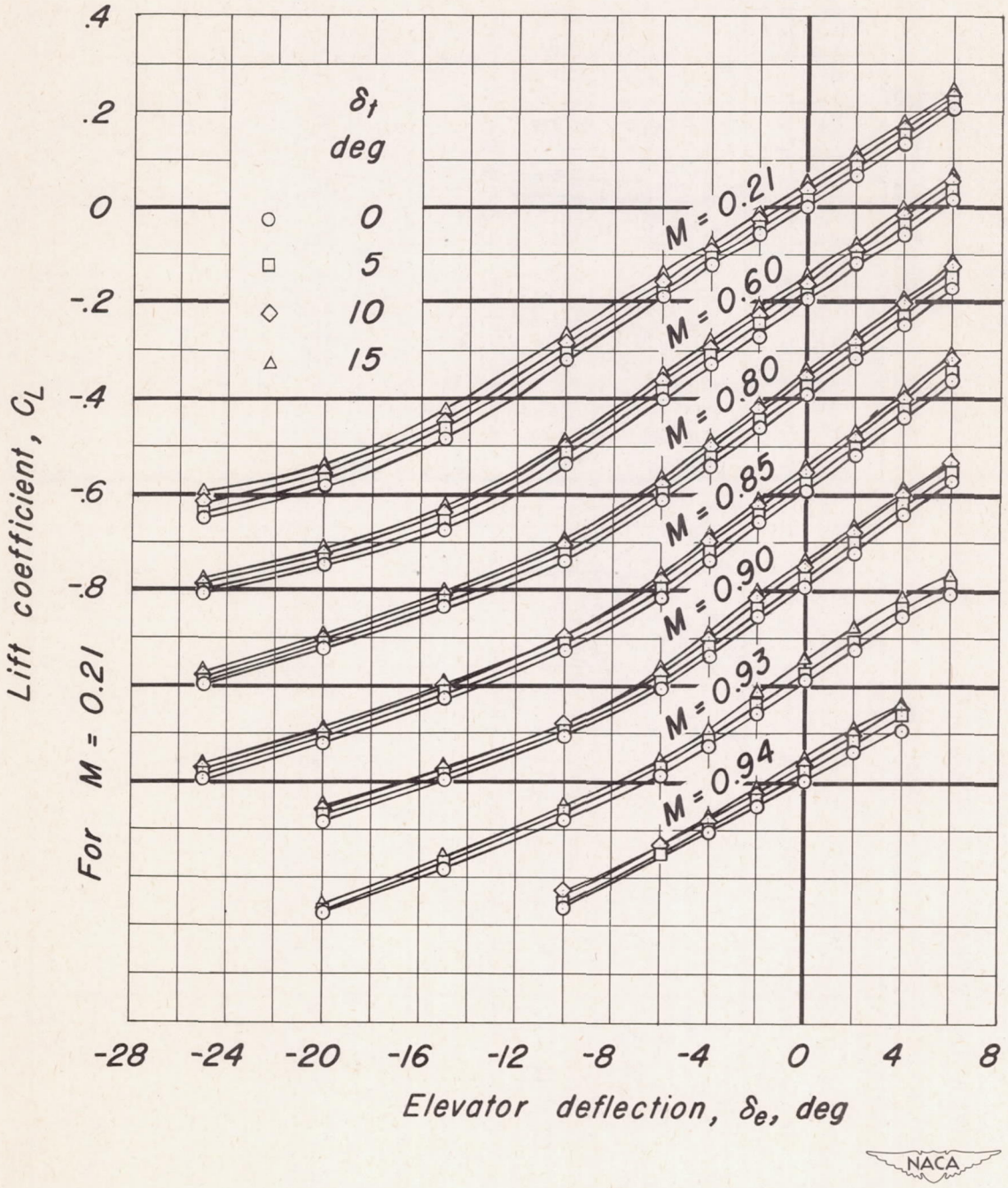

Figure 17.— The variation of lift coefficient with elevator deflection. α_u, 0°; R, 2,000,000.

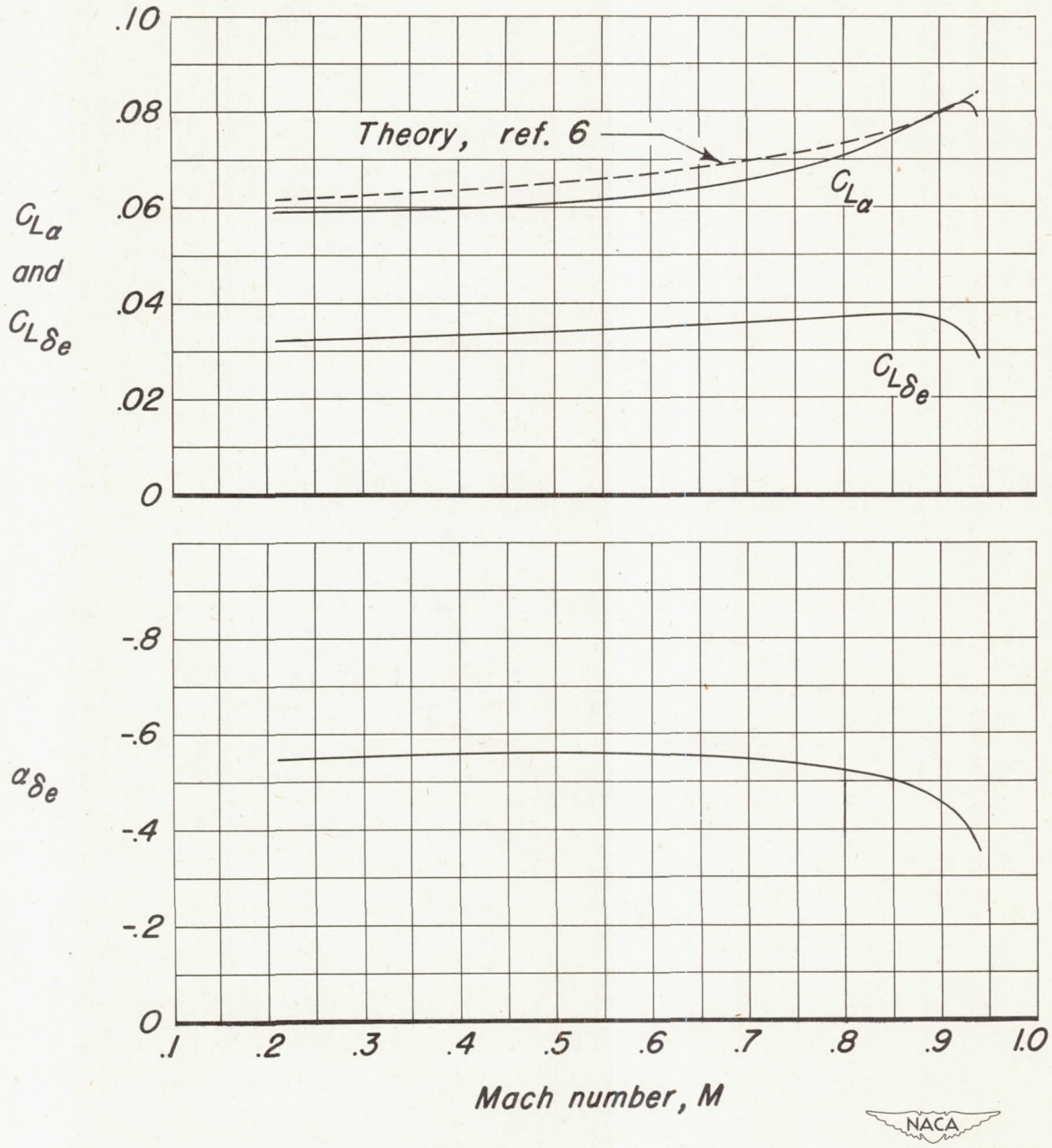

Figure 18.— The variations of lift parameters C_{L_α}, $C_{L_{\delta_e}}$, and α_{δ_e} with Mach number. R, 2,000,000.

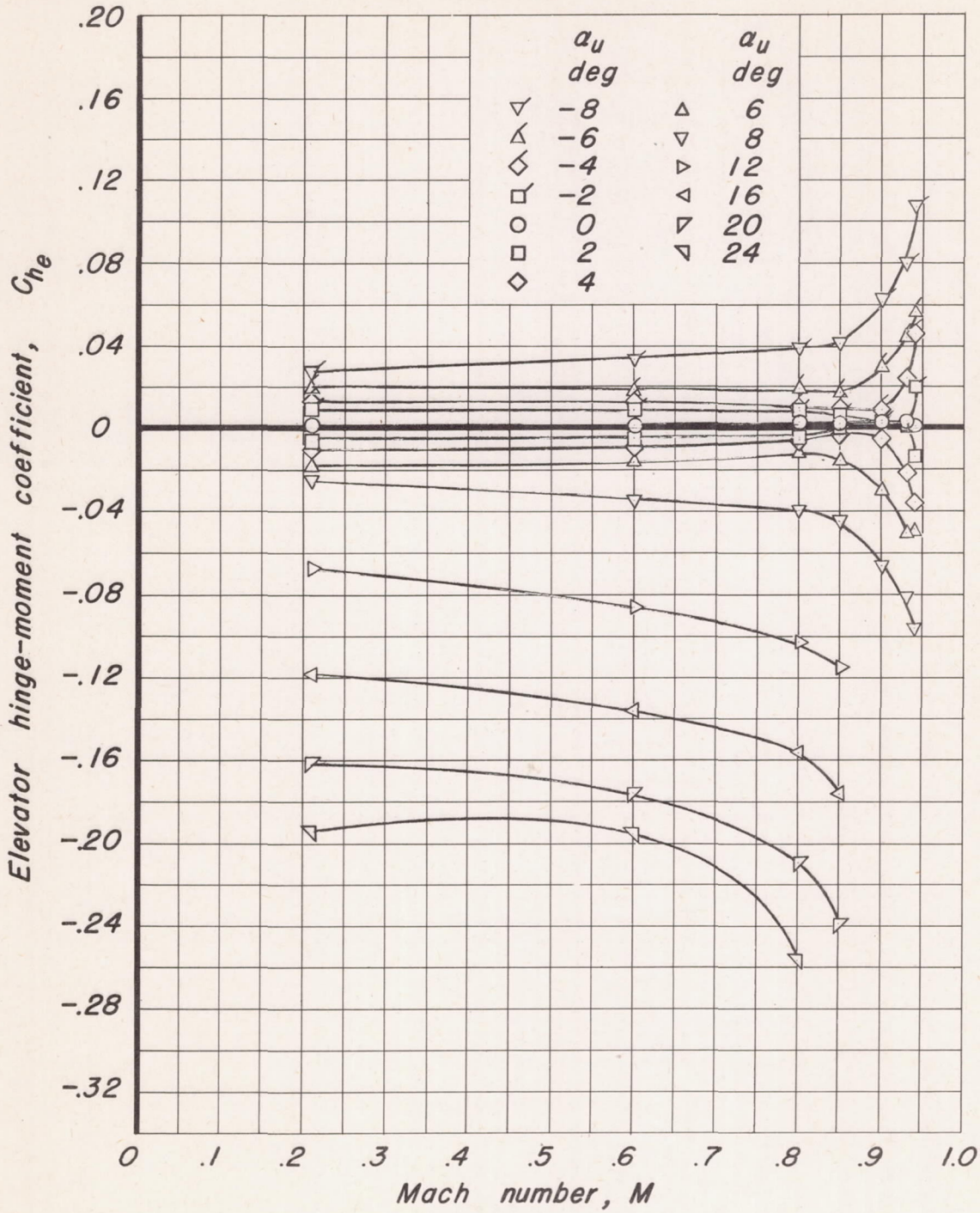

(a) $\delta_e = 0°$.

Figure 19.—The variation of elevator hinge-moment coefficient with Mach number. δ_t, 0°; R, 2,000,000.

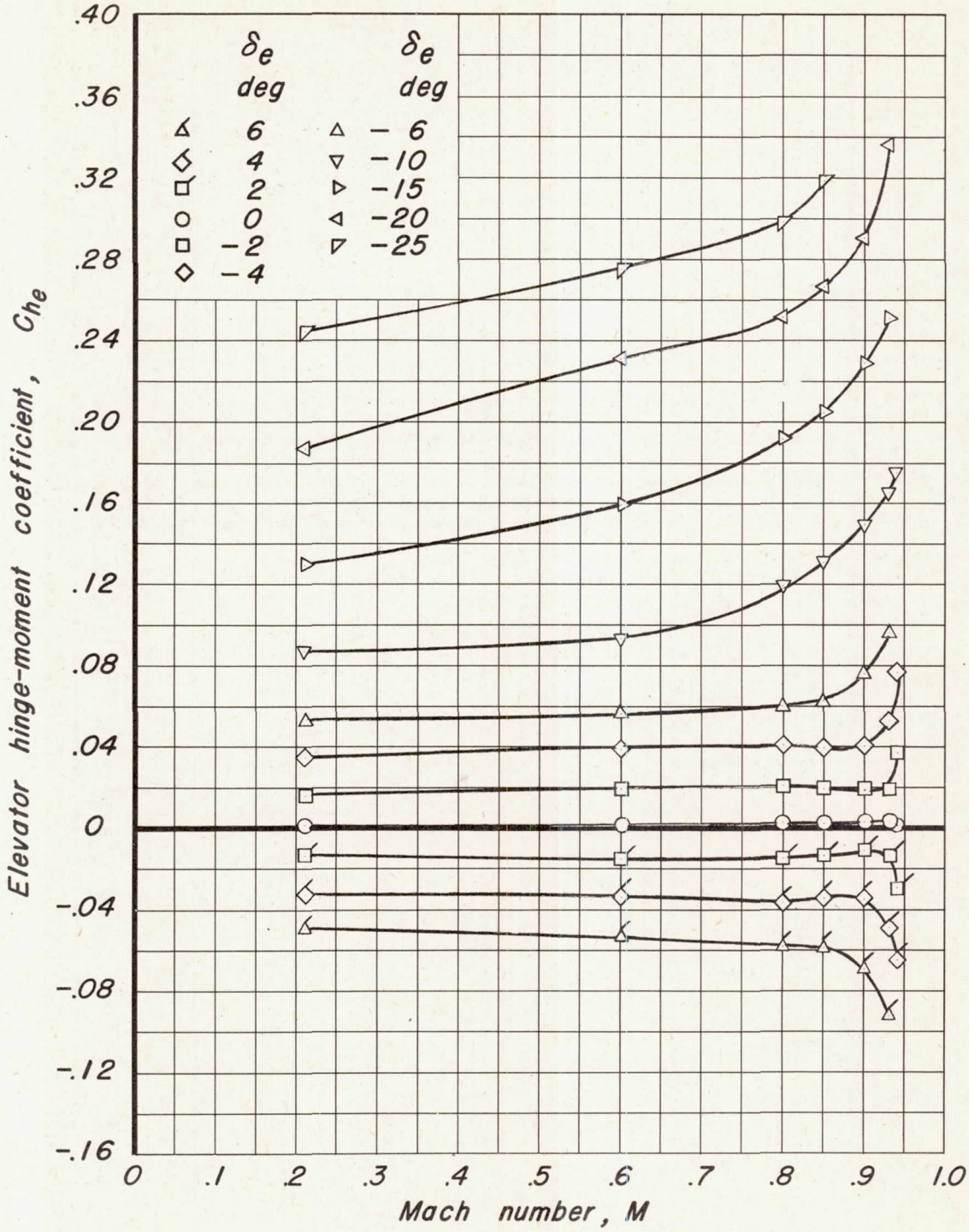

(b) $\alpha_u = 0°$.

Figure 19.– Concluded.

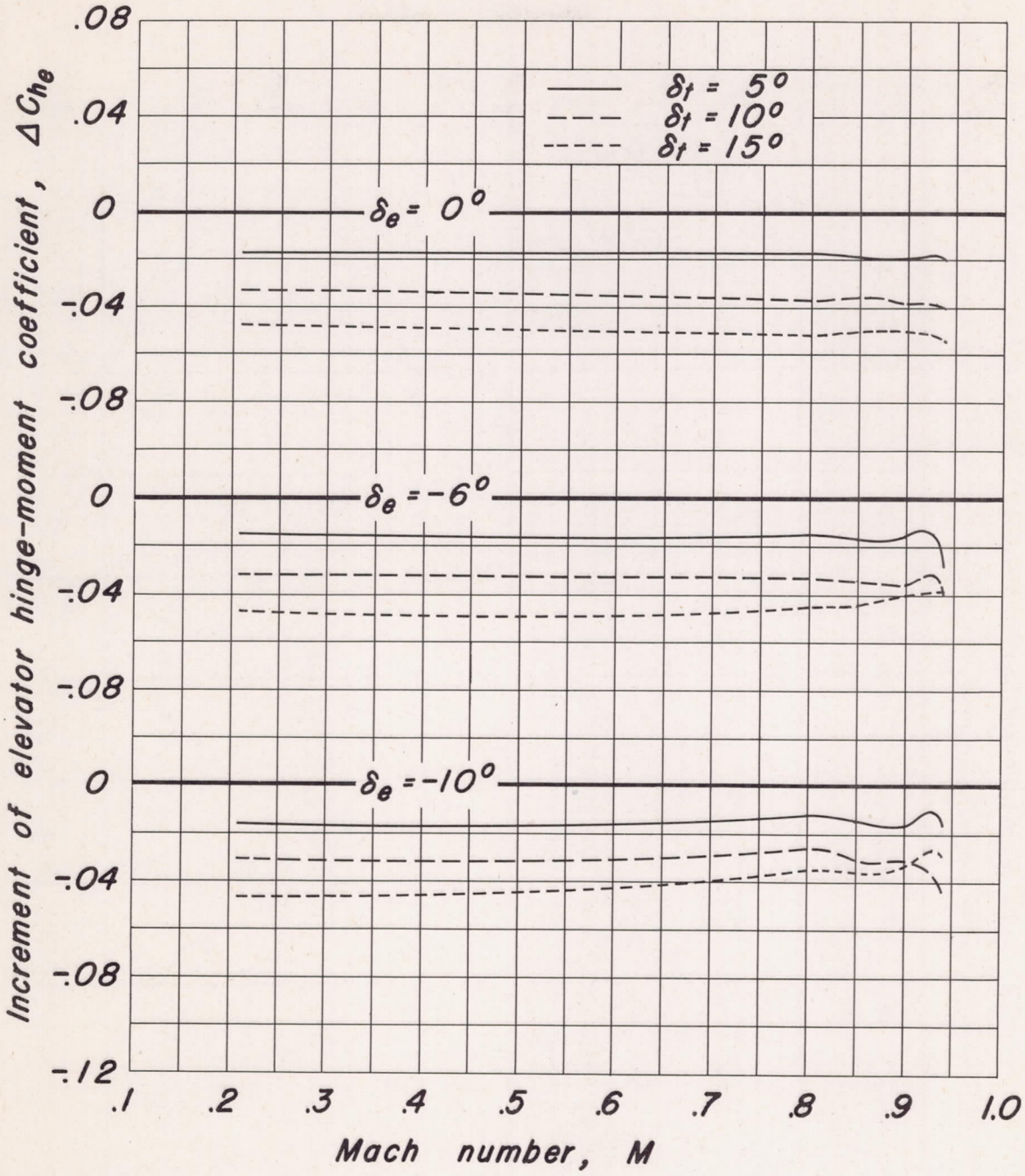

Figure 20.– The variation of increment of elevator hinge-moment coefficient due to tab deflection with Mach number. a_u, 0°; R, 2,000,000.

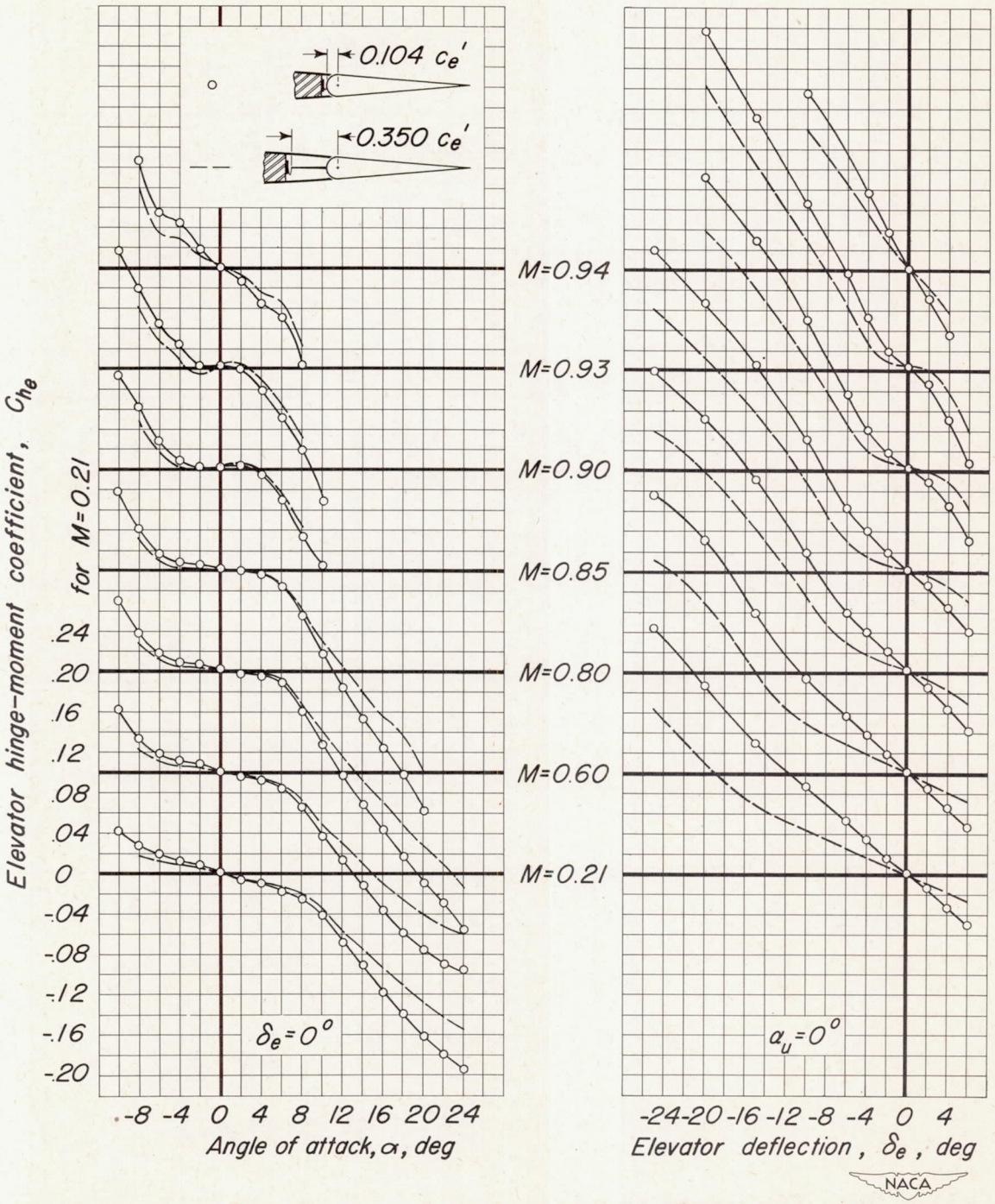

Figure 21.– The computed effect of a sealed, internal, aerodynamic balance on the variation of elevator hinge-moment coefficient with angle of attack and with elevator deflection. δ_t, 0°; R, 2,000,000.

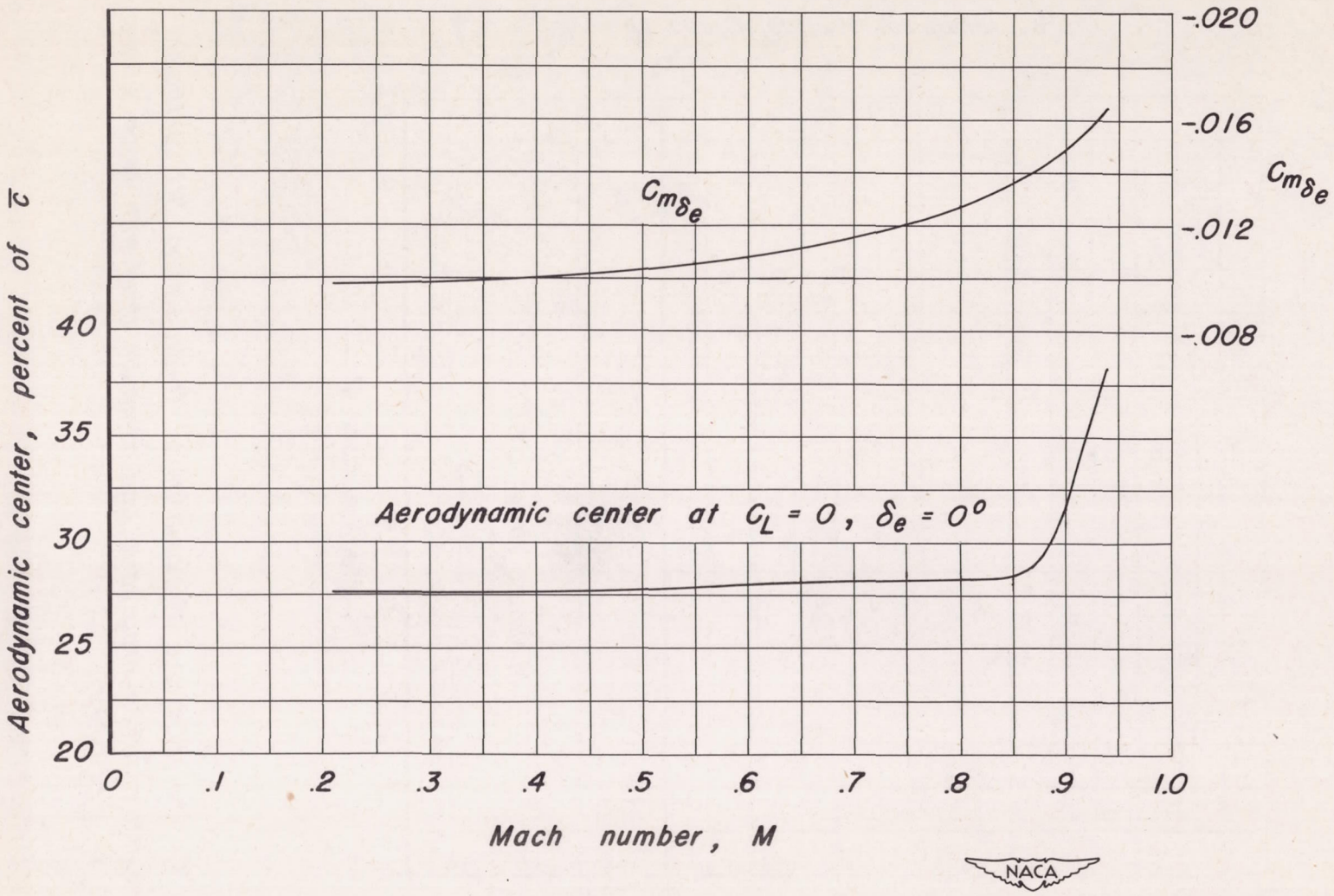

Figure 22.– The variations of pitching-moment parameter $C_{m_{\delta_e}}$ and aerodynamic-center location with Mach number. δ_t, 0°; R, 2,000,000.

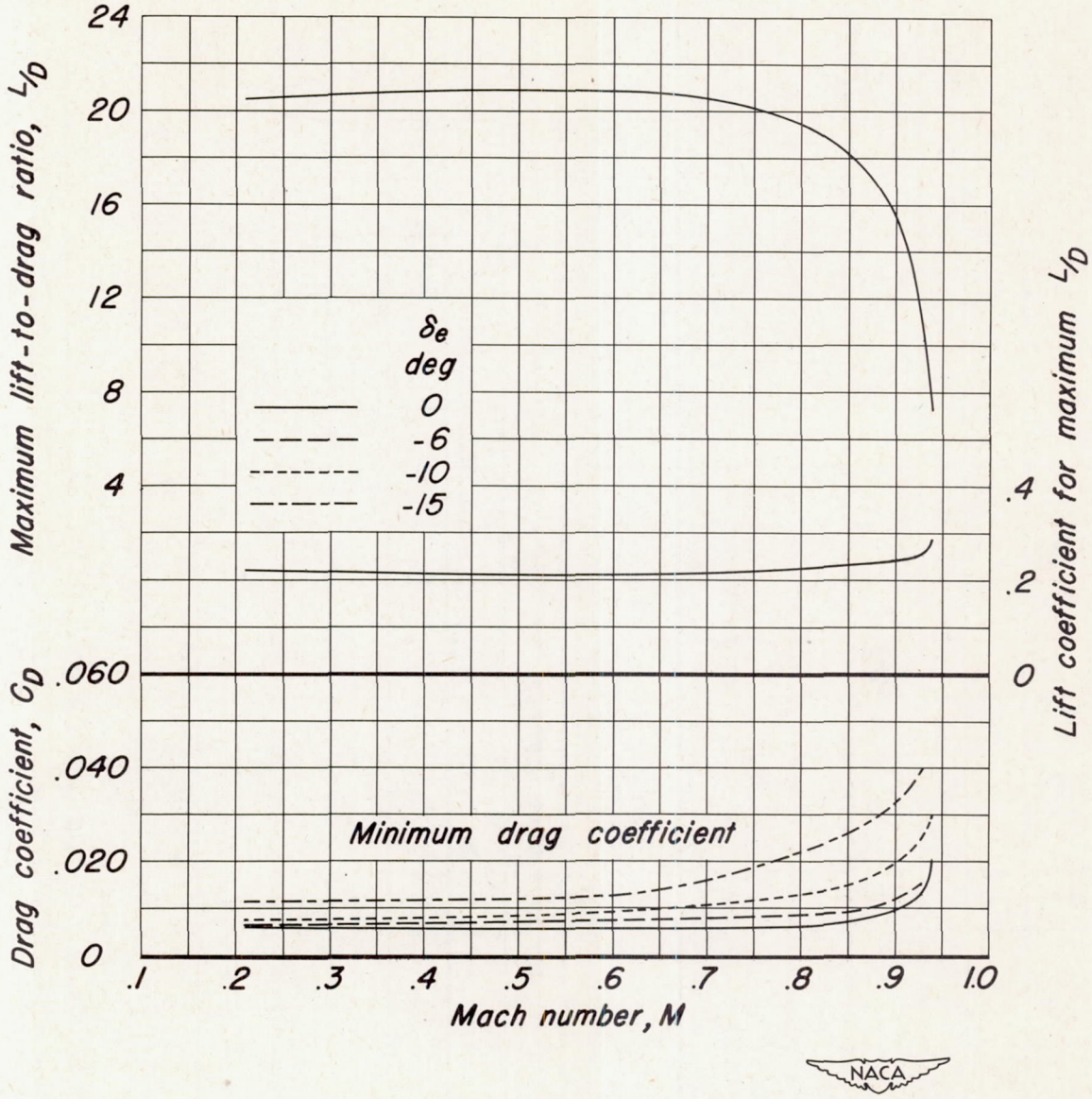

Figure 23.– The variations of maximum lift-to-drag ratio, lift coefficient for maximum lift-to-drag ratio, and minimum drag with Mach number. δ_t, 0°; R, 2,000,000.

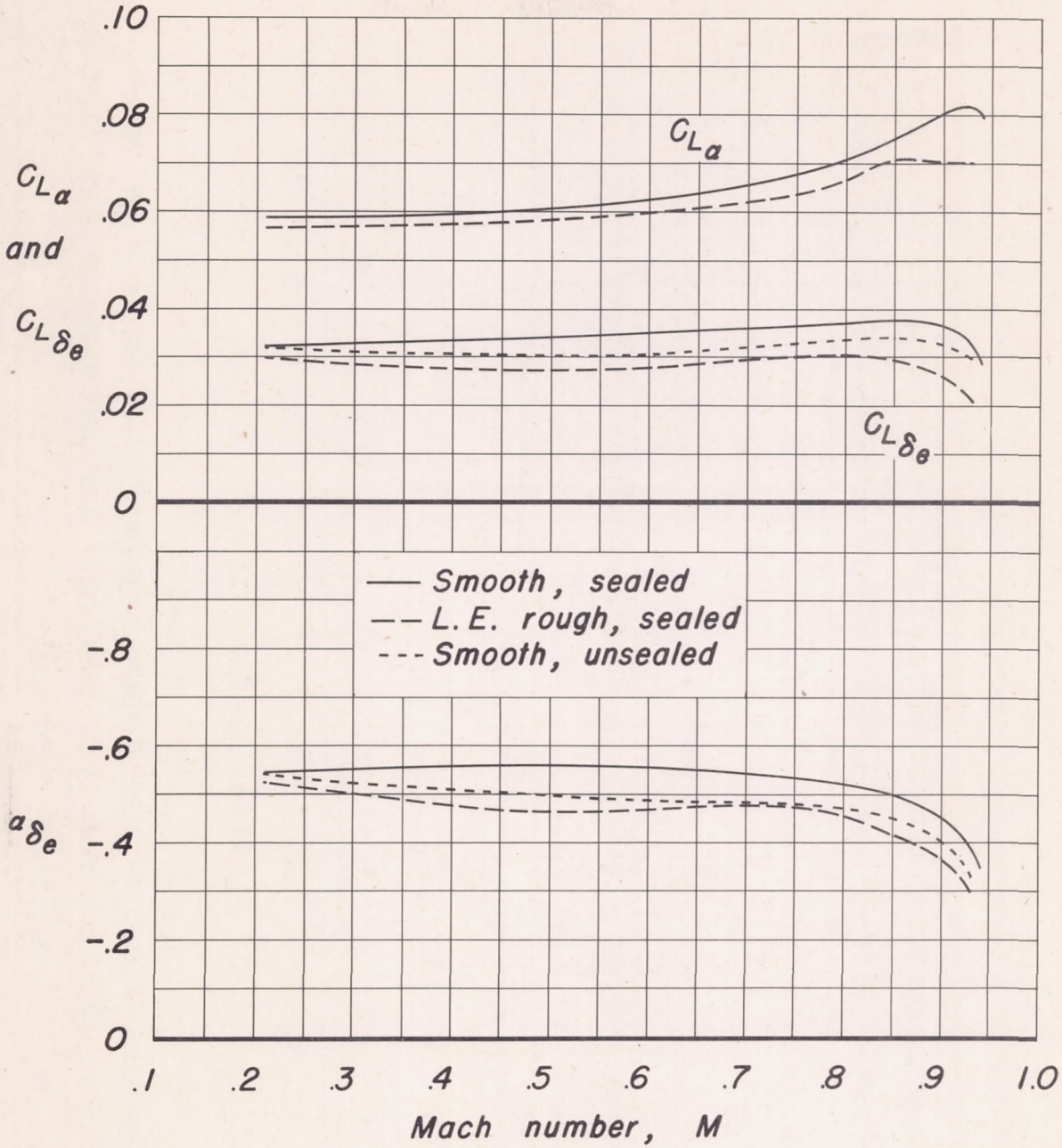

Figure 24.— The independent effects of leading-edge roughness and removal of the elevator-nose seal on the variations of lift parameters C_{L_α}, $C_{L_{\delta_e}}$, and a_{δ_e} with Mach number. R, 2,000,000.

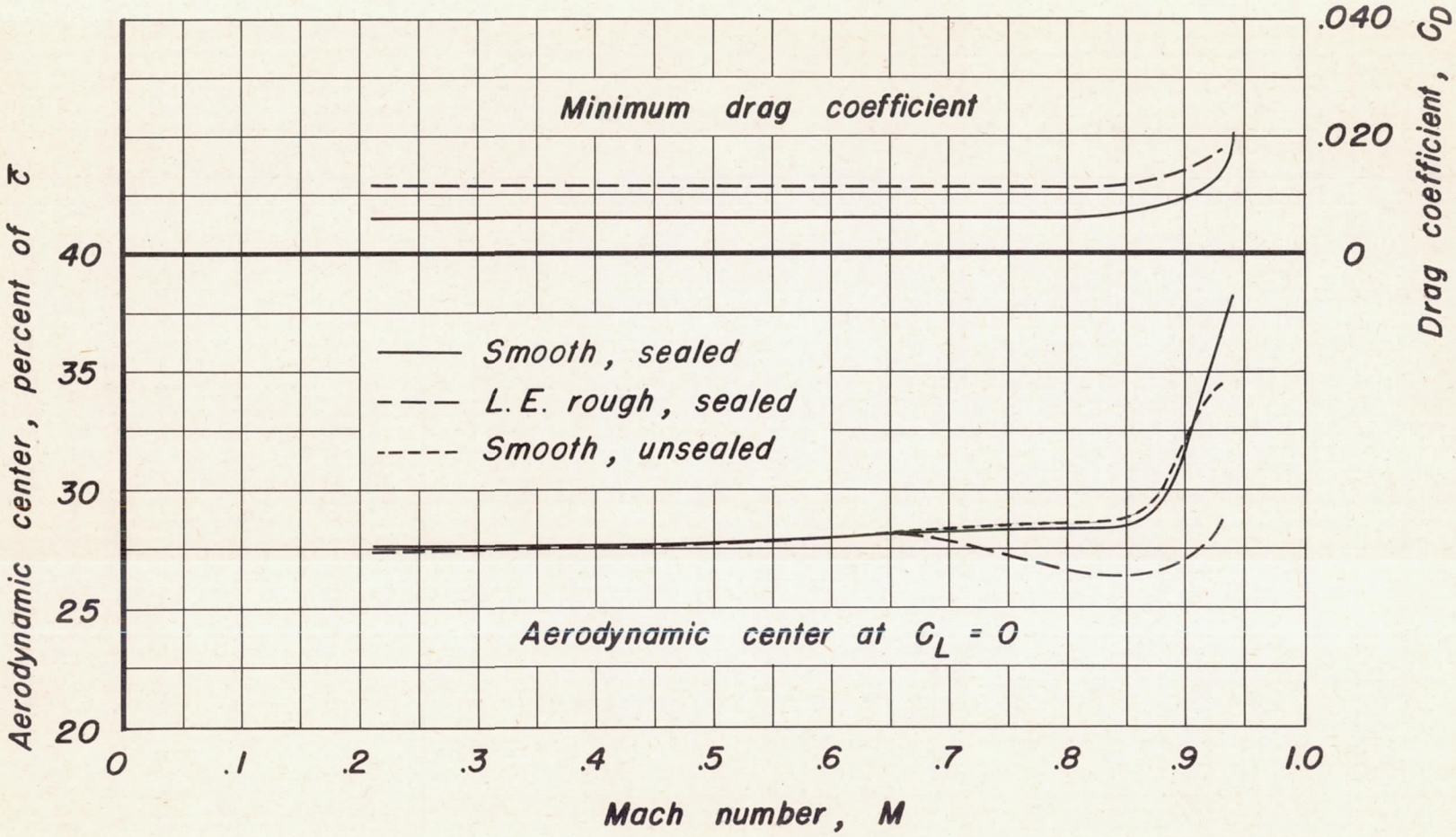

Figure 25.— The independent effects of leading-edge roughness and removal of the elevator-nose seal on the variations of minimum drag coefficient and aerodynamic-center location with Mach number. δ_e, 0°; δ_t, 0°; R, 2,000,000.

NACA-Langley - 9-9-49 - 250